

## ABSTRACT

Title of Thesis: IGNITION QUALITY TESTER  
CHARACTERIZATION WITH PURE  
COMPONENT AND CONVENTIONAL  
NAVY FUELS

Jacob L Mendelson, Master of Science, 2016

Thesis Directed By: Dr. Ashwani K. Gupta  
Department of Mechanical Engineering

The U.S. Navy is attempting to reduce dependence on conventional diesel fuels as a part of the environmental initiative commonly referred to as “The Great Green Fleet”. The purpose of this research was to characterize the measurements of ignition delay gathered by the Advanced Engine Technology Ignition Quality Tester (IQT) with conventional Navy diesel fuels, pure component biodiesel fuels, primary cetane standards, and toluene-hexadecane blends. The use of computational analysis with pressure traces gathered from the IQT allowed for the comparison of IQT ignition delay results with various methods of calculating start of combustion for various fuels. Physical and chemical ignition delays of each fuel were also calculated using different separation techniques and the chemical ignition delay results were compared with prior academic literature and with chemical ignition delays calculated with Lawrence Livermore kinetic theory.

IGNITION QUALITY TESTER CHARACTERIZATION WITH PURE  
COMPONENT AND CONVENTIONAL NAVY FUELS

by

Jacob Lee Mendelson

Thesis submitted to the Faculty of the Graduate School of the  
University of Maryland, College Park, in partial fulfillment  
of the requirements for the degree of  
Master of Science  
2016

Advisory Committee:

Dr. Ashwani K. Gupta, Professor, Chair  
Dr. Jim Cowart, Professor  
Dr. Bao Yang, Professor  
Dr. Gary Pertmer, Professor

© Copyright by  
Jacob Lee Mendelson  
2016

## Acknowledgements

I would like to take this time to thank Dr. Ashwani Gupta for taking me in as a member of his research team over the past year. It is difficult to find an advisor who is willing to accept a student with a one-year M.S. timeline such as myself, but Dr. Gupta did not hesitate in his commitment to help me succeed and accomplish my goal of earning a degree from the University of Maryland.

To Dr. Jim Cowart, your commitment to guiding my research and your technical knowledge of the field is unparalleled. I am gracious for your patience in guiding me towards greater knowledge regarding my research and to instill what it means to be a graduate student.

I would like to also thank Dr. Bao Yang and Dr. Gary Pertmer for taking the time to be members of my advisory committee.

I would also like to thank Dr. Len Hamilton for your efforts in guiding the technical approach to my analysis. Your expertise with MATLAB is a rare gift and I am forever grateful for your guidance and support that you have given me over the course of my research.

To my parents, Mark and Teresa Mendelson, you have supported me all my life and over the course of my studies with positive energy and enthusiasm, and have pushed me towards success despite the hardships of a rigorous academic program.

Lastly, I would also like to thank my sister, Leah Mendelson, who helped to open my eyes to the idea of becoming a graduate student and who offered guidance when I faced difficult courses and unfamiliar material.

# Table of Contents

Acknowledgements.....	ii
Table of Contents.....	iii
List of Tables.....	iv
List of Figures.....	v
Chapter 1: Motivation and Objectives.....	1
Chapter 2: Background and Literature Review.....	5
Chapter 3: Experimental Setup.....	9
Advanced Engine Technology Ignition Quality Tester.....	9
Fuels.....	10
Experimental Procedure.....	11
Methods for Determining Start of Combustion.....	14
Physical and Chemical Delay Separation.....	15
Chapter 4: Experimental Results and Analysis.....	17
Ignition Delay of Analyzed Fuels.....	17
Ignition Delay of Toluene-Hexadecane Blends.....	19
Separation of Physical and Chemical Delays.....	22
Comparison of CHRR Ignition Delays with IQT Ignition Delays.....	32
Fuel Properties Analysis.....	35
Comparison of Results with Lawrence Livermore Kinetics.....	41
Chapter 5: Conclusions and Recommendations for Future Work.....	44
Conclusions.....	44
Recommendations for Future Work.....	46
Appendices.....	51
Bibliography.....	111

## List of Tables

Table 3-1: Various Fuel Property Values for F76 and JP5.....	10
--	----

## List of Figures

Figure 3-1: An Advanced Engine Technology Ignition Quality Tester .....	9
Figure 3-2: Heat release rate figure for a single combustion event .....	12
Figure 3-3: A pressure trace for a single combustion event .....	13
Figure 3-4: An illustration depicting SOC methods .....	14
Figure 4-1: Ignition delay metrics for analyzed fuels .....	18
Figure 4-2: Ignition delay metrics for Tol-Hex blends .....	19
Figure 4-3: Ignition delays relative to IQT delays .....	20
Figure 4-4: Ignition delays relative to IQT delays less mindP .....	21
Figure 4-5: WSU method for analyzed fuels .....	22
Figure 4-6: WSU method for Tol-Hex blends .....	23
Figure 4-7: 25% mindP method for analyzed fuels .....	24
Figure 4-8: 25% mindP method for Tol-Hex blends .....	25
Figure 4-9: 50% mindP method for analyzed fuels .....	26
Figure 4-10: 50% mindP method for Tol-Hex blends .....	27
Figure 4-11: ddP method for analyzed fuels .....	28
Figure 4-12: ddP method for Tol-Hex blends .....	29
Figure 4-13: Separation methods for nC7 .....	30
Figure 4-14: Separation methods for CN30 .....	31
Figure 4-15: Separation methods for nC16 .....	32
Figure 4-16: CHRR ignition delays for nC7 .....	33
Figure 4-17: nC7 ignition delays relative to IQT delay .....	34
Figure 4-18: Modified droplet diameter vs. fuel .....	38

Figure 4-19: Modified droplet diameter vs. DCN .....	38
Figure 4-20: Weber number vs. fuel .....	39
Figure 4-21: Weber number vs. DCN.....	39
Figure 4-22: Break-up time vs. fuel.....	40
Figure 4-23: Break-up time vs. DCN.....	40
Figure 4-24: LLK/ddP comparison for pure component fuels.....	42
Figure 4-25: LLK/ddP comparison for Tol-Hex blends .....	43



## List of Abbreviations

CHCD-76 – Catalytic Hydrothermal Conversion Diesel Fuel  
CHCJ-5 – Catalytic Hydrothermal Conversion Jet Fuel  
CHRR – Cumulative Heat Release Rate  
CVCA – Constant Volume Combustion Apparatus  
DCN – Derived Cetane Number  
ddP – Second Derivative Inflection Point Analysis  
IHRR – Immediate Heat Release Rate  
IQT – Ignition Quality Tester  
LLK – Lawrence Livermore Kinetics  
mindP – Minimum Change in Pressure Integration  
nC7 – Pure Component Heptane  
nC10 – Pure Component Hexane  
nC16 – Pure Component Hexadecane  
SOC – Start of Combustion  
SOI – Start of Injection  
Tol-Hex – Toluene-Hexadecane Fuel Blend  
WSU – Wayne State University

## Chapter 1: Motivation and Objectives

In the modern era, the U.S. Navy is attempting to reduce its dependency on conventional, petroleum based fuels. As such, a year-long effort colloquially known as the “Great Green Fleet” has been implemented to transform the energy use of the U.S. Navy [1]. The Navy is seeking “drop-in” replacements which would prevent the need for excessive engine overhauls or changes in the operational procedures of the engine [1].

The Navy intends to apply renewable energy sources to shore installations as well as ships which would allow for continued operation of Navy facilities if grid power becomes unavailable or disrupted [1]. The U.S. Navy is trying to expand the use of renewable energy beyond afloat commands and aviation to allow for greater flexibility of the entire fighting force.

Ray Mabus, the current Secretary of the Navy, has stated in an interview that “By no later than 2020, at least half of all energy that the navy and marines use afloat, ashore, and in the air will come from non-fossil fuel sources” [2]. Motions are already being made towards this goal and the use of biofuels is beyond testing in the laboratory. The USS Makin Island has been launched as the first hybrid ship which utilizes an electric drive when travelling at speeds less than 12 knots and a normal diesel engine for any higher speeds [2].

The use of biofuels will not only affect the readiness of the US Navy, but will positively affect its expenditures as well. As stated by Ray Mabus, “Every time the price of a barrel of oil goes up a dollar it costs the navy \$30 million” [2]. The

previously mentioned USS Makin Island saved \$2 million on fuel costs for a recent underway which emphasizes the monetary value of replacing conventional fuels with biofuels [2].

The Navy has utilized biofuels in many tactical displays since the motion to move the Navy towards renewable energy sources. U.S. ships and aircraft utilized biofuels derived from many sources such as algae in the Rim of the Pacific exercise [3]. These algae fuels qualify as “drop-in” replacements for conventional diesel fuels and will soon be competitive in cost with petroleum based diesel fuels [3].

Rather than ethanol and standard biodiesel, the Navy is interested in fuels that have the same energy density as petroleum-based fuels and contain lower levels of oxygen [4]. Political moves have already been made as the United States has encouraged foreign government cooperation and offered to share test and certification data for alternative fuels [4].

The Navy has recently deployed a part biofuel-powered carrier strike group containing the USS John C. Stennis [5]. The destroyers and fast combat support ship that comprise the carrier strike group are powered with a biofuel blend made from 90% petroleum fuel and 10% rendered beef fat [5]. This fuel proves to be cost competitive and allows for future progress with biofuel blends that aim to end the dependency on petroleum-based fuels [5].

In previous research conducted by LT Kevin Burnett, USN, the quality of ignition was experimentally determined for potential pure component fuels like normal heptane, normal hexane, and normal hexadecane [6]. Conventional Navy fuels were also tested as control data points [6]. The fuels were tested in a single-cylinder

diesel Combined Fuels Research engine with varying compression ratio and air-fuel ratio [6]. Improvements in startup performance were caused by increasing compression ratio, increasing the cetane number of the fuel, and decreasing the air-fuel ratio of the fuel mixture [6]. This research served to characterize the startup performance of the pure component biodiesel fuels and whether they could serve as viable “drop-in” replacements given their behavior on engine startup.

With the Navy desiring advancements in the use of compatible biofuels, it becomes necessary to test the ignition and combustion characteristics of many different biofuels and biofuel blends. There are combustion attributes that are missing from biofuel-centric experimentation and data that could prove of use to the U.S. Navy in its quest of moving towards renewable energy sources.

The Ignition Quality Tester (IQT) developed by Advanced Engine Technology is a viable device capable of analyzing new biofuels and biofuel blends that could be possible energy sources for the U.S. Navy’s Green Fleet power requirements. The focus of this research is to provide experimental data to accomplish goals in connecting the IQT to biofuel research.

Firstly, there is no clear connection between the ignition delays calculated with the IQT and the ignition characteristics of cumulative heat release rate (CHRR) which are derived from the first law of thermodynamics. CHRR is a method that is commonly used when producing combustion data with engines such as the Waukesha CFR engine that was utilized in LT Burnett’s experimentation and analysis. This start of combustion (SOC) metric is useful in analyzing engine performance and a clear

connection is needed between the IQT and CHRR data in order to provide useful intuition on the combustion of biofuels in the IQT.

A second objective of this research is to produce experimental ignition delay data of fundamental fuels relevant to the Navy. The selection of fuels is explained thoroughly in Chapter 3. Pure component biofuels, primary cetane standards, toluene-hexadecane blends, and conventional Navy fuels were all analyzed and evaluated as to provide a comprehensive set of data that could be used to determine the IQT performance as it pertains to a myriad of different fuels.

A tertiary objective of this research was to develop an improved understanding of the IQT and combustion characteristics of biofuels with respect to the chemical properties of the fuel. This objective was not entirely accomplished as the fuel properties analysis conducted in this research remains inconclusive. Chapter 4 of this document will highlight some key areas of the experimentation and data and figures are attached in the appendices.

Lastly, this research aimed to determine methods of separating the physical and chemical ignition delays. The physical ignition delay refers to the breakdown of molecules of each fuel which corresponds with the break-up time and vaporization. The chemical ignition delay refers to the decomposition of each individual molecule as the combustion reaction takes place.

## Chapter 2: Background and Literature Review

In 1997, a team of researchers began work analyzing the efficacy of utilizing a CVCA which could rapidly test diesel fuels and develop values for ignition quality [7]. The team analyzed the testing method of the IQT to determine the repeatability of the method and the accuracy of the prediction of cetane value of each tested fuel [7]. 123 test fuels were utilized to validate the results of the IQT against the ASTM D-613 test which produces a resulting cetane value [7]. It was concluded that the repeatability of the IQT test over the 40 to 56 CN range was 0.40 CN which was within the standards of the D-613 ASTM test [7].

Their research was continued when the team attempted to improve the CN model and continue to refine the fuel injection system of the IQT [8]. 38 fuel samples were tested and characterized to meet the D-613 test method and 97% of the test fuels had an IQT predicted cetane number within the quoted ASTM limits [8].

In 2001, the same team conducted experimentation on an IQT unit with a wide variety of different diesel fuels to determine the precision of the instrument [9]. The team also had the objective of determining if the device could meet the American Society for Testing and Materials (ASTM) and Institute of Petroleum (IP) testing methods [9]. It was concluded that the IQT maintained adequate precision over the 40 to 55 CN range and met the standards of the ASTM D613 Test Method [9]. It was also concluded that the use of the IQT to measure blended fuels was adequate, where blending fuels is a common practice used to optimize diesel fuels [9].

In 2014, members of a Wayne State University research team investigated the matching of fuel properties to develop JP-8 surrogates and the use of an ignition quality tester to validate their results [10]. The team examined properties such as boiling point, volatility, density, surface tension, and viscosity to isolate possible surrogates that would behave similarly to JP-8 in terms of autoignition and combustion [10]. These properties could then be used to construct surrogates of different fuel components that would best match the properties of the original JP-8 fuel [10]. The team tested their possible surrogates in an ignition quality tester to develop a derived cetane number [10]. Overall, the team discovered that the six surrogates all closely matched the fuel properties of JP-8 and that JP-8 surrogate matching increased as the number of fuel components increased from two to four [10]. This surrogate matching is important because it is the process of creating alternative biofuels that can be utilized by the U.S. Navy as drop-in replacements for their traditional diesel fuels.

In 2014, a research team attempted to utilize computational fluid dynamics to model the combustion of n-Alkanes in the IQT [11]. It was concluded that the computational fluid dynamics could accurately predict the ignition delay for n-heptane and n-hexadecane over a wide range of temperatures [11]. The IQT was discovered to be of use in validating the results of chemical kinetics and other simulation methods that attempt to model combustion and determine the ignition delay of diesel fuels [11].

In 2012, Donna Post Guillen of Idaho National Laboratory conducted experimentation of the autoignition of cyclopentane, a flammable hydrocarbon, in an

IQT [12]. Ignition delay of the cyclopentane decreased as either temperature or equivalence ratio of the chamber increased [12]. No ignition was observed at lean operating conditions with an equivalence ratio equal to 0.5 [12].

Additional research was completed in 2016 that investigated the negative temperature coefficient region within the ignition quality tester for fuel blends of iso-octane and ethanol [13]. The IQT could capture the two-stage ignition of these fuel mixtures which aids in the comparison between experimental combustion data and ignition data generated with a chemical kinetics scheme [13]. It was determined that evaporative cooling, a major aspect of the physical ignition delay, was not highly affected as temperature was varied during the experimentation [13]. It was concluded that increases in the ethanol concentration of the mixture produced shorter ignition delay times over the range of temperatures used in the experimentation [13].

In efforts to increase the knowledge regarding the use of biodiesels in the IQT, research was conducted that determined the cetane numbers of straight-chain and branched fatty esters [14]. 29 different ester molecules were tested in an IQT to determine their ignition properties [14]. It was concluded that the additional branches of branched esters as compared to straight-chain esters did not significantly affect the ignition properties [14]. The branched esters have better properties at low temperatures compared to the straight-chain esters making them viable additives to biodiesel blends given they did not affect the ignition properties in this experimentation [14].

Two-stage Lagrangian (TSL) modeling of the IQT was researched by a team under Adamu Alfazazi [15]. The TSL modeling utilized two-stage mixing of two



fluid frames of reference and allowed for the analysis of chemical kinetics and fluid flow during combustion [15]. It was concluded that there was acceptable agreement between the results from the TSL model and the experimental data gathered for various fuels with and without an Ignition Quality Tester (IQT) [15]. It proved to be most efficient in simulating the ignition of fuels with long delays in the IQT and variables such as ambient pressure and ambient oxygen concentration could be altered which affected the ignition delay of isooctane [15].

Lastly, additional research was completed in comparing ignition delay times generated with an IQT to the octane numbers of fuels [16]. Primary reference fuels of isooctane and n-heptane as well as toluene reference fuels of toluene and n-heptane were examined in the research along with various gasolines and certification gasolines [16]. The team measured the ignition delay of each of the test fuels in an IQT and compared the ignition delay results with an octane index to determine an expression for the octane number of the test fuels given only ignition delay [16]. This experimentation will help to mathematically connect fuel descriptions like the octane number to possible future experimentation with the IQT. Furthermore, the team introduced a correlation between octane number and derived cetane number that will aid in designing fuels by allowing for the use of the IQT in research modes [16].

## Chapter 3: Experimental Setup

### Advanced Engine Technology Ignition Quality Tester

The IQT was the sole piece of equipment used in the production and analysis of ignition quality data for this set of experiments. The instrument was located at the United States Naval Academy in Annapolis, MD.



Figure 3-1: An Advanced Engine Technology Ignition Quality Tester

The IQT is capable of testing standard and alternative diesel fuels and can measure ignition quality based on ignition delay [17]. The device boasts a short testing time of approximately twenty minutes for fuels and is sensitive to diesel additives and various diesel mixtures which makes the device ideal for testing diesel blends and how they affect ignition performance [17]. The IQT uses a low volume of

fuel allowing for cheap and accurate ignition testing of a wide range of diesel fuels [17].

The IQT is outfitted with temperature and pressure sensors that are used to maintain consistent testing settings as well as output a form of pressure data that can be used for analysis. Both the pressure and temperature sensors are utilized in this research as both can be used to formulate various definitions of ignition delay.

### Fuels

The Navy standard F76 diesel fuel and JP5 jet fuel were the two conventional Navy fuels used for experimentation and analysis. These fuels are the standard diesel and standard aviation fuels utilized by the navy and are entirely petroleum based. Properties of these fuels can be found below in Table 3-1. Additional property values can be found in Appendix A.

**Table 3-1: Various Fuel Property Values for F76 and JP5**

	F76	JP5
Density at 15 °C (kg/L)	0.833	0.8048
Viscosity at -20 °C (mm <sup>2</sup> /s)		4.8
Viscosity at 40 °C (mm <sup>2</sup> /s)	2.3	
Flash Point (°C)	66	61
Surface Tension (dyne/cm)	28.4	27.6
Freezing Point (°C)		-50

The conventional fuels were also complemented with pure component heptane (nC7), hexane (nC10), and hexadecane (nC16). Pure component heptane is the calibration fuel used for the IQT. These fuels were analyzed for startup performance

in the prior thesis work of LT Kevin Burnett [6] and are important to be considered for potential navy application in the quest for new alternative biodiesel fuels.

The primary cetane standards of CN30, CN45, and CN60 were also tested with the IQT. These primary standards were composed of mixtures of n-hexadecane and 2,2,4,4,6,8,8-heptamethylnonane (HMN). For this research, the cetane values of interest were decomposed into the mixtures that contained a certain percentage of n-hexadecane and a certain percentage of HMN.

Lastly, various toluene-hexadecane blends were added to the experimental list of fuels. Toluene is a common diesel additive that adds lubricity to diesel fuel and can help to minimize normal wear and tear of mechanical diesel engine components. Various blends of toluene and hexadecane show how the addition of toluene affects ignition quality of the pure component hexadecane diesel fuel. These mixtures are denoted by the percent toluene and the percent hexadecane that make up the specific mixture. The cetane number of the fuel generally increases as the percent of hexadecane increases which intuitively means that the mixture is comprised of lower amounts of toluene.

### Experimental Procedure

Each fuel was tested with the default IQT testing procedure which consists of 32 tests that run over the course of 20 to 30 minutes. This creates a series of 32 pressure traces that were used in a MATLAB analysis to produce results for various ignition delays explained below.

MATLAB was used to calculate various types of ignition delays and to separate the physical and chemical ignition delays of each fuel. The MATLAB

Ignition Delay Analyzer code is attached in Appendix B. The code produces a series of plots for each of the 32 tests for each diesel fuel analyzed.

The first plot is a heat release rate plot that shows the valve lift which determines start of injection (SOI). This plot is produced for each individual combustion event, so a total of 32 plots are generated over the course of one complete testing cycle for a given fuel. The figure shows both CHRR and immediate heat release rate (IHRR) and prints various calculated ignition delays with the various methods. The CHRR for each test is used to determine the analyzed ignition delays based on start of combustion (SOC) occurring at five percent of the CHRR value and ten percent of the CHRR value. The plot of the heat release rates for nC7 is shown below in Figure 3-2.

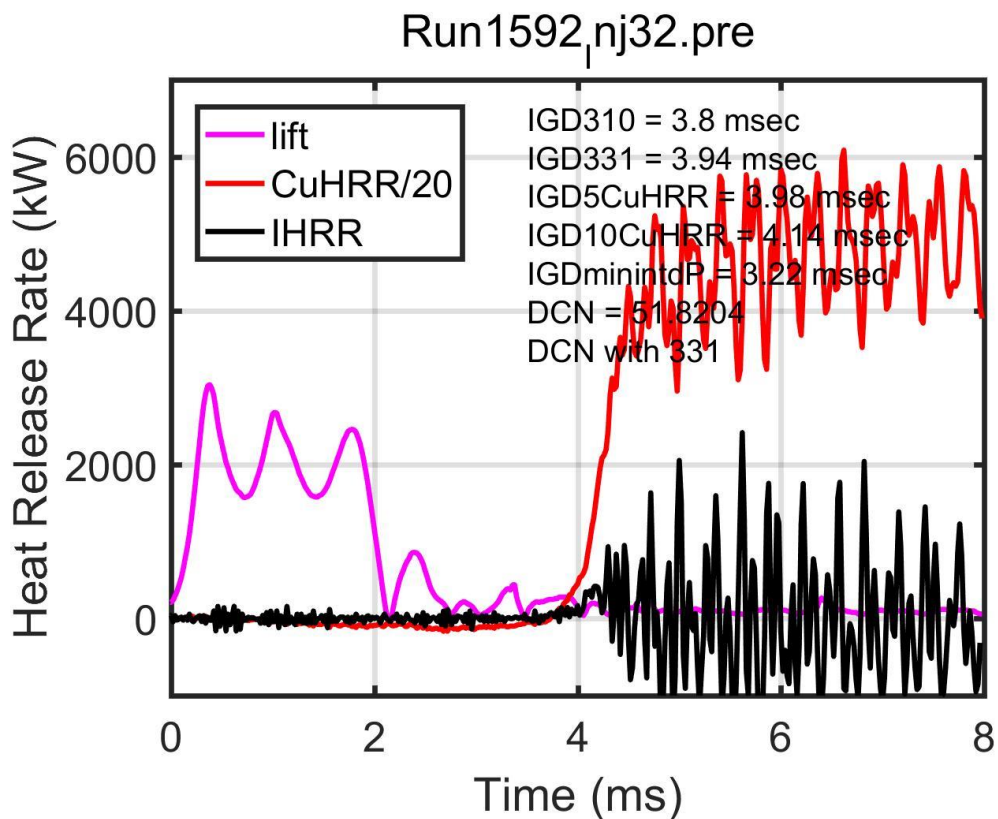


Figure 3-2: A heat release rate figure produced for one test of the nC7 fuel.

The analyzer code also produces a figure for each individual pressure trace that is recorded by the IQT testing cycle. For 32 individual tests for a given fuel, 32 different pressure traces are recorded. These pressure traces are then smoothed with a curve fitting function in the MATLAB code which becomes useful when analyzing the pressure trace for the point of inflection. The figure also depicts valve lift which, as previously mentioned, is the metric for determining SOI of the fuel. The pressure trace figure for one test of nC7 can be seen below in Figure 3-3.

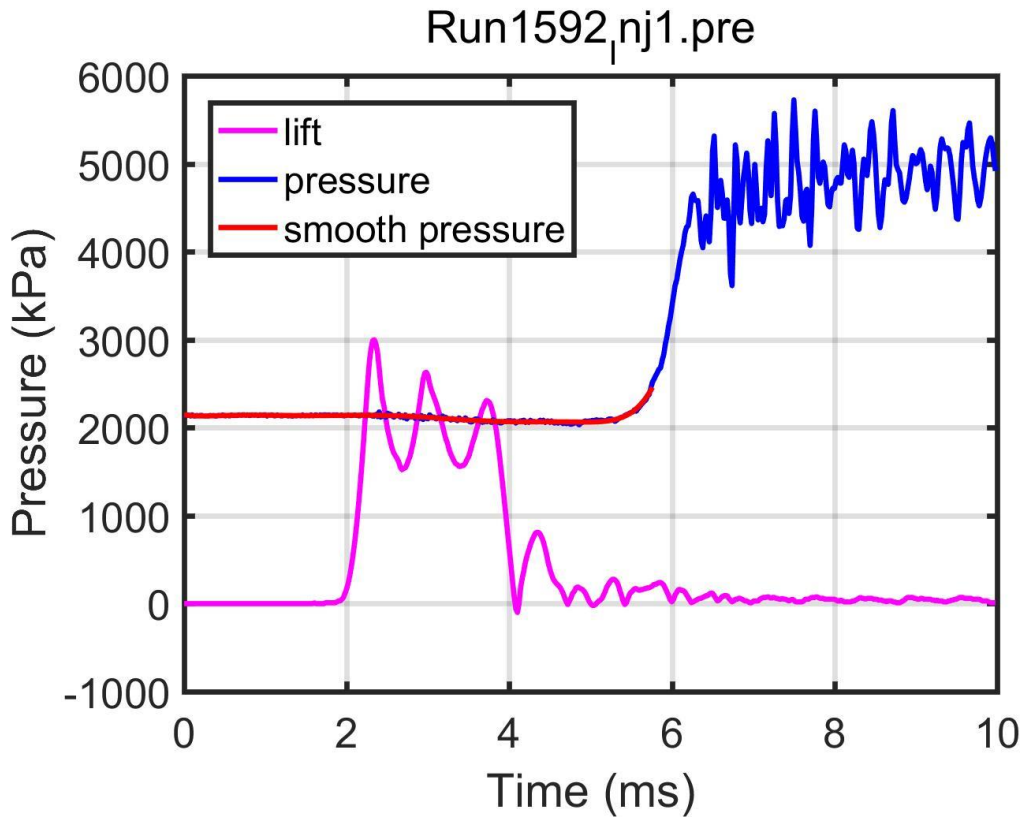


Figure 3-3: A pressure trace figure for one test of the nC7 fuel.

Methods for Determining Start of Combustion

Start of combustion (SOC) was determined using many different analytical methods that were applied to pressure traces that were gathered from the IQT. The methods used are depicted below by Figure 3-4:

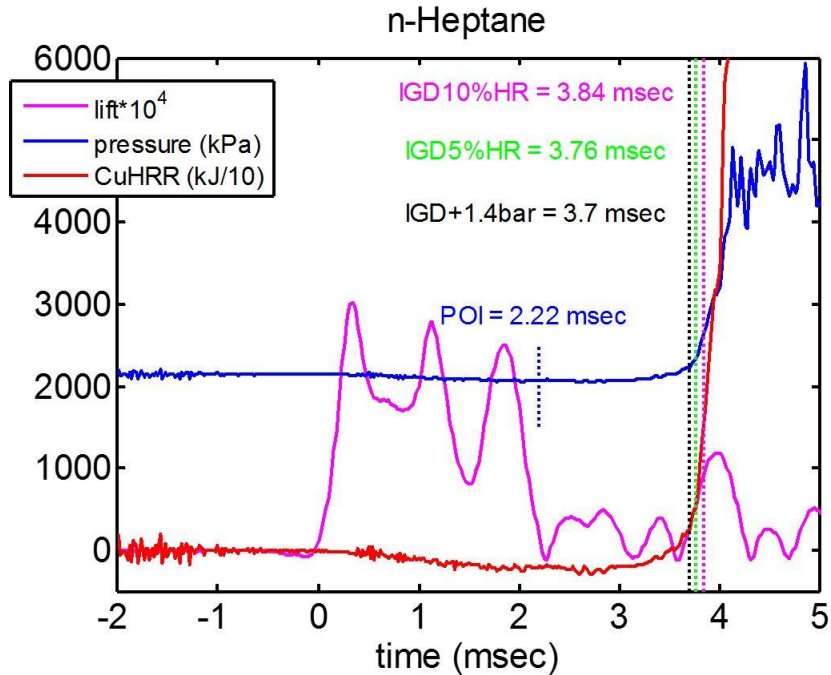


Figure 3-4: Depiction of the methods used to calculate SOC.

The first method used to determine SOC was the 331 psi standard. This equates to an achieved pressure of 331 psi which is 21 psi, or 1.4 bar, higher than the 310 psi initial combustion state of the IQT. The black line in Figure X-X shows where the 331 psi standard determined SOC for normal heptane.

A second method for determining SOC was the 310 psi standard. 310 psi is the normal steady state operating pressure of the IQT. All combustion tests begin with the chamber pressurized to 310 psi. The pressure drops after injection due to

evaporative cooling, and this method places SOC at the point where the pressure recovers to the initial 310 psi.

Cumulative heat release rate (CHRR) is another method for determining SOC. CHRR is a method that is frequently used in operating engines to determine SOC. Using the pressure trace and characteristics of the IQT, CHRR can be calculated for each test for a given fuel. For this research, both 5% CHRR and 10% CHRR were analyzed as possible measures for SOC. These SOC points are shown in Figure X-X as the green and purple dotted lines, respectively.

The mindP method for determining SOC involved using a minimum change in pressure integration. As soon as the cumulative sum of the change in pressure reached a minimum, the analysis used that time as SOC. This produced a very short ignition delay compared to the pressure and CHRR metrics for SOC, and thus is much more useful as a baseline for separating the physical and chemical ignition delays of each fuel.

#### *Physical and Chemical Delay Separation*

Along with the metrics to determine SOC, various methods were used to determine the separation between the physical ignition delay and chemical ignition delay of the analyzed diesel fuels. The physical and chemical delays are important aspects of diesel fuel combustion since the physical delay is highly determined by the properties of the fuel such as droplet diameter, break-up time, and response to evaporative cooling while the chemical delay is intuitively associated with the chemical composition of the fuel molecules such as molecular chain length and the



strength of the individual bonds in the molecule. The measure of each delay provides insight as to how important the fuel properties are for the combustion of a given diesel fuel and lead to more precise predictions for possible conventional diesel fuel alternatives.

As previously mentioned, the mindP (WSU) method serves as a baseline for determining the separation of the physical and chemical ignition delays, and was highly analyzed by a fuel research team at Wayne State University. This provides a high-end estimate for a possible point of separation.

The 25% mindP separation point determined the time at which the mindP integration achieved 25% of its minimum value. Similarly, the 50% mindP separation method labeled physical/chemical delay separation at the point where the mindP integration achieved 50% of its minimum value.

An additional separation method was implemented in this research which involved analyzing the second derivative of the pressure trace gathered from each test. This point of inflection method, or “ddP” method utilized the location of the point of inflection of the pressure trace as the separation between the physical and chemical delays. In other words, at the point at which the pressure trace began to show signs of recovery, the ddP method labeled this point as the separation between the physical and chemical delays.

## Chapter 4: Experimental Results and Analysis

### Ignition Delay of Analyzed Fuels

Complete IQT testing cycles were completed for each of the analyzed fuels as well as the additional toluene-hexadecane blends. The ignition delays for the previously mentioned methods were calculated and compared with results gathered from the IQT. All IQT summary sheets can be found in Appendix C of this document. The MATLAB code was also utilized to calculate statistical data which is compiled in a master spreadsheet attached as Appendix D. The plots were generated with a separate MATLAB plotting code that references the master data sheet. This code along with all generated plots, some of which are used in the discussion of the results, are attached as Appendix E.

Figure 4-1 below shows the ignition delays as well as confidence intervals of two standard deviations for the conventional navy diesel fuels, the pure component fuels, and the primary standards.

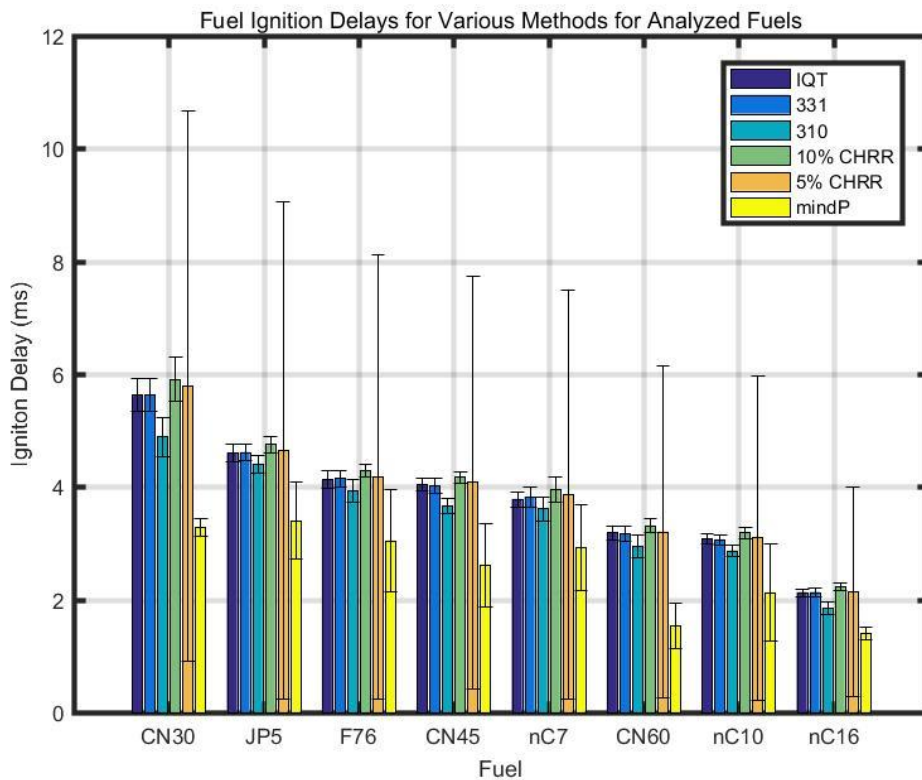


Figure 4-1: Ignition delay values and confidence intervals for analyzed fuels.

From this data, the ignition delay values calculated by the IQT most closely match the 331 psi standard for all analyzed fuels. This is valuable information since it helps to isolate the possible calculation methods of the IQT which are not published.

All the fuels show similar trends with regards to the ignition delay calculation methods. The ten percent CHRR values create a connection to actual engine data and boast appropriate confidence intervals. The five percent CHRR ignition delays have very large confidence intervals which could be the result of inconsistent valve lift at SOI and a rapidly changing temperature and pressure signal in the region where the MATLAB code attempts to isolate SOC.

Ignition Delay of Toluene-Hexadecane Blends

Another master figure was created that bears similarity to Figure 4-1, that contained ignition delay values for all analyzed methods for the toluene-hexadecane blends. The results of these blends are also compared with the conventional navy fuels F76 and JP5. These ignition delays can be seen below in Figure 4-2.

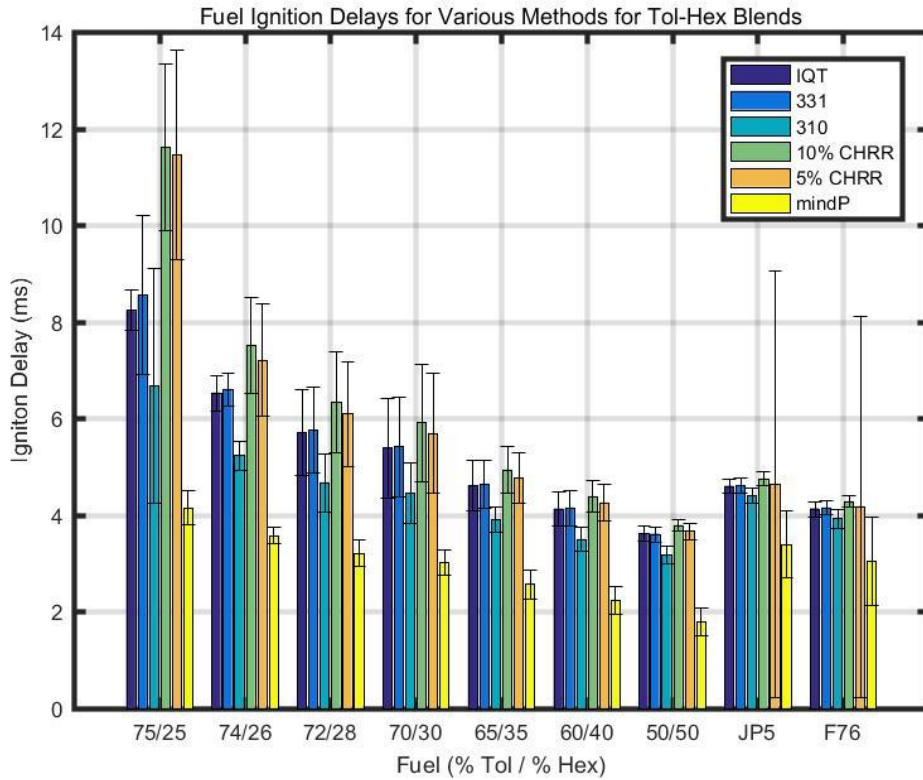


Figure 4-2: Ignition delay values and confidence intervals for toluene-hexadecane blends.

The 331 psi standard again most closely matched the IQT produced value for ignition delay. The CHRR ignition delays are calculated and shown for all of the fuels. Higher confidence intervals are seen for the CHRR ignition delay values at higher percentages of toluene which corresponds to lower cetane number values. As the percent hexadecane, and thus the cetane number, increases, the confidence

intervals of the CHRR values shrink which corresponds to the conclusion that more reliable data can be produced from fuels that possess higher cetane values. Larger error values are seen for the toluene-hexadecane data with fuels of lower cetane values, but the higher cetane value fuels produce similarly consistent data as the analyzed fuels shown in Figure 4-1. The toluene-hexadecane blends produce more reliable data for CHRR than the analyzed fuels at all cetane values.

*IQT and Calculated Ignition Delay Comparison*

It is important to compare the ignition delays calculated with the MATLAB analysis with the ignition delay values produced by the IQT. Figure 4-3 below shows a plot that shows the calculated fuel ignition delays relative to the IQT ignition delays in terms of milliseconds.

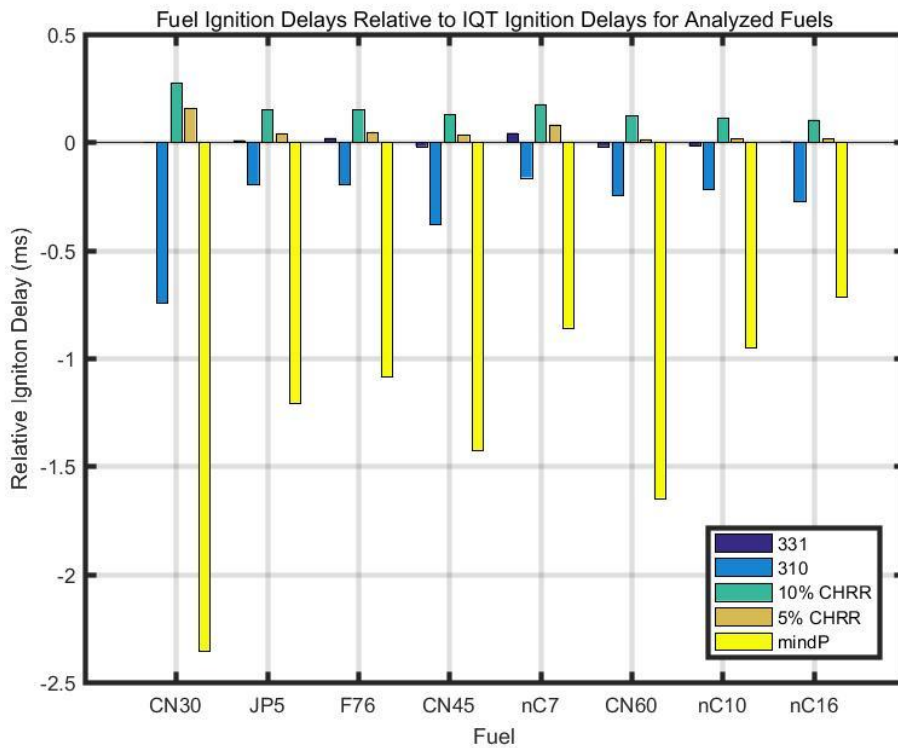


Figure 4-3: Calculated ignition delay values relative to IQT ignition delay values.

This figure illustrates how closely the 331 psi standard coincides with the IQT calculated ignition delays. The 310 psi standard is significantly more distant from the IQT ignition delay value than the 331 psi standard. The mindP calculated value for ignition delay shows large deviation from the IQT value which supports its inclusion as a baseline method for separating the physical and chemical ignition delays rather than the total ignition delay. For the heat release rate ignition delays, the five percent CHRR delay is the closest to the IQT delay each of the depicted fuels which strengthens the connection between the IQT calculated ignition delay and the ignition delays calculated from smaller percentages of CHRR.

This same data is plotted below in Figure 4-4 with the mindP ignition delays removed. This offers better resolution for comparing the pressure calculated ignition delays and CHRR ignition delays with that produced by the IQT.

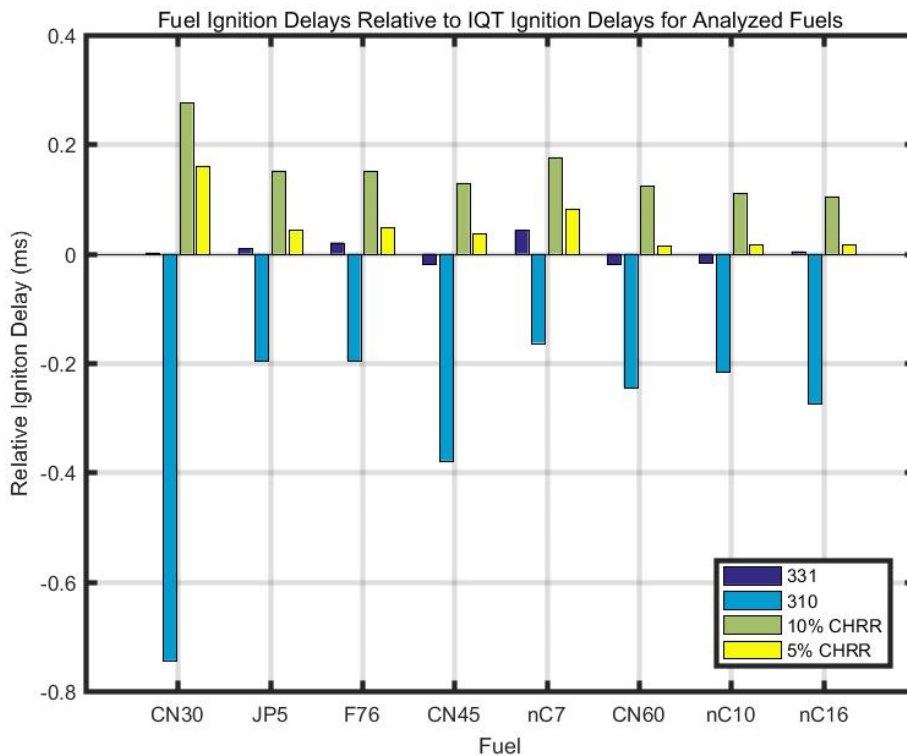


Figure 4-4: Calculated ignition delay values less mindP relative to IQT ignition delay.

Separation of Physical and Chemical Delays

Along with the calculation of the total ignition delays for each of the analyzed fuels, experimental data was analyzed with numerous methods to separate the physical and chemical delays. Figure 4-5 below illustrates the results of using the WSU method which places the end of the physical ignition delay and start of the chemical ignition delay at the time calculated using the mindP method.

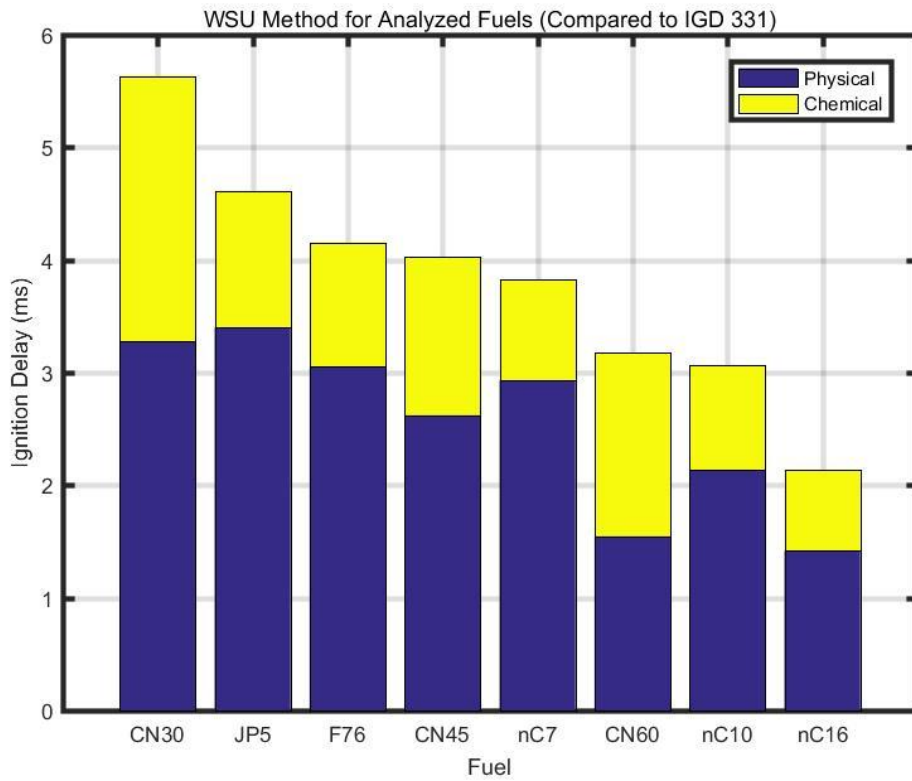


Figure 4-5: Physical and chemical delay separation with the WSU method.

The results show that this method produces a very large physical delay as compared to the chemical delay for each of the fuel molecules. The fuels are arranged in order of increasing DCN along the bottom axis. Larger molecules such as nC10 and nC16 have large physical ignition delays as compared to their chemical ignition delays when the WSU method is used for separation. Larger molecules have a higher

ratio of weaker secondary bonds to stronger primary bonds than smaller molecules so the chemical delay is expected to be less dominant in larger diesel fuel molecules. Given the high physical ignition delays experienced by smaller molecules such as nC7, the WSU method overstates the probable physical delay of the fuel on the lower end of cetane values.

Figure 4-6 below shows the application of the WSU separation method on the Tol-Hex fuel blends analyzed in this research.

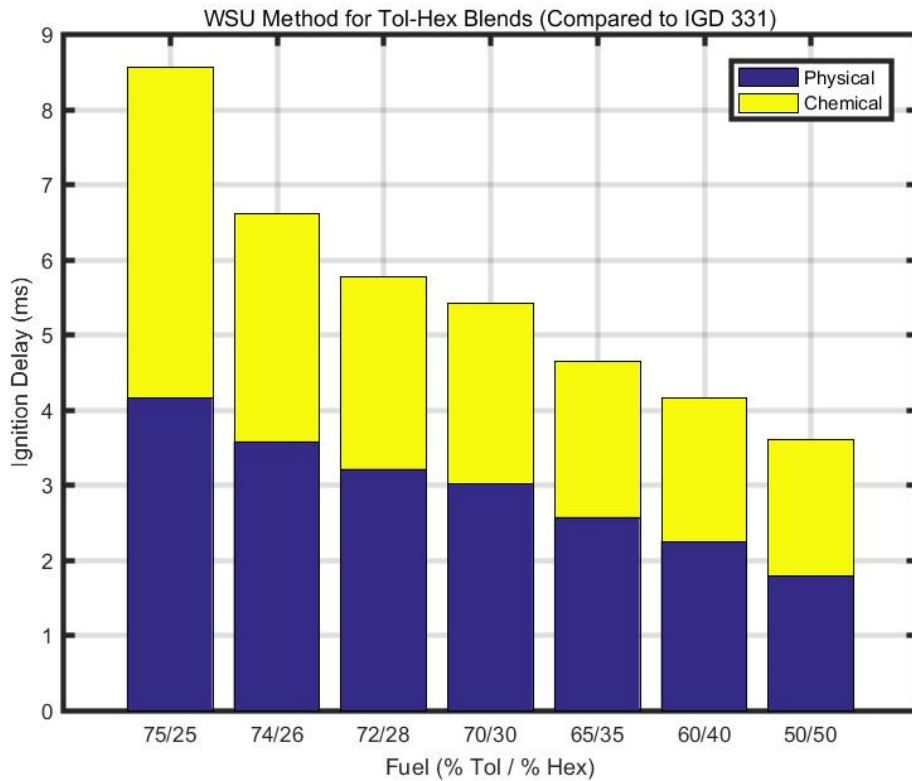


Figure 4-6: Physical and chemical delay separation with the WSU method for Tol-Hex blends.

The Tol-Hex fuels experience a much smaller change in fuel properties over the wide range of blends which explains the similar relative physical and chemical



ignition delays for each fuel. Physical ignition delay decreases at a slower rate than total ignition delay which follows the trend of larger-chained molecules having a more dominant physical ignition delay.

The 25% mindP method provided a baseline from which to start the analysis of separating the physical and chemical ignition delays. Figure 4-7 below shows the total 331 psi ignition delay split into the physical and chemical components for the analyzed fuels.

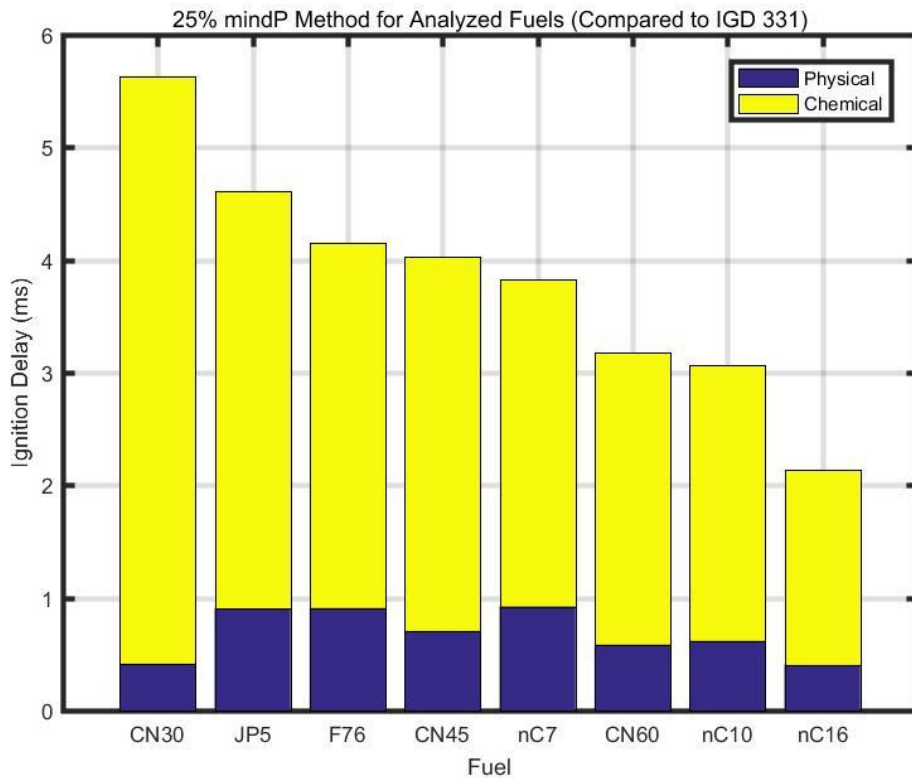


Figure 4-7: Physical and chemical delay separation with the 25% mindP method.

Based on the figure, the 25% mindP method creates a dominant chemical delay and largely insignificant physical delay in the analyzed fuels. This method overstates the chemical delay with larger-chained molecules and does not produce

any visible trends with the change of the physical or chemical ignition delays relative to the overall ignition delay for each fuel.

Figure 4-8 uses the 25% mindP method for the Tol-Hex blends. Very little change is seen in the physical delays between each of the fuels and the chemical ignition delay is still highly overstated as the physical delay is nearly insignificant for each of the fuel blends.

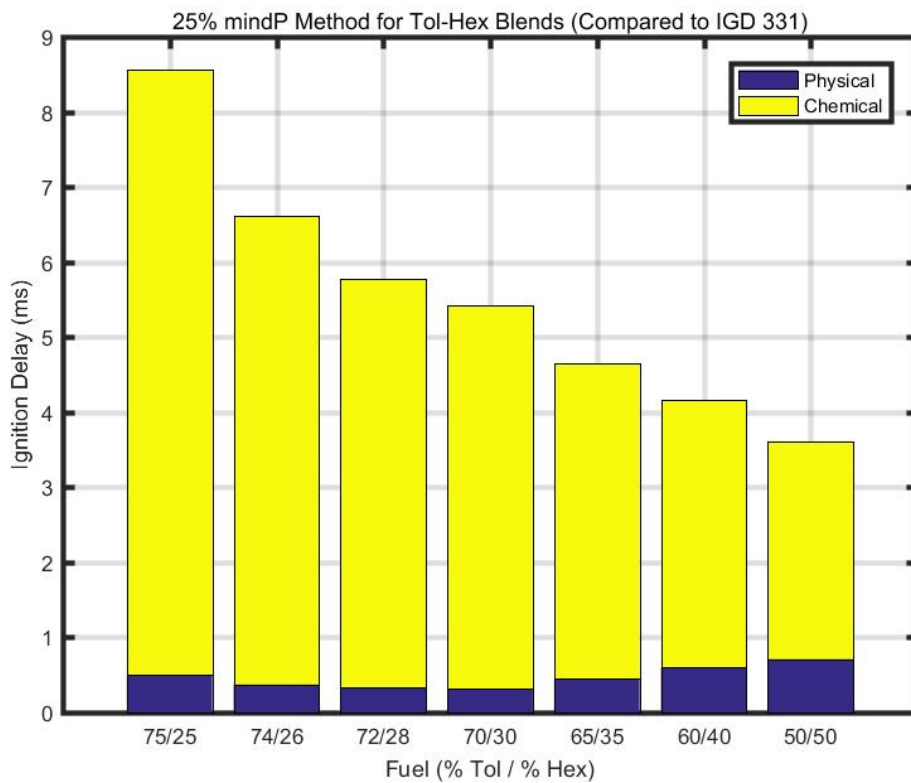


Figure 4-8: 25% mindP ignition delay separation for Tol-Hex blends.

As stated, fuel properties change very little between the different mixtures of toluene and hexadecane which would indicate that similar physical delays would be seen between each of the diesel blends. However, despite the high level of consistency in the physical ignition delay, the chemical delay is still highly dominant over the entire cetane range.

The physical and chemical ignition delay separation using the 50% mindP method for the analyzed fuels is seen in Figure 4-9. Larger chemical delays relative to the total ignition delay are seen at the lower end of the cetane values at the left side of the graph. As cetane value increases, overall ignition delay increases along with the calculated physical ignition delay.

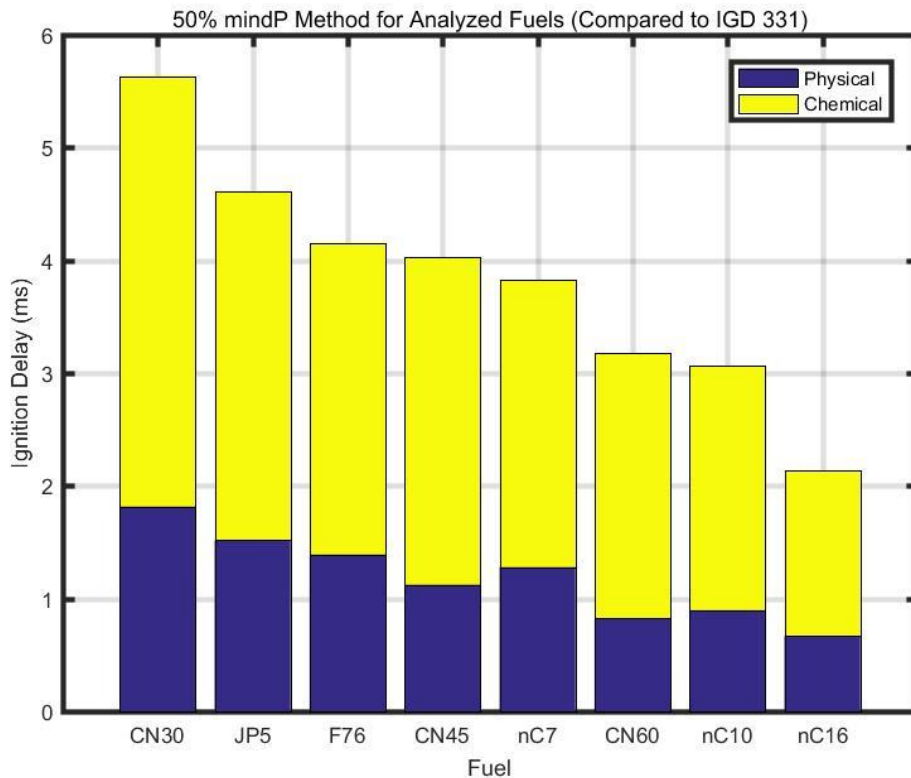


Figure 4-9: Physical and chemical delay separation with the 50% mindP method.

The 50% mindP method was also used to separate possible physical and chemical delays for the Tol-Hex blends shown by Figure 4-10. Physical delay remained constant over the range of Tol-Hex blends which agrees with the hypothesis that the physical delay should be consistent among the fuels. Total ignition delay and chemical delay decrease in a smooth trend as the fuels increase in cetane number.

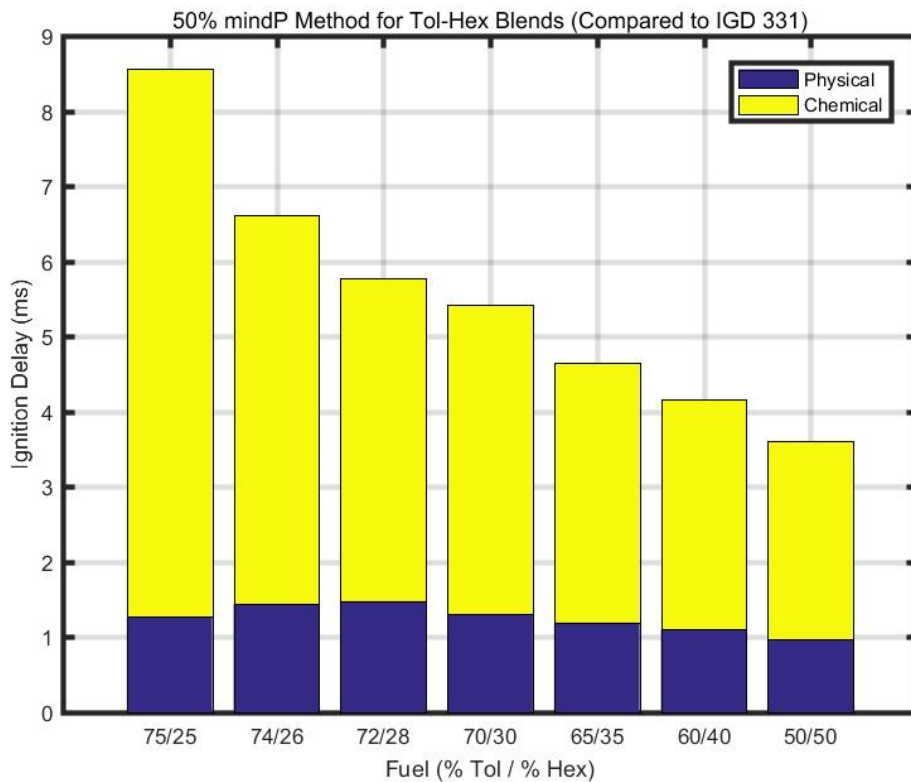


Figure 4-10: 25% mindP ignition delay separation for Tol-Hex blends.

The last separation method used was the ddP (point of inflection) method.

This analysis used a code developed by CAPT Leonard Hamilton, USN (Ret.) and is referenced in Appendix F. Figure 4-11 shows the ignition delays compared to the 331 psi standard with the physical and chemical separation placed at the calculated point of inflection of the pressure trace. An outlying physical delay exists for the CN30 primary standard. This could be the result of unreliable combustion that occurs at very low cetane values which result in distorted pressure data leading to possible errors in the analysis.

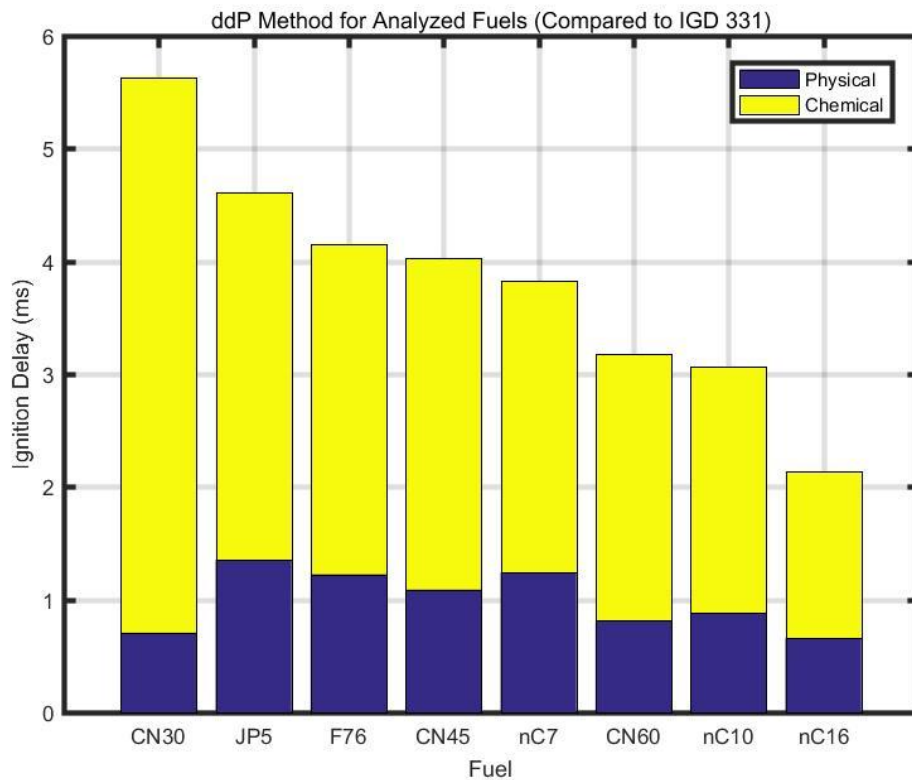


Figure 4-11: Physical and chemical delay separation with the ddP method.

The results of the Tol-Hex blends from the ddP analysis can be seen in Figure 4-12. Physical ignition delay again remains relatively constant over the range of the diesel blends while overall ignition delay compared to the 331 psi standard steadily decreases as the fuels increase in cetane value. The 74/26 blend of toluene/hexadecane has an unusually low physical delay compared to the other blends in the series. The blends with high percentages of toluene have low cetane values and can produce errant pressure traces which could explain the low value for physical delay for the 74/26 Tol-Hex blend.

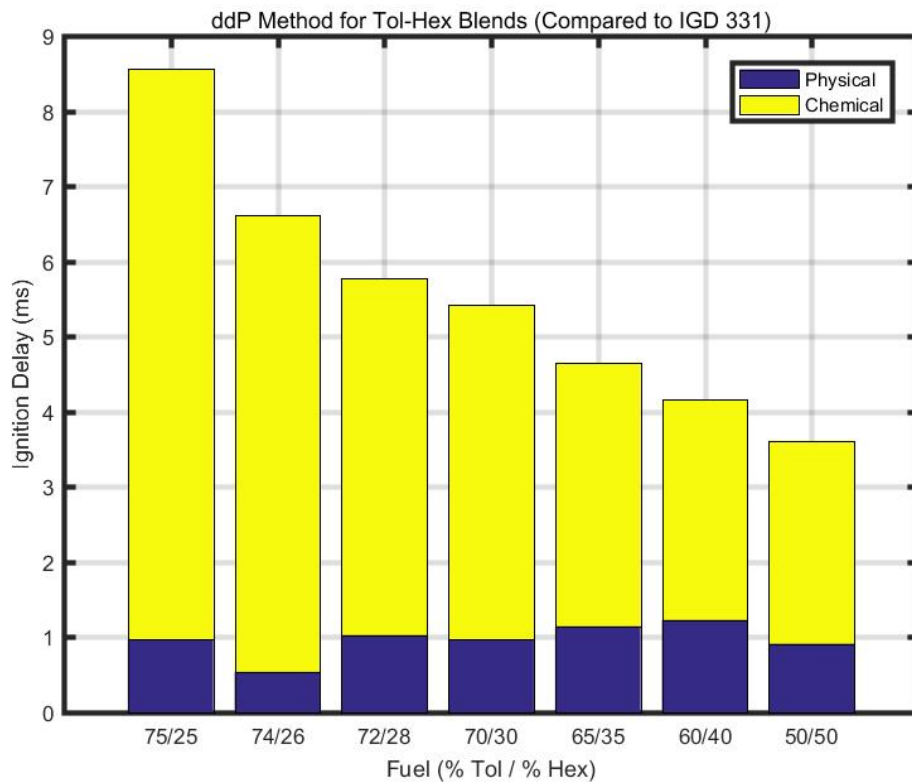


Figure 4-12: ddP ignition delay separation for Tol-Hex blends.

It was important to compare the physical delay and chemical delay separation methods for the same fuel as to create experimental results that directly compare the separation methods to one another. Figure 4-13 below shows the 331 psi ignition delays separated into the physical and chemical delay for each of the separation methods for the nC7 pure component IQT calibration fuel.

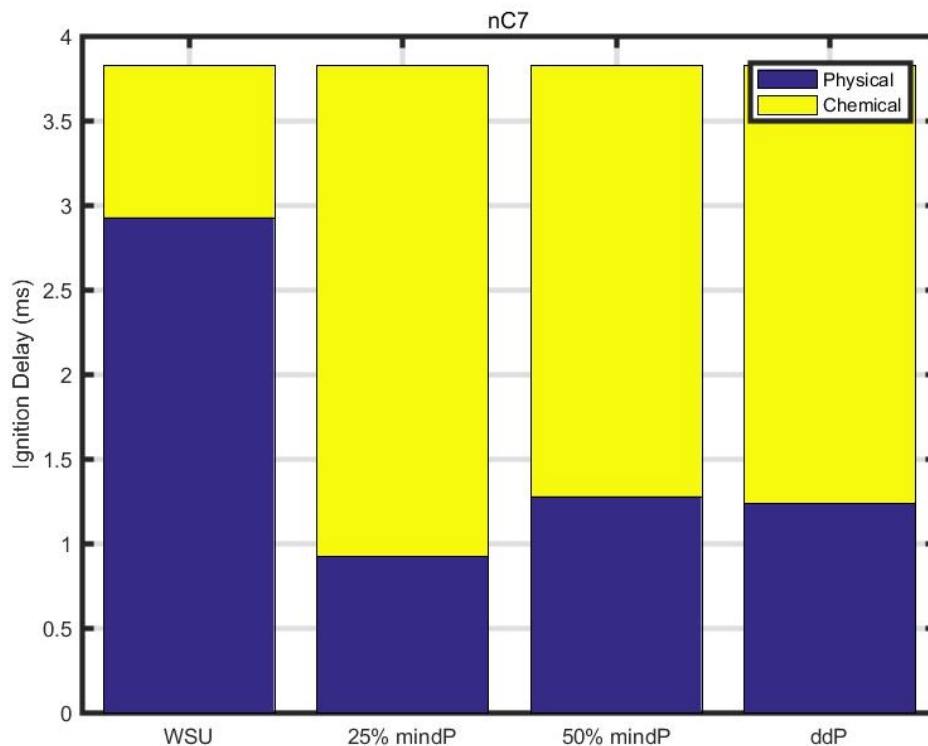


Figure 4-13: Separation methods for nC7.

As predicted, the WSU method creates a large physical delay compared to the chemical delay for the nC7 pure component fuel. The 25% mindP and mindP methods serve to create minimum and maximum values for possible physical and chemical separation points. It is important to note how the 50% mindP separation and ddP separation are almost identical meaning that they could both be viable for use as ignition delay separation methods. However, the ddP method is highly supported in previous literature while there is no scientific basis for the 50% mindP method, indicating that the ddP method serves as a better calculation method for the separation of the physical and chemical delays.

At low cetane values, a much larger difference is seen between the 50% mindP and ddP methods. Figure 4-14 shows the separation methods for the CN30

primary standard. It becomes more difficult to process the pressure trace into a smooth curve at low cetane values due to the inherent “rough running” characteristics of low cetane diesel fuels and as such it is much harder to isolate the point of inflection which is sensitive to the curvature of the pressure trace. While the ddP method proves useful with higher cetane fuels, more tedious analysis will be necessary to perfect the method for fuels with low cetane numbers.

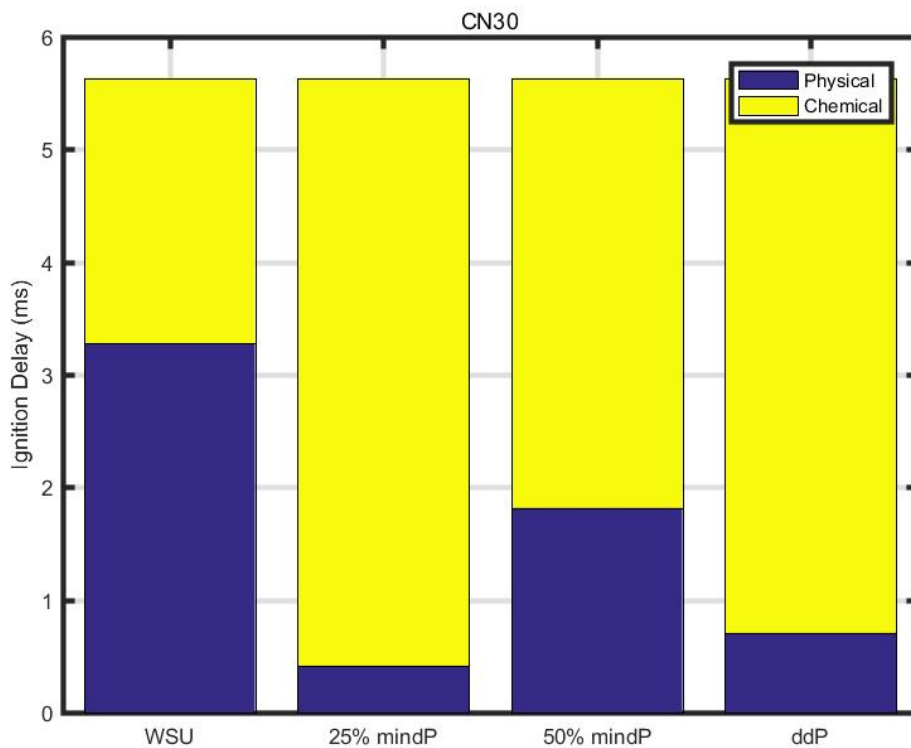


Figure 4-14: Separation methods for CN30.

With higher cetane fuels, the ddP method proves to be more consistent with the 50% mindP method indicating more reliable data. Figure 4-15 depicts the physical and chemical separation methods for nC16 pure component hexadecane. This fuel boasts the highest cetane value out of the entire plethora of analyzed fuels. The ddP and 50% mindP separation points are nearly the same for the nC16. The higher cetane



fuels produce more consistent pressure traces which are easier to fit to a curve. It then becomes easier to isolate the point of inflection as the required sensitivity for the ddP method to be effective is achieved.

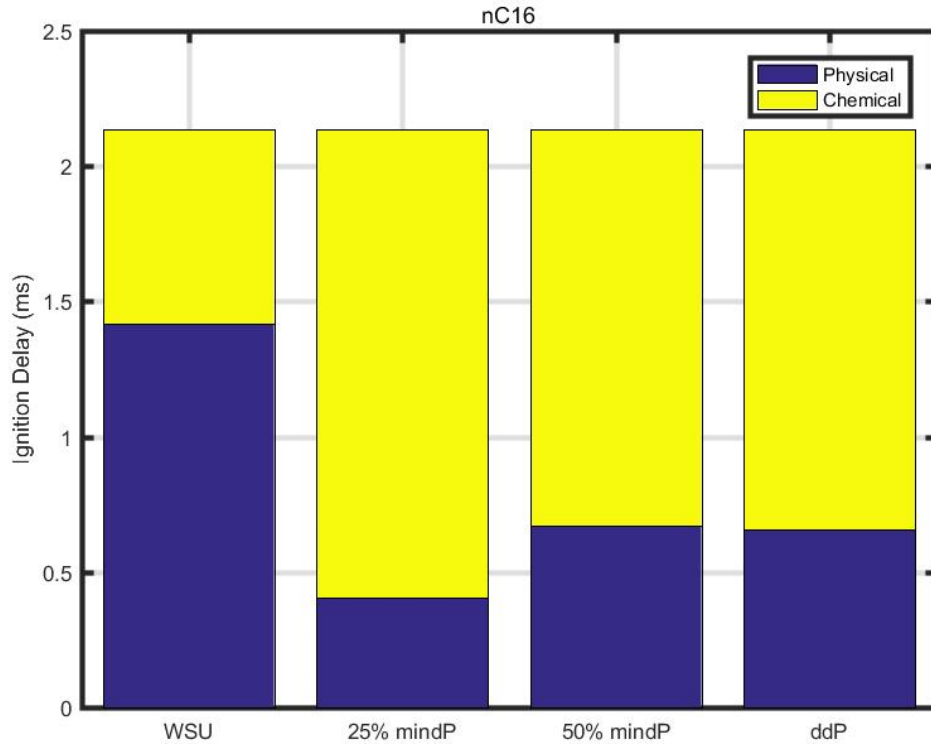


Figure 4-15: Separation methods for nC16.

Comparison of CHRR Ignition Delays with IQT Ignition Delays

An important objective of this research was to connect CHRR ignition delay analysis with the ignition delay results generated by the IQT. Cumulative heat release rate is a calculated quantity and is an important bridge between the IQT and actual diesel engine combustion.

CHRR ignition delays in percentages ranging from two percent to ten percent were calculated for nC7. In different words, as soon as the specified percentage of

CHRR has been achieved, the analysis marks that time as SOC. Figure 4-16 shows these ignition delays for nC7.

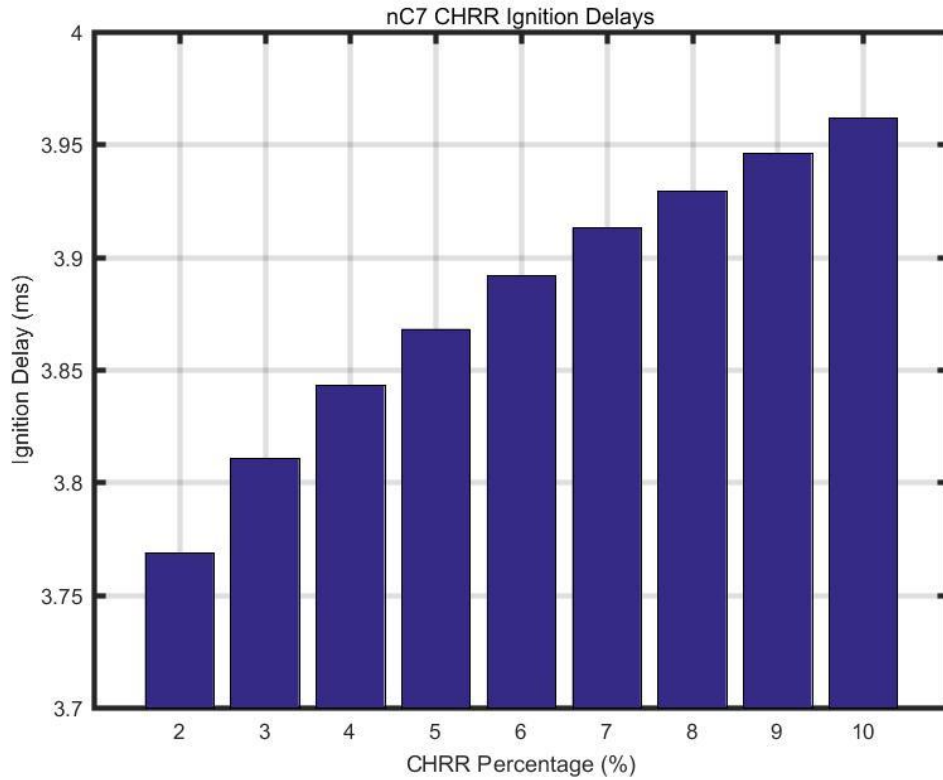


Figure 4-16: CHRR ignition delays for nC7.

A clear trend is seen from the data as ignition delay steadily increases as percentage CHRR increases, which is expected. From previous results, lower percentages of CHRR tended to produce large confidence intervals indicating a tradeoff between accurate ignition delay measurement and possible error in the results. From Figure 4-15, ignition delay varies from two to ten percent CHRR over a range of approximately 0.2 milliseconds which illustrates how little ignition delay changes versus change in percentage CHRR.

The nC7 CHRR results were also compared relative to the IQT ignition delay value. Figure 4-17 shows the same range of two percent CHRR to ten percent CHRR and how the results compared to the IQT generated ignition delay value.

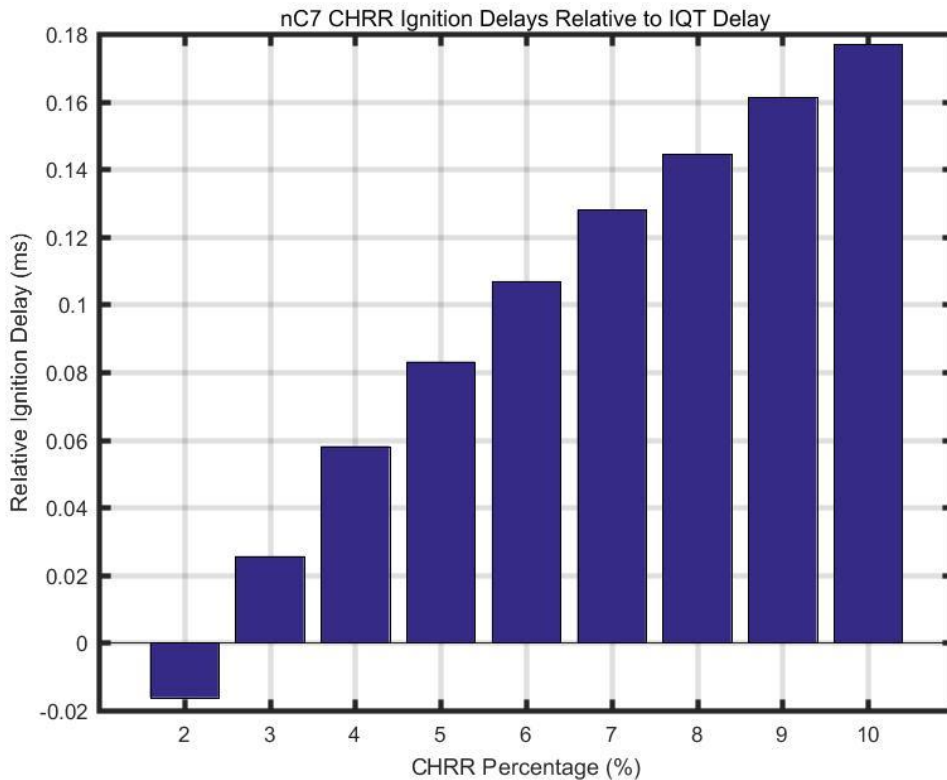


Figure 4-17: CHRR ignition delays for nC7 relative to IQT ignition delay.

The results from this analysis would indicate that the closest CHRR percentage to match the IQT produced ignition delay value would lie in between two and three percent. As previously mentioned, lower CHRR values produce large margins for error meaning it is difficult to accurately measure CHRR and produce the same ignition delay as the IQT. Possible results are that the IQT may understate the ignition delays which would result in higher generated derived cetane numbers when compared to actual cetane numbers given that the matching CHRR percentages are comparatively low. A curve fit analysis when calculating CHRR may allow for better

isolation of lower CHRR percentages but this could be at the expense of removing actual experimental data.

### Fuel Properties Analysis

A fuel properties analysis was completed to determine trends with regards to various property metrics and cetane value of the fuel. The three metrics were the modified droplet diameter, the Weber number, and the fuel break-up time. Equations were referenced from John Heywood's Internal Combustion Engine Fundamentals [18]. Modified droplet diameter was calculated with Equation 4-1 below:

$$D_d = \frac{2\pi\sigma}{\rho_g v_r^2} \quad (4-1)$$

Equation 4-1 determines modified droplet diameter, where  $\sigma$  is the liquid fuel surface tension,  $\rho_g$  is the gas density of the fuel, and  $v_r$  is the relative velocity between the liquid and the gas which is taken to be injection velocity [18]. This equation is minus a constant  $C$  and a wavelength number  $\lambda$  which were determined to not be of use when comparing the values of droplet diameter among several fuels. Droplet diameter is another important physical delay metric since smaller droplet diameters result in increased surface area which can reduce physical delays and aid fuel evaporation. Weber number was calculated with Equation 4-2 below:

$$We = \frac{\rho_l v_j^2 l}{\sigma} \quad (4-2)$$

Equation 4-2 calculates the dimensionless Weber number, where  $\rho_l$  is the density of the liquid fuel in kilograms per cubic meter,  $v_j$  is the injection velocity in meters per second,  $l$  is a characteristic length such as the droplet diameter in meters, and  $\sigma$  is the surface tension in Newtons per meter [18]. Fuel break-up time was calculated with Equation 4-3 below:

$$t_{break} = \frac{29\rho_l d_n}{(\rho_g \Delta p)^{1/2}} \quad (4-1)$$

Equation 4-3 determines break-up time in seconds, where  $\rho_l$  denotes the liquid density of the fuel in kilograms per cubic meter,  $d_n$  denotes the injector nozzle diameter in meters,  $\rho_g$  indicates the gas density of the fuel in kilograms per cubic meter, and  $\Delta p$  is the pressure drop across the nozzle in pascals [18]. Break-up time is a useful metric that determines how quickly a diesel fuel spray breaks and evaporates as it enters the combustion chamber and is highly related to the physical delay of the fuel.

It was necessary to determine the values of fuel properties like density and surface tension for each of the primary standards to complete the analysis. Given the specified mixture, the fuel properties could be determined with respect to the tables provided by the literature regarding the primary standards [19]. These fuels strengthened the data of variation between the IQT's produced derived cetane number

(DCN) and actual fuel cetane values. The calculated values of these properties can be seen on the spreadsheet attached as Appendix G.

The spreadsheet containing the calculation of these values for all fuels can be viewed in Appendix H. Figure 4-18 shows the calculated modified droplet diameters for each of the eight analyzed fuels. Figure 4-19 shows the same results with the DCN of each fuel replacing the name of the fuel. Figure 4-20 shows the calculated Weber number for each fuel where Figure 4-21 again shows the same data plotted against DCN. Figure 4-22 depicts the break-up time of each fuel and Figure 4-23 plots the results against DCN.

It is evident that there are no discernable trends in the modified droplet diameter, Weber number, or break-up time as the derived cetane number of the fuel increases. At first glance, this would indicate inconclusive results from the attempted fuel properties analysis of the eight analyzed fuels and the Tol-Hex blends. However, it is noteworthy to mention that reliable ignition delay data with discernable trends was gathered with the previously mentioned analysis with pressure and CHRR methods.

This would indicate that it is possible to conclude that the fuel properties are not as important in the ignition delay analysis as other factors namely the chemical composition of the fuel. It is also possible that a different physical property, such as bulk modulus, dominates the physical ignition delay of fuels while properties such as the break-up time, the modified droplet diameter, and the Weber number are less important.

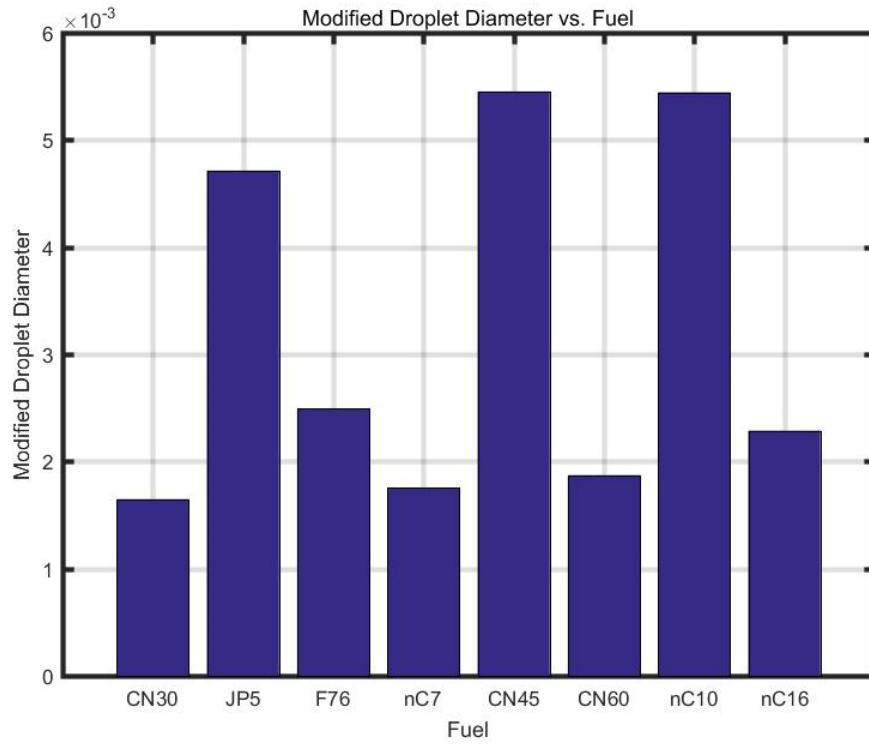


Figure 4-18: Modified droplet diameter for each of the analyzed fuels.

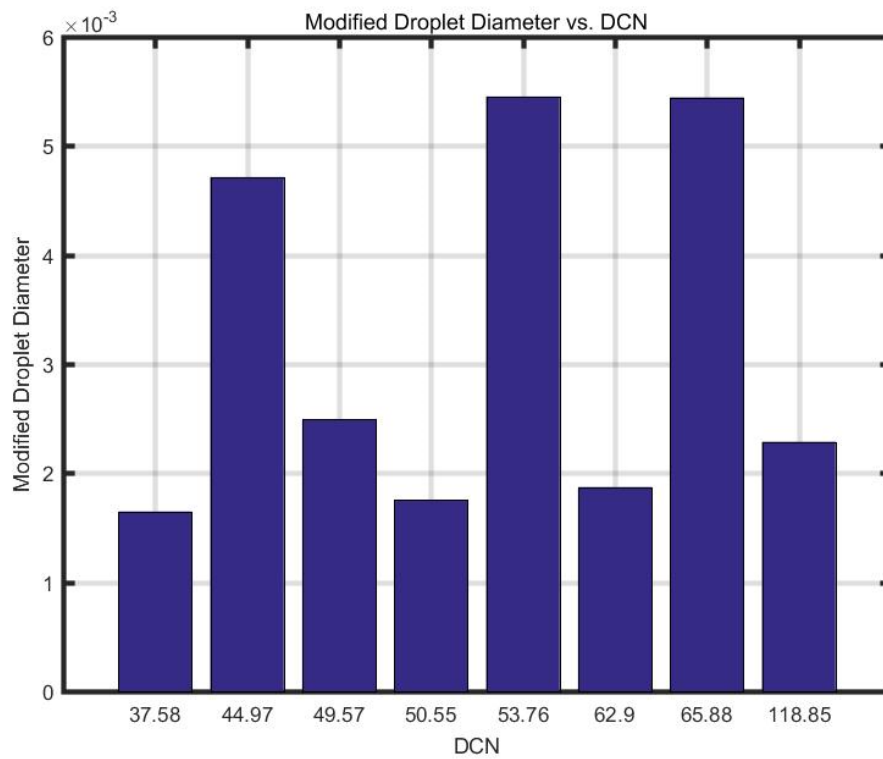


Figure 4-19: Modified droplet diameter plotted against the DCN of each fuel.

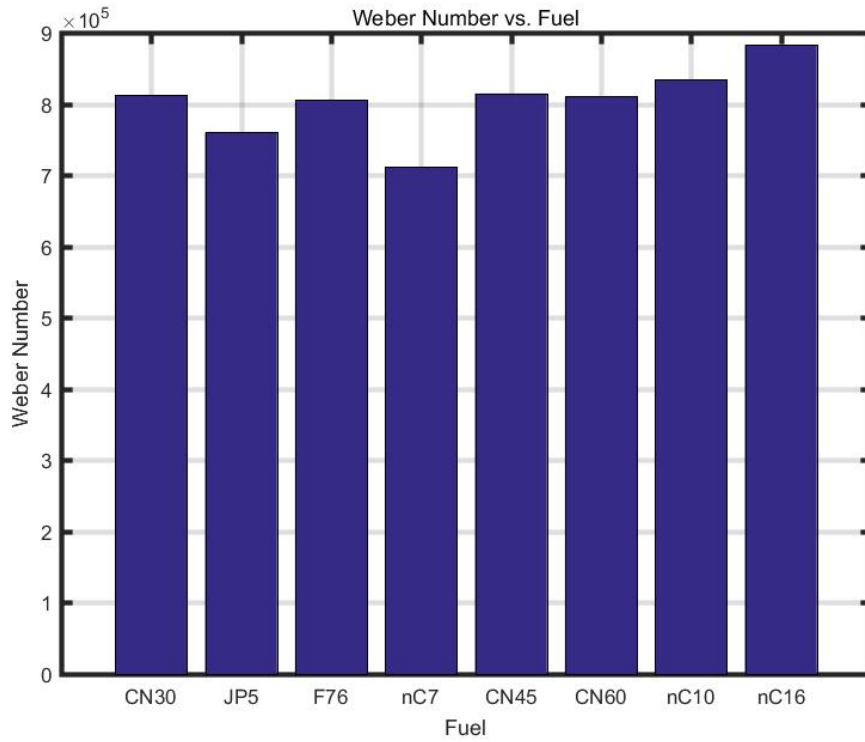


Figure 4-20: Weber number for each of the analyzed fuels.

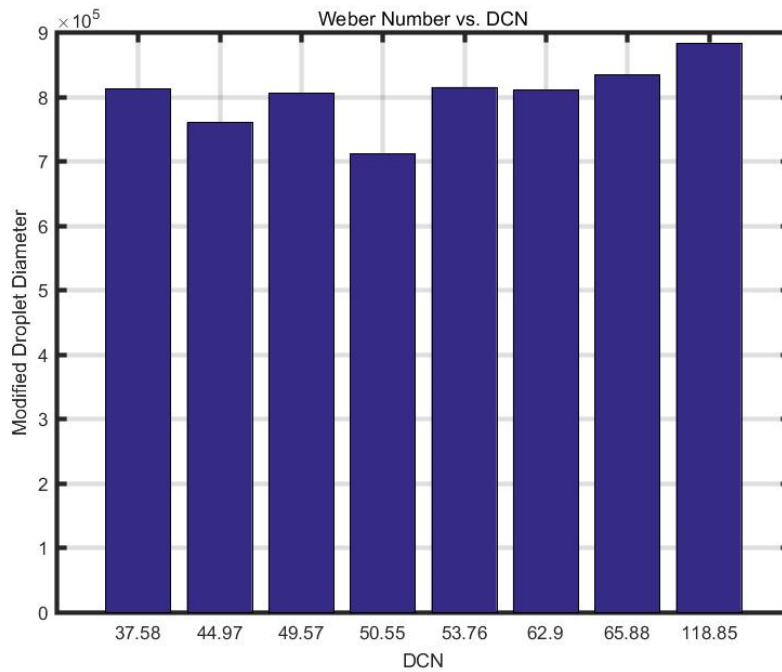


Figure 4-21: Weber number plotted against the DCN of each fuel.



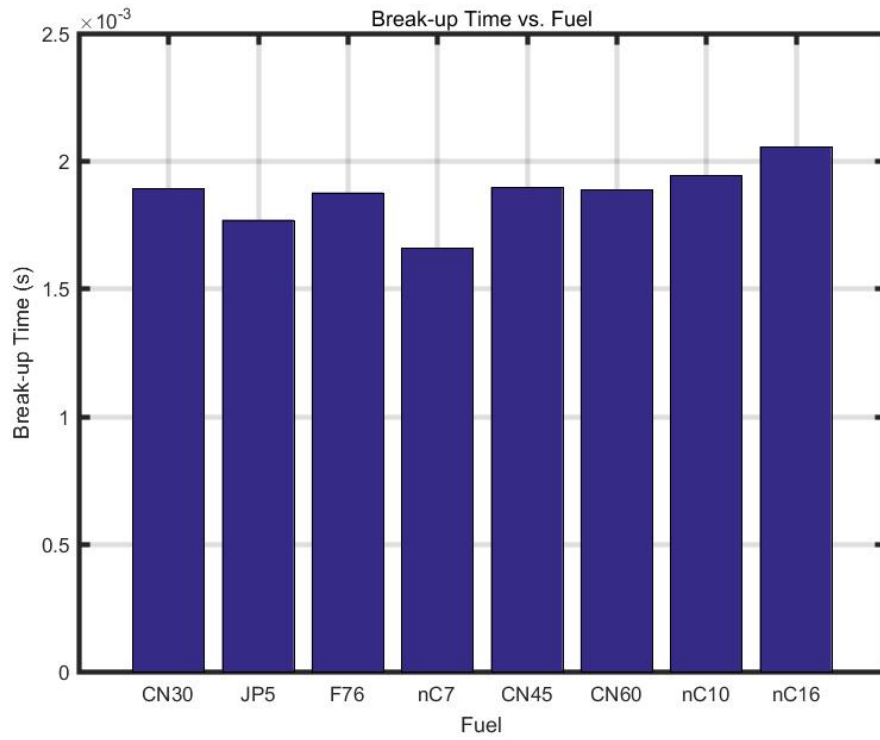


Figure 4-22: Break-up time for each of the analyzed fuels.

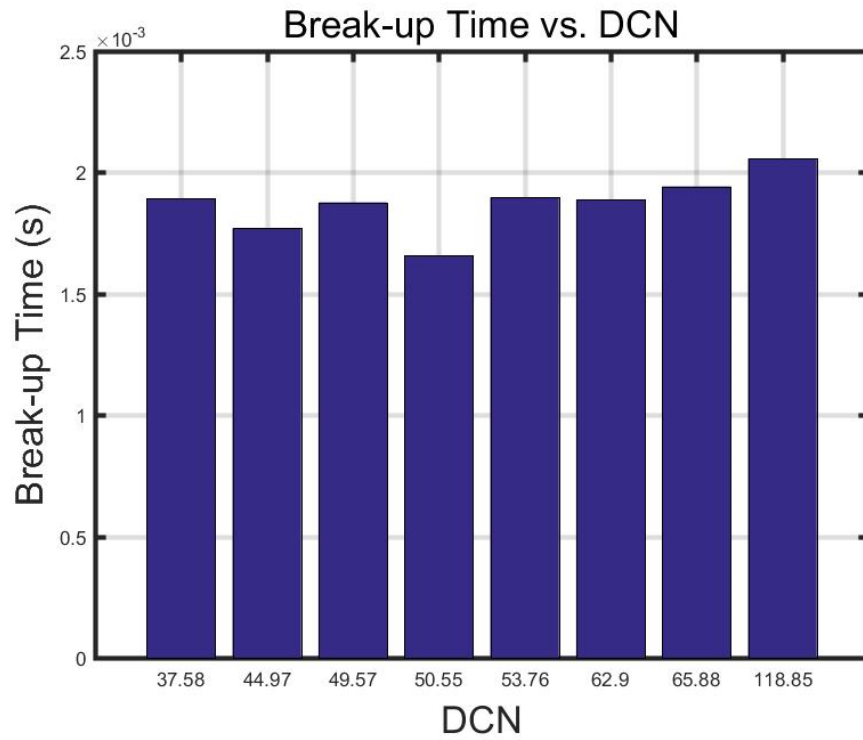


Figure 4-23: Break-up time plotted against the DCN of each fuel.

No conclusive results were determined from the fuel properties analysis contained within this research. Further experimentation is needed with properties such as bulk modulus to create a better comparison between the physical properties of diesel fuels and their behavior in the IQT and with calculated ignition delay metrics.

#### *Comparison of Results with Lawrence Livermore Kinetics*

Lawrence Livermore National Laboratory developed an advanced simulation used to determine the chemical ignition delay of combustion for various fuels. These Lawrence Livermore Kinetics (LLK) model the various reaction pathways for different temperatures are input into large simulations involving thousands of reactions which allows for an iterative calculation to determine the ignition delay of n-alkane hydrocarbons [20].

The ignition delays used as a comparison in this research were processed at the United States Naval Academy. Figure 4-23 shows the comparison between the ddP calculated chemical ignition delay and the chemical delay generated with LLK.

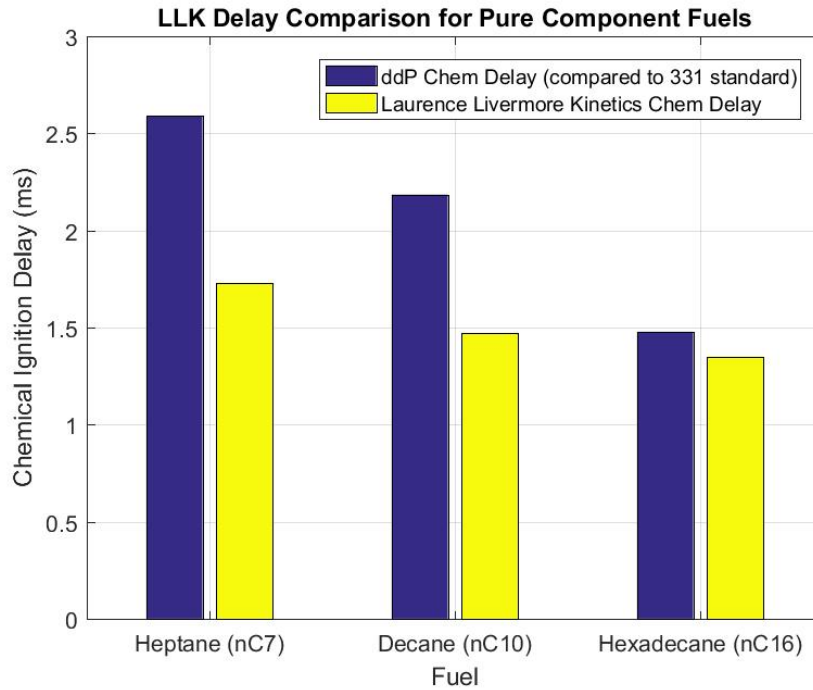


Figure 4-24: Comparison of ddP delay for pure component fuels with LLK.

From the results, it is seen that there is relative agreement between the ddP calculated delays and the LLK ignition delays. The LLK method tends to overstate the chemical delay compared to the experimental results gathered from the IQT data for the pure component fuels of nC7, nC10, and nC16. This comparison shows the remarkable advancement of kinetic theory attained by Lawrence Livermore National Laboratory and how future combustion processes may be modeled accurately without the need for costly experimentation.

LLK is based on the calibration fuel of nC7 and the other pure component fuels are then modeled based on only the difference in size of the molecules of the fuels [20]. This could explain the trend of the general increase in similarity between the LLK method and the ddP method as cetane number increases.

Figure 4-24 compares the ddP chemical delay results for the Tol-Hex blends against LLK calculations with select Tol-Hex blends.

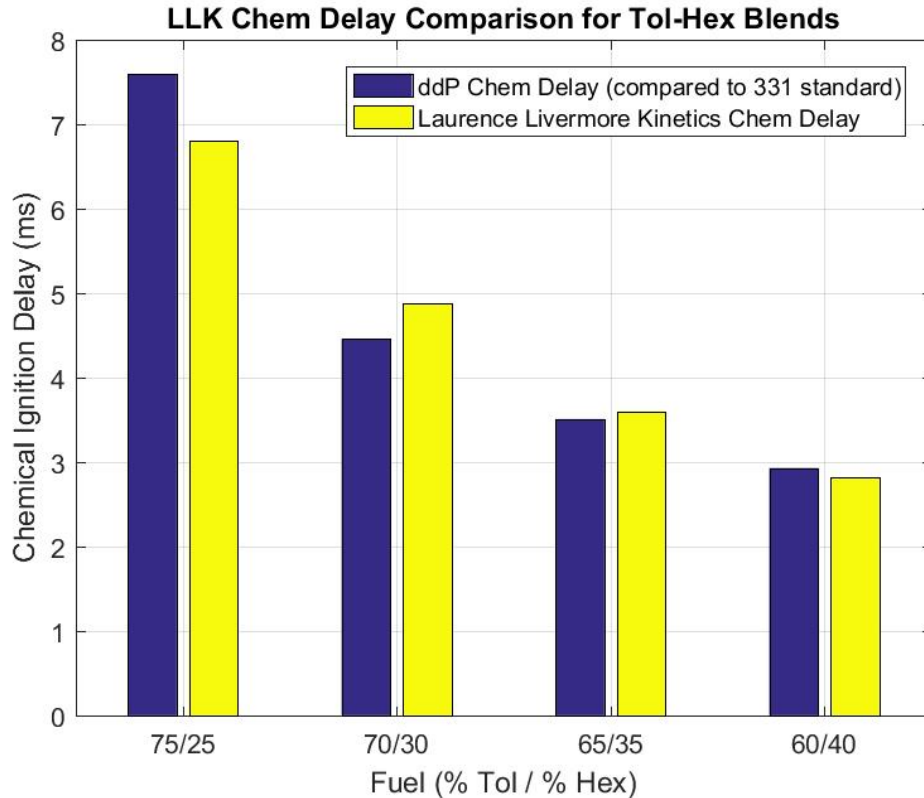


Figure 4-25: Comparison of ddP delay for Tol=Hex blends with LLK.

There is a high level of agreement between the LLK generated chemical delays and the ddP calculated chemical delays. The fuel properties vary little among different Tol-Hex blend percentages which could allow for greater accuracy in calculating ignition delays with LLK methods than using the same methods for pure component fuels.

As the properties vary more definitively with the pure component fuels of nC7, nC10, and nC16, the LLK model produces results that are not as precise to the ddP calculated results. More research is needed to determine the relationship between the LLK simulated reaction methods and the properties of the individual fuel.

## Chapter 5: Conclusions and Recommendations for Future Work

### Conclusions

The IQT is an effective means to analyze conventional fuels, pure component fuels, and various diesel and biodiesel blends with an acceptable amount of precision. Because testing in engines like the Combined Fuels Research single cylinder diesel engine can be costly and time consuming, the IQT can aid the U.S. Navy by allowing for the testing of newly developed biodiesels and biodiesel blends that will aid in the development of the Great Green Fleet.

The 331 psi standard most closely resembles the ignition delay produced by the IQT for each of the eight analyzed fuels and each of the seven Tol-Hex blends. Although the IQT ignition delay calculation method is not published, it can be concluded that the 331 psi pressure recovery method is calculation that the IQT uses to generate the ignition delay of the fuel.

There is a clear connection between ignition delay results produced with CHRR percentages and the ignition delays of the IQT which connects the IQT to real engine data. Lower percentages of CHRR lead to calculated ignition delay with large amounts of error which is expected given the inconsistency in early combustion and valve lift which introduces inherent error in the calculation of CHRR metrics.

The comparison between CHRR and the IQT for nC7 shows that the IQT calculates ignition delay at a corresponding percentage of CHRR that lies between two and three percent. Since the IQT calculates a DCN that is higher than the actual cetane value of the fuel, as proven by the primary standards in this research, the IQT

and the 331 psi standard may understate the actual ignition delay of the fuel for fuels with lower cetane values.

Analysis of the Tol-Hex blends show that at higher cetane values, the CHRR ignition delays and the IQT ignition delays show greater levels of agreement. The CHRR calculated data for the Tol-Hex blends has less error than the eight analyzed primary standards, pure component fuels, and conventional Navy diesel fuels.

The point of inflection (ddP) method is a calculation method that separates the physical and chemical ignition delays of both the analyzed fuels and the Tol-Hex blends with believable results and is supported by prior literature in the field. This makes the ddP method a better means of calculation the physical and chemical ignition delays than the 50% mindP method which does not hold scientific background. The ddP method does not overstate the physical ignition delay of the fuel as much as the WSU method in which the physical ignition delay dominates the chemical delay for the fuels analyzed in this research.

The fuel properties analysis proved inconclusive in this research but offered insight that the physical properties of modified droplet diameter, Weber number, and break-up time may not be as paramount in the ignition delays calculated by the IQT and by the MATLAB calculated delays as other fuel properties such as bulk modulus.

Lawrence Livermore Kinetics created similar chemical delays to the chemical delays calculated with the point of inflection method for the pure component fuels of nC7, nC10, and nC16. Very precise results were seen between the LLK chemical delays and the ddP chemical delays for the Tol-Hex blends. Since the Tol-Hex blends have little variation in physical properties, it can be inferred that the LLK methods are

accurate for fuels with similar physical properties but require adjustment for the pure component fuels in which they only vary their reaction theory based on size of the fuel molecule.

### *Recommendations for Future Work*

For future research, a detailed fuel properties analysis is needed to determine which physical properties most significantly impact the ignition delay of diesel fuels. This will aid the U.S. Navy since biodiesels can be analyzed based on specific fuel properties and the similarity between fuels can be analyzed with fewer steps. Additionally, the physical properties might aid in the connection between Lawrence Livermore Kinetics and the chemical delays calculated with the point of inflection method. Fuel properties can also be used to hone the results produced by the IQT and may account for the calculation of a higher-than-normal DCN by the device.

Further research is needed to develop a cumulative heat release rate analysis that shrinks the amount of error that is present when calculation ignition delays with lower percentages of heat release rate. This will aid in a more direct connection between the ignition delays calculated with the IQT and the combustion characteristics determined with a heat release analysis for an actual diesel engine.

## Appendix A: Fuel properties for F-76 and JP-5.

### Conformance to F-76 Chemical and Physical Properties per MIL-DTL-16884N

Test (Units)	Method	Minimum	Maximum	Neat CHCD-76	F-76
Appearance at 25°C	D4176	Clear & Bright		Clear & Bright	Clear & Bright
Demulsification at 25°C (minutes)	D1401		10	3	3
Density at 15°C (kg/m <sup>3</sup> )	D4052	800	876	819	833
Distillation	D86				
10% Recovered (°C)		Report		240	200
50% Recovered (°C)		Report		271	249
90 % Recovered (°C)			357	289	324
End Point (°C)			385	298	353
Residue + Loss (volume %)			3.0	1.6	1.7
Cloud Point (°C)	D5773		-1	-8	-10
Color	D6045		3	<0.5	1.3
Flash Point (°C)	D93	60.0		96	66
Particulate Contamination (mg/L)	D5452		10	0	1
Pour Point (°C)	D5949		-6	-12	-21
Viscosity at 40°C (mm <sup>2</sup> /s)	D445	1.7	4.3	2.7	2.3
Acid Number (mg KOH/g)	D974		0.30	0.06	0.01
Ash (mass %)	D482		0.005	0.000	0.000
Aromatics (mass %)	D6591	8.1 <sup>1</sup>		11.5	27.6
Carbon Residue on 10% Bottoms (mass %)	D524		0.20	0.05	0.1
Copper Strip Corrosion at 100 °C	D130		1	1a	1a
Hydrogen Content (mass %)	D7171	12.5		14.0	13.3
Ignition Quality	D6890	42		62.6	48.9
Storage Stability, Total Insolubles (mg/100mL)	D5304		3.0	0.6	2
Sulfur Content					
XRF(mass %), or UV Fluorescence (mg/kg)	D4294		0.0015 <sup>2</sup>	<0.0001	0.0515
	D5453		15	-	-
Trace Metals (mg/kg)	D7111				
Ca			1.0	0.0	0.0
Pb			0.5	0.0	0.1
Na + K			1.0	0.3	0.5
V			0.5	0.0	0.0
Lubricity <sup>3</sup> (µm)	D6079		460	430	350
Surface Tension (dyne/cm) <sup>4</sup>	D1331			28.5	28.4
Existent Gum (mg/100 mL) <sup>4</sup>	D381			2.2	39.2

\* CHCD-76 - Catalytic Hydrothermal Conversion Diesel Fuel



**Conformance to JP-5 Chemical and Physical Properties per MIL-DTL-16884N**

<b>Test (Units)</b>	<b>Method</b>	<b>Minimum</b>	<b>Maximum</b>	<b>CHCJ-5</b>	<b>JP-5</b>
Color, Saybolt	D6045	Report		>30	19
Total Acid Number (mgKOH/g)	D3242		0.015	0.001	0.003
Aromatics (volume %)	D1319	8.0 <sup>a</sup>	25.0	9.5	19.2
Sulfur, Mercaptan (mass %) or, Doctor Test	D3227		0.002	0.000	0.000
	D4952		Negative	-	-
Sulfur, Total XRF (mass %), or UV Fluorescence (mg/kg)	D4294		0.20	0.0009	0.14
	D5453		2000	-	-
Distillation	D86				
Initial (°C)			Report	176	177
10% Recovered (°C)			205	186	190
20% Recovered (°C)			Report	191	195
50% Recovered (°C)			Report	200	207
90 % Recovered (°C)			Report	222	235
End Point (°C)			300	236	253
Residue (volume %)			1.5	1.3	1.4
Loss (volume %)			1.5	0.1	0.1
Flash Point (°C)	D93	60.0		64	61
Density at 15 °C (kg/L)	D4052	0.788	0.845	0.803	0.8048
Freezing Point (°C)	D5972		-46	-52	-50
Viscosity at -20 °C (mm <sup>2</sup> /s)	D445		8.5	4.4	4.8
Net Heat of Combustion (MJ/kg)	D4809	42.6		43.2	42.7
Ignition Quality, Derived Cetane Number	D6890	Report		49.3	46.6
Hydrogen Content (mass %)	D7171	13.4		14.0	13.9
Smoke Point (mm)	D1322	19.0		30.0	23.6
Copper Strip Corrosion, two hours at 100 °C	D130		1	1a	1a
Thermal stability					
Pressure Drop (mm Hg)	D3241		25	0	0
Heater Tube Deposit			<3	1	<1
Existent Gum (mg/100 mL)	D381		7.0	0.8	15.6
Particulate Matter (mg/L)	D5452		1.0	0.5	0.4
Filtration Time (minutes)	MIL-DTL- 5624V		15	6	6
Micro Separometer Rating	D7224	<sup>b</sup>		96	69
Fuel System Icing Inhibitor (volume %)	D5006	0.10	0.15	0.00	0.13
Lubricity- BOCLE (mm)				0.57	0.57
Lubricity- HFRR (µm)	D6079			670	740
Surface Tension (dyne/cm)	D1331			27.5	27.6
Viscosity at 40°C (mm <sup>2</sup> /sec)	D445			1.3	1.4

\* CHCJ-5 - Catalytic Hydrothermal Conversion Jet Fuel

## Appendix B: Ignition delay analyzer code for nC7 run.

```
%this program evaluates SOI and SOC in constant volume spray vessel
%L.J. Hamilton 12-19-2014

%edits include filtering the initial pressure drop response in order to
%analyze 25%, 50%, and the ddP inflection point of the pressure trace in
%order to find delay times corresponding to the physical and chemical
%delays of the fuel
%J.L. Mendelson 3-23-2016

clear all
format compact
close all
clc

%inputs

% data=xlsread('Run658_Inj2bx.xlsx');
% time = data(:,1);
% Pvesse1 = data(:,2)*101.325/14.7; %kPa
% lift = data(:,3);

% file='run1415Inj27.txt';
%file='Run653Inj1.txt';
% file='F76Run1400Inj3.txt'; %3, 18, 29
% file='JP5Run1340Inj3.txt'; %3,20,29
%file='HeptaneRun1440Inj2.txt'; % 2,21,31
%file='6040Run654_Inj5.txt'; % 5
%file='6535Run658_Inj5.txt'; % 5
%file='7030Run653_Inj6.txt'; % 6
%file='7525Run655_Inj5.txt'; % 5
%file='7228Run664_Inj6.txt'; % 6
%load(file)
% time=run1408_Inj29(:,1);
% Pvesse1=run1408_Inj29(:,2)*101.325/14.7;
% lift=run1408_Inj29(:,3);

for k=1:32
    k
    % have all 32 for CN30, 45 and 60
    num=1592; %1597 CN60 (DCN 62.9), 1595 CN30 (DCN 37.6), 1598 CN45 (DCN 50.6)
    %data=load(file)
    filename = strcat('Run',num2str(num),'_Inj',num2str(k),'.pre'); %change below also
    data=importdata(filename);
    data=csvread(filename,2,0);

    time=data(:,1);
    Pvesse1=data(:,2)*101.325/14.7;
    lift=data(:,3);

    deltime = (time(2)-time(1))/1e3; %time between samples (sec)

    P1 = mean(Pvesse1(100:150)); %kPa - initial air pressure of spray vessel
    T1 = 550 + 273.15; %K, initial air temp in spray vessel
```

```

V1 = 0.21/1000; %m^3 - volume of spray vessel
Rbar = 8.314; %kJ/kmol-K
Z = 1; %compressibility factor
phi = 0.8; %fuel-air equivalence ratio
M = 28.97; %molar mass of air
R = Rbar/M;

%calculations
Mair = P1*V1/Z/R/T1; %kg
Tair = Pvessel*V1/Mair/Z/R;

Cpbar = 28.11 + 0.1967e-2*Tair + 0.4802e-5*Tair.^2 - 1.966e-9*Tair.^3;
Cvbar = Cpbar-Rbar;
Cv = Cvbar/M; %kJ/kg-K

CuHRR = (1/deltime)*Mair*Cv.*(Tair-T1); %kw
IHRR = diff(CuHRR); %cumulative heat release rate

%creating a new set of pressure values to only include the initial pressure
%drop without the large pressure increases due to combustion
maxP = max(Pvessel); %defining the maximum pressure reading
maxcut = P1+(0.1*(maxP-P1)); %determining the cutoff value for the smooth pressure signal
cutloc = min(find(Pvessel > maxcut)); %determining the position of the cutoff value
Pvessel_drop = Pvessel(1:cutloc); %creating a new matrix of only the pressure drop signal

% using a curve fit to filter the initial pressure data and smooth the response
time2 = time(1:size(Pvessel_drop));
COEF = polyfit(time2,Pvessel_drop,8);
Pvessel_drop_fit = polyval(COEF,time2);

dPvessel = diff(Pvessel_drop_fit); %1st derivative of pressure
ddPvessel = diff(Pvessel_drop_fit,2); %2nd derivative of pressure
cumsumdP = cumsum(dPvessel);
cumsumddP = cumsum(ddPvessel);
time3 = time(1:size(dPvessel));
time4 = time(1:size(ddPvessel));

%finding SOI based on 10% of max fp
[SOI_loc,SOI_y] = min(find(lift > 0.05*max(lift)));
SOI = time(min(find(lift > 0.05*max(lift))));

%SOI and IGD
%based on pressure recovery to 310 psi
press=Pvessel*14.7/101.325;
SOC310 = time(max(find(press < 310)));
IGD310 = SOC310 - SOI;
%based on pressure recovery to 331 psi
prsabv=331; %138 kPa above initial = 21 psi per D6890
SOC331 = time(max(find(press < prsabv)));
IGD331 = SOC331 - SOI;
%based on 2% CumHRR
SOC2CuHRR = time(max(find(CuHRR < 0.02*max(CuHRR))));
IGD2CuHRR = SOC2CuHRR - SOI;
%based on 3% CumHRR
SOC3CuHRR = time(max(find(CuHRR < 0.03*max(CuHRR))));
IGD3CuHRR = SOC3CuHRR - SOI;

```

```

%based on 4% CumHRR
SOC4CuHRR = time(max(find(CuHRR < 0.04*max(CuHRR))));
IGD4CuHRR = SOC4CuHRR - SOI;
%based on 5% CumHRR
SOC5CuHRR = time(max(find(CuHRR < 0.05*max(CuHRR))));
IGD5CuHRR = SOC5CuHRR - SOI;
%based on 6% CumHRR
SOC6CuHRR = time(max(find(CuHRR < 0.06*max(CuHRR))));
IGD6CuHRR = SOC6CuHRR - SOI;
%based on 7% CumHRR
SOC7CuHRR = time(max(find(CuHRR < 0.07*max(CuHRR))));
IGD7CuHRR = SOC7CuHRR - SOI;
%based on 8% CumHRR
SOC8CuHRR = time(max(find(CuHRR < 0.08*max(CuHRR))));
IGD8CuHRR = SOC8CuHRR - SOI;
%based on 9% CumHRR
SOC9CuHRR = time(max(find(CuHRR < 0.09*max(CuHRR))));
IGD9CuHRR = SOC9CuHRR - SOI;
%based on 10% CumHRR
SOC10CuHRR = time(max(find(CuHRR < 0.10*max(CuHRR))));
IGD10CuHRR = SOC10CuHRR - SOI;
%based on min delP integration
[mindP, locdP] = min(cumsumdP);
SOCminintdP = time(locdP);
IGDminintdP = SOCminintdP - SOI;
%based on 25% mindP
cumsumdPcut = cumsumdP(SOI_loc+10:end);
time_cumsumdPcut = time3(SOI_loc+10:end);
mindP25 = time_cumsumdPcut(min(find(cumsumdPcut < 0.25*mindP)));
IGDmindP25 = mindP25 - SOI;
check25 = isempty(IGDmindP25);
if check25 == 1
    IGDmindP25 = IGDmindP25_past;
end
IGDmindP25_past = IGDmindP25;
%based on 50% mindP
mindP50 = time_cumsumdPcut(min(find(cumsumdPcut < 0.5*mindP)));
IGDmindP50 = mindP50 - SOI;
check50 = isempty(IGDmindP50);
if check50 == 1
    IGDmindP50 = IGDmindP50_past;
end
IGDmindP50_past = IGDmindP50;

%based on point of inflection (ddP~=0)
ddPvesse1cut = ddPvesse1((SOI_loc+10):end); %limiting the region of interest for point of inflection to after
SOI, 10 positions added to remove initial pressure fluctuations
timeddP = time4((SOI_loc+10):end);
s_ddP = sign(ddPvesse1cut); %creating a list of sign values for the truncated ddP data
diffsign = diff(s_ddP);
zeros = find(diffsign == 2 | diffsign == -2);
%returns inflection point locations
POI = timeddP(zeros(1));
IGDDDP = POI-SOI;

% derived cetane number calculation

```

```

dcn = 4.46 + (186.6/IGD331);
if (IGD331>6.5 | IGD331<3.1)
    dcn = 83.99*(IGD331-1.512)^- .658+3.547% ID<3.1 and ID>6.5
end

figure(1)
plot(time,10e4*lift,'m')
hold on
grid
plot(time,Pvessel,'b')
plot(time2,Pvessel_dropfit,'r')
%plot(time(1:length(dPvessel)),10*dPvessel,'g')
%plot(time(1:length(ddPvessel)),10*ddPvessel,'g')
%plot(time,Tair,'r')
hold off
legend('lift','pressure','smooth pressure','Location','northwest');
ylabel('Pressure (kPa)');
xlabel('Time (ms)');
% text(4,14000,['\fontsize{12}IGD310 = ',num2str(IGD310),' msec'])
% text(4,13000,['\fontsize{12}IGD331 = ',num2str(IGD331),' msec'])
% text(4,12000,['\fontsize{12}IGD5CuHRR = ',num2str(IGD5CuHRR),' msec'])
% text(4,11000,['\fontsize{12}IGD10CuHRR = ',num2str(IGD10CuHRR),' msec'])
% text(4,10000,['\fontsize{12}IGDminintdP = ',num2str(IGDminintdP),' msec'])
% text(4,9000,['\fontsize{12}IGDmindP25 = ',num2str(IGDmindP25),' msec'])
% text(4,8000,['\fontsize{12}IGDmindP50 = ',num2str(IGDmindP50),' msec'])
% text(4,7000,['\fontsize{12}IGDddP = ',num2str(IGDDDP),' msec'])
% text(4,6000,['\fontsize{12}DCN = ',num2str(dcn)])
% text(4,5000,['\fontsize{12}DCN with ', num2str(prsabv)])
title(filename)
plotfixer;

figure(2)
plot(time-2,10e4*lift,'m')
hold on
grid
plot(time-2,CuHRR/20,'r')
plot(time(1:length(IHRR))-2,IHRR/10,'k')
axis([0 8 -1000 7000])
hold off
legend('lift','CuHRR/20','IHRR','Location','northwest');
text(3.5,6500,['\fontsize{12}IGD310 = ',num2str(IGD310),' msec'])
text(3.5,6000,['\fontsize{12}IGD331 = ',num2str(IGD331),' msec'])
text(3.5,5500,['\fontsize{12}IGD5CuHRR = ',num2str(IGD5CuHRR),' msec'])
text(3.5,5000,['\fontsize{12}IGD10CuHRR = ',num2str(IGD10CuHRR),' msec'])
text(3.5,4500,['\fontsize{12}IGDminintdP = ',num2str(IGDminintdP),' msec'])
text(3.5,4000,['\fontsize{12}DCN = ',num2str(dcn)])
text(3.5,3500,['\fontsize{12}DCN with ', num2str(prsabv)])
title(filename)
xlabel('Time (ms)')
ylabel('Heat Release Rate (kw)')
plotfixer;

filename2 = strcat(num2str(num),'_',num2str(k),'m.mat');
save(filename2)
end

```

```

pressure_master = [];
for k=1:32
    filename2 = strcat(num2str(num),'_',num2str(k),'m.mat');
    load(filename2)
    igd_331(k)=IGD331;
    igd_cum10(k)=IGD10CuHRR;
    igd_cum5(k)=IGD5CuHRR;
    igd_cum2(k)=IGD2CuHRR;
    igd_cum3(k)=IGD3CuHRR;
    igd_cum4(k)=IGD4CuHRR;
    igd_cum6(k)=IGD6CuHRR;
    igd_cum7(k)=IGD7CuHRR;
    igd_cum8(k)=IGD8CuHRR;
    igd_cum9(k)=IGD9CuHRR;
    igd_mndp(k)=IGDminintdP;
    igd_310(k)=IGD310;
    igd_mindP25(k)=IGDmindP25;
    igd_mindP50(k)=IGDmindP50;
    igd_ddP(k)=IGDDDP;
    physdelay_mindP25(k)= IGDmindP25;
    chemdelay_mindP25(k)= IGD331-IGDmindP25;
    physdelay_mindP50(k)= IGDmindP50;
    chemdelay_mindP50(k)= IGD331-IGDmindP50;
    physdelay_ddP(k)= IGDDDP;
    chemdelay_ddP(k)= IGD331-IGDDDP;
    physdelay_wsu(k)= IGDminintdP;
    chemdelay_wsu(k)= IGD331-IGDminintdP;

end

test=1:32;
wsu_ratio = chemdelay_wsu./physdelay_wsu;
mindP25_ratio = chemdelay_mindP25./physdelay_mindP25;
mindP50_ratio = chemdelay_mindP50./physdelay_mindP50;
ddP_ratio = chemdelay_ddP./physdelay_ddP;
figure(3)
plot(test,igd_331,'gx')
hold on
plot(test,igd_cum10,'bo')
plot(test,igd_cum5,'kd')
plot(test,igd_mndp,'mx')
plot(test,igd_310,'co')
plot(test,igd_mindP25,'ms')
plot(test,igd_mindP50,'ro')
plot(test,igd_ddP,'b*')
xlabel('test #')
ylabel('IGD (msec)')
legend('331','Cum10','Cum5','MindP','310','mindP25','mindP50','ddP');
name=strcat('IQT Run#',num2str(num))
title(name)
plotfixer;

%creating the plot for chem/phys delay ratio
figure(4)
plot(test,wsu_ratio,'bs')
hold on

```

```

plot(test,mindP25_ratio, 'kx')
plot(test,mindP50_ratio, 'g*')
plot(test,ddP_ratio,'ko')
xlabel('test #')
ylabel('Chemical Delay / Physical Delay (ms)')
legend('wsu','mindP25','mindP50','ddP')
title(name)
plotfixer;

% calculating average values in ms for chemical and physical delays
mnphyswsu = mean(physdelay_wsu);
mnchemwsu = mean(chemdelay_wsu);
mnphysmindp25 = mean(physdelay_mindP25);
mnchemmindp25 = mean(chemdelay_mindP25);
mnphysmindp50 = mean(physdelay_mindP50);
mnchemmindp50 = mean(chemdelay_mindP50);
mnphysddP = mean(physdelay_ddP);
mnchemddP = mean(chemdelay_ddP);

width1 = 0.5; % bar graph - 1st bar width
width2 = 0.25; % 2nd bar width

%bar graph depicting chemical vs. physical delay for each method in ms
chem_tot = [mnchemwsu, mnchemmindp25, mnchemmindp50, mnchemddP];
phys_tot = [mnphyswsu, mnphysmindp25, mnphysmindp50, mnphysddP];
x_methods = {'wsu','mindP25','mindP50', 'ddP'};
figure(5)
bar(chem_tot,width1,'FaceColor',[0.2 0.2 0.5]);
set(gca, 'XTick', 1:5, 'XTickLabel', x_methods);
hold on;
bar(phys_tot,width2,'FaceColor',[0 0.7 0.7]);
title(name)
grid on
xlabel('Separation Method')
ylabel('Ignition Delay (ms)')
plotfixer;
legend('Chemical Delays','Physical Delays');

%printing statistical data
mn331=mean(igd_331)
std331=std(igd_331)
mncum5=mean(igd_cum5)
stdcum5=std(igd_cum5)
mncum10=mean(igd_cum10)
stdcum10=std(igd_cum10)
mn310=mean(igd_310)
std310=std(igd_310)
mnmndp=mean(igd_mndp)
stdmndp=std(igd_mndp)
mnmin25=mean(igd_mindP25)
stdmin25=std(igd_mindP25)
mnmin50=mean(igd_mindP50)
stdmin50=std(igd_mindP50)
mnddp=mean(igd_ddP)
stdddp=std(igd_ddP)
mnwsuratio=mean(wsu_ratio)

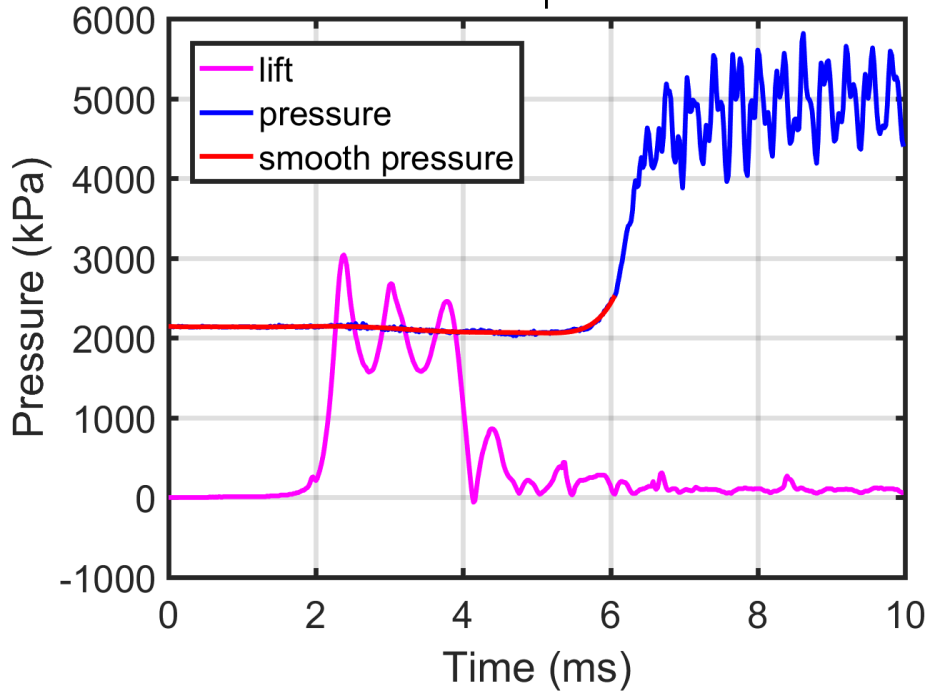
```

```
mnmin25ratio=mean(mindP25_ratio)
mnmin50ratio=mean(mindP50_ratio)
%save('cn30iqtm')
```

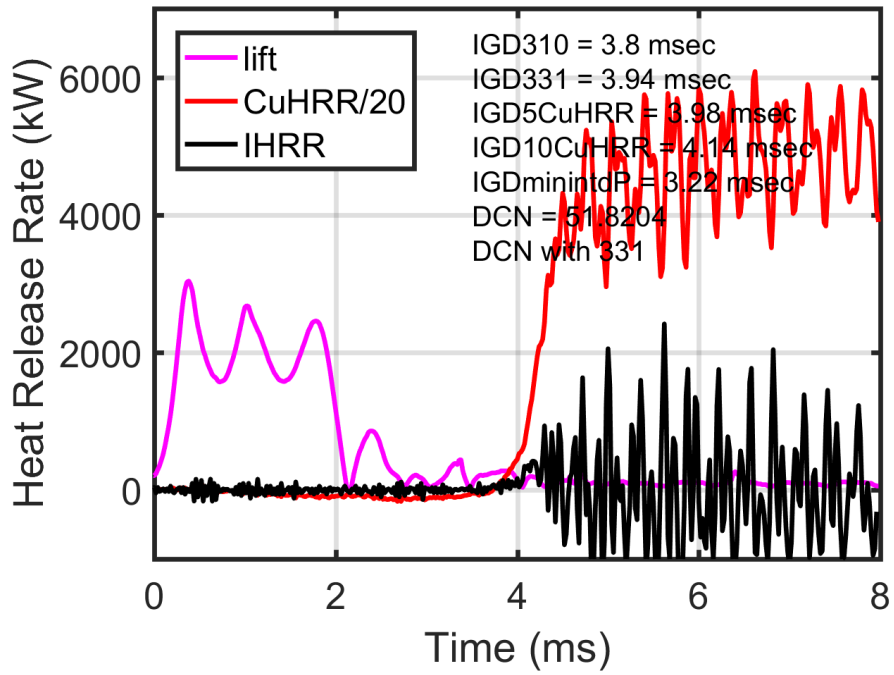
```
mn331 =
    3.8281
std331 =
    0.0916
mncum5 =
    3.8681
stdcum5 =
    0.0883
mncum10 =
    3.9619
stdcum10 =
    0.0905
mn310 =
    3.6219
std310 =
    0.1067
mnmdp =
    2.9275
stdmdp =
    0.3823
mnmin25 =
    0.9225
stdmin25 =
    0.0978
mnmin50 =
    1.2775
stdmin50 =
    0.1003
mnmdp =
    1.2369
stdmdp =
    0.0920
mnwsuratio =
    0.3337
mnmin25ratio =
    3.1912
mnmin50ratio =
    2.0109
```

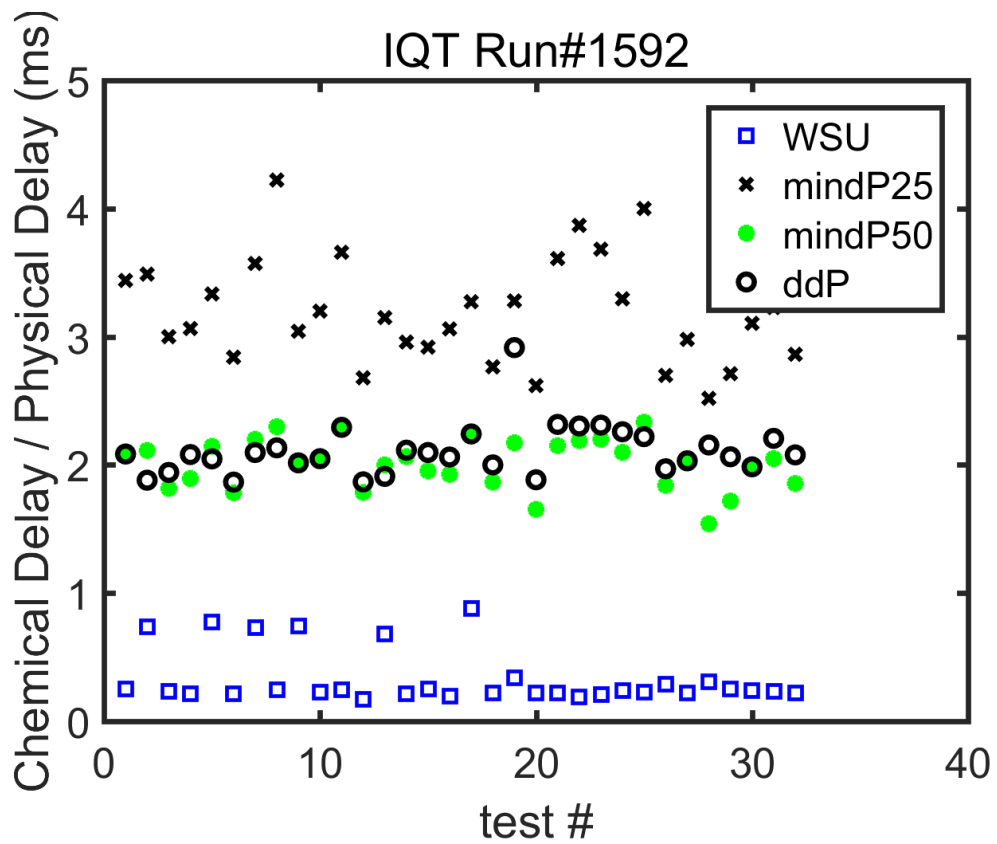
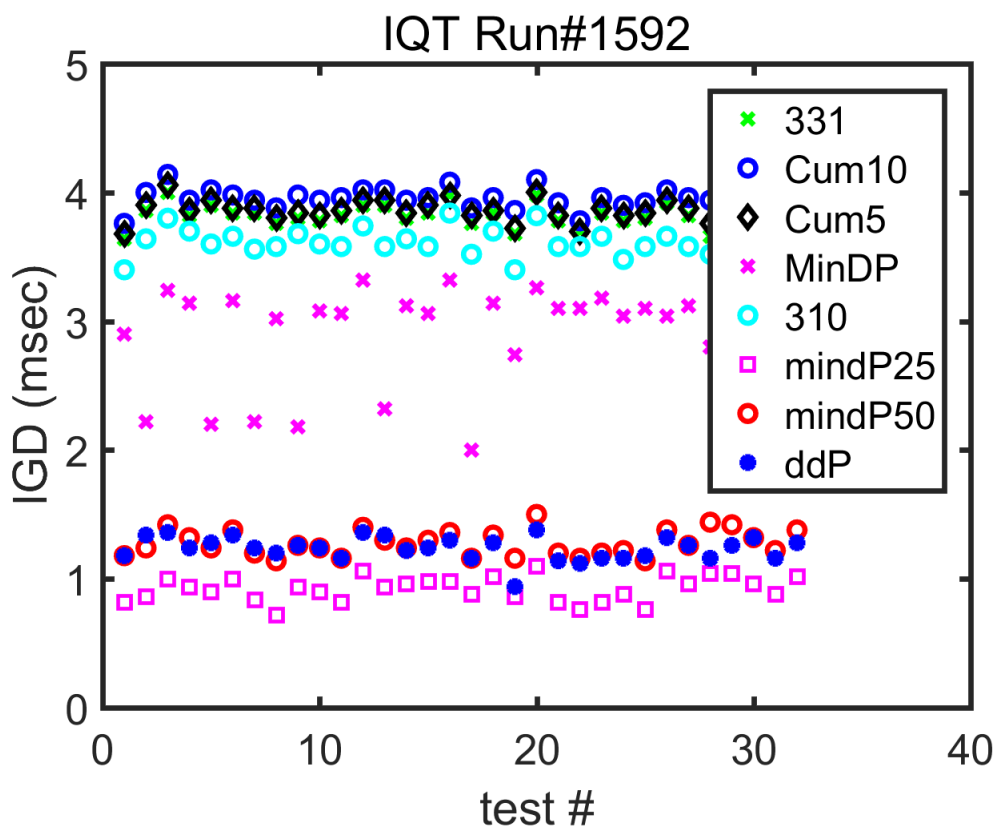


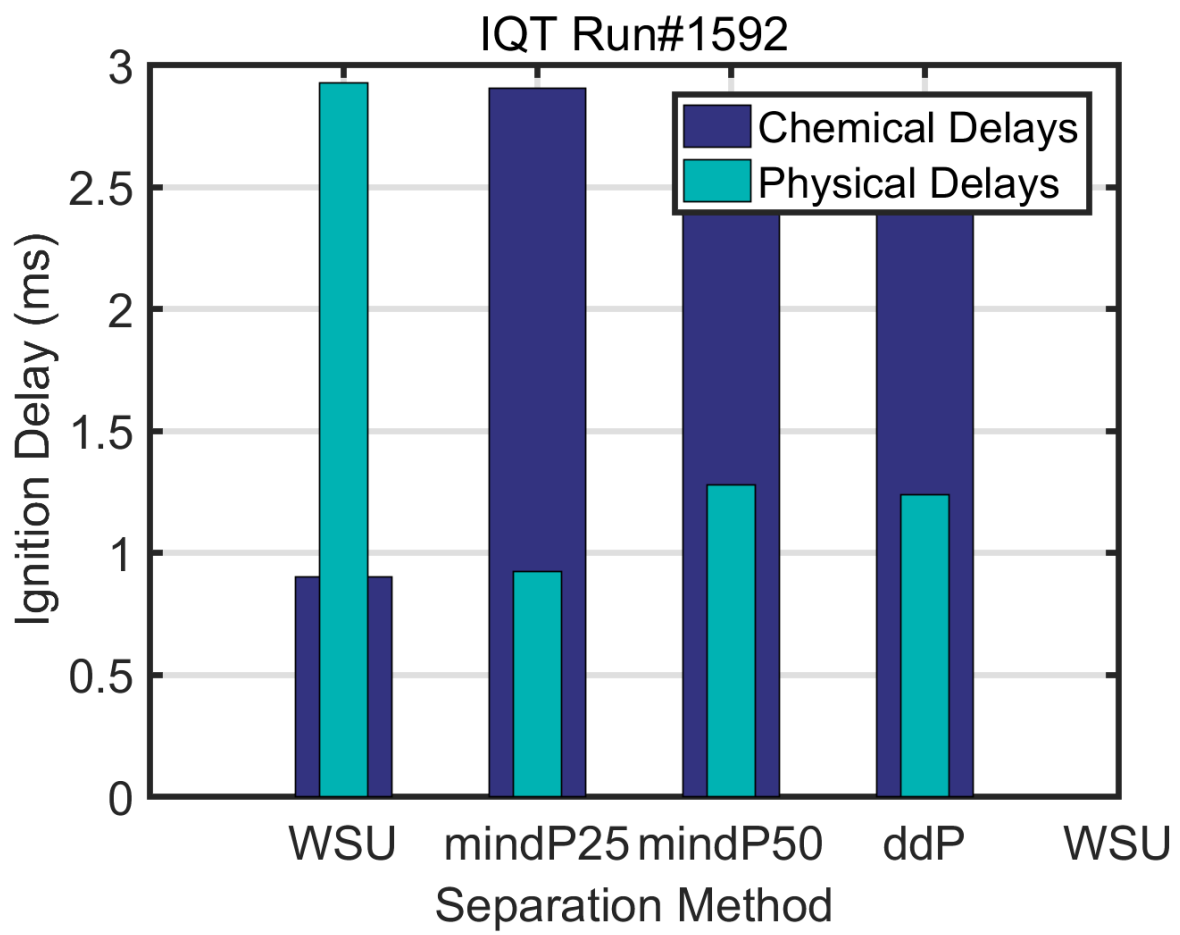
Run1592\_nj32.pre



Run1592\_nj32.pre







Published with MATLAB® R2016a

# Appendix C: IQT fuel run summary sheets.

## IQT™ Results - Run Details

Fuel ID: heptane

ISS version: 3.40a, rev. 13c / 2014-04-28

Setpoint: 576.5

Test Method: ASTM D6890-13b

Inj. #	ID	DCN	Charge P.	Inj. P.	Test T.	Trans. T.	Nozzle T.	Coolant T.	Air B. T.	Pump T.
1	3.631	55.84	309.7	175.6	558.2	127.0	49.3	42.7	587.3	35.7
2	3.781	53.81	309.7	175.6	558.1	127.3	48.5	42.6	587.2	35.3
3	3.932	51.92	309.8	175.6	558.2	127.2	48.4	42.6	588.0	35.6
4	3.782	53.80	309.7	175.6	558.3	127.4	49.3	42.5	586.9	35.3
5	3.859	52.81	309.7	175.6	558.1	127.4	50.0	42.6	587.3	36.7
6	3.745	54.28	309.8	175.6	558.5	127.7	48.7	42.8	588.2	36.0
7	3.859	52.82	309.8	175.6	558.5	128.0	50.8	42.7	587.3	35.3
8	3.763	54.05	309.8	175.6	558.1	128.3	49.7	42.8	586.9	35.6
9	3.741	54.34	309.8	175.7	558.3	128.4	48.7	42.8	588.3	35.3
10	3.796	53.62	309.7	175.7	558.3	128.7	49.3	42.8	587.5	36.0
11	3.786	53.75	309.8	175.7	558.1	128.6	48.7	42.8	587.9	36.0
12	3.771	53.94	309.8	175.6	558.5	128.7	48.9	42.9	588.6	35.3
13	3.858	52.83	309.8	175.6	558.5	128.8	49.0	42.9	587.3	36.6
14	3.744	54.30	309.8	175.7	558.2	128.8	49.5	42.7	587.6	35.9
15	3.766	54.01	309.7	175.6	558.5	129.0	49.4	42.8	588.9	35.3
16	3.898	52.33	309.8	175.6	558.5	129.1	50.0	42.8	587.9	36.3
17	3.770	53.96	309.8	175.6	558.0	129.1	49.6	42.7	587.9	35.6
18	3.757	54.12	309.7	175.6	558.5	129.4	49.5	42.8	589.2	35.2
19	3.693	54.99	309.8	175.6	558.5	129.5	49.6	42.8	588.1	37.3
20	3.883	52.52	309.8	175.6	557.9	129.4	50.4	42.9	588.1	36.3
21	3.784	53.77	309.8	175.7	558.3	129.6	49.0	42.8	588.9	35.6
22	3.701	54.88	309.8	175.7	558.3	129.9	50.8	42.8	587.9	35.1
23	3.830	53.19	309.8	175.6	558.0	130.1	49.0	42.9	588.2	36.5
24	3.785	53.75	309.8	175.7	558.4	130.0	48.7	42.8	589.3	35.6
25	3.813	53.39	309.8	175.7	558.2	129.7	49.1	42.8	588.6	35.3
26	3.813	53.40	309.7	175.6	558.1	129.6	49.5	42.8	587.4	36.5
27	3.722	54.60	309.8	175.7	558.2	129.7	48.3	42.8	589.1	35.7
28	3.672	55.28	309.8	175.6	558.1	129.4	50.0	42.9	588.6	35.3
29	3.765	54.02	309.7	175.7	558.3	129.5	50.4	42.8	588.6	37.3
30	3.826	53.24	309.7	175.6	558.6	129.4	50.4	42.9	589.4	36.3
31	3.724	54.56	309.7	175.6	558.5	129.6	49.4	42.9	587.8	35.6
32	3.865	52.74	309.8	175.6	558.5	129.4	49.1	42.8	587.9	35.2
Avg.:	3.785	53.76	309.8	175.6	558.3	128.9	49.4	42.8	588.1	35.8
Min:	3.631	51.92	309.7	175.6	557.9	127.0	48.3	42.5	586.9	35.1
Max:	3.932	55.84	309.8	175.7	558.6	130.1	50.8	42.9	589.4	37.3
Range:	0.301	3.93	0.1	0.1	0.7	3.0	2.5	0.4	2.6	2.3
Std. Dev.:	0.067	0.87	0.0	0.0	0.2	0.9	0.7	0.1	0.7	0.6

All test results within limits of test method

# IQT™ Results - Run Details

ruel ID: cn30

ISS version: 3.40a, rev. 13c<sup>1</sup> / 2014-04-28

Setpoint: 576.5

Test Method: ASTM D6890-13b

Inj. #	ID	DCN	Charge P.	Inj. P.	Test T.	Trans. T.	Nozzle T.	Coolant T.	Air B. T.	Pump T.
1	5.279	39.81	309.8	175.6	559.1	128.0	49.7	43.1	587.3	35.4
2	5.554	38.06	309.8	175.6	559.1	128.0	49.7	43.2	588.7	35.5
3	5.472	38.56	309.8	175.6	559.5	128.4	50.0	43.2	588.6	35.1
4	5.617	37.68	309.7	175.6	559.5	128.8	49.0	43.2	587.6	35.3
5	5.494	38.43	309.7	175.5	559.8	129.1	50.0	43.2	588.9	35.9
6	5.425	38.86	309.7	175.6	559.8	129.1	49.8	43.2	588.8	36.0
7	5.445	38.73	309.7	175.6	559.6	129.4	51.1	43.2	587.6	35.3
8	5.545	38.11	309.8	175.6	559.7	129.5	48.7	43.2	589.8	35.7
9	5.599	37.79	309.7	175.6	559.8	129.7	49.3	43.2	589.4	35.3
10	5.649	37.49	309.7	175.6	559.5	129.8	49.7	43.2	587.7	36.7
11	5.534	38.18	309.8	175.6	559.5	129.8	50.0	43.2	589.2	36.3
12	5.576	37.92	309.8	175.6	559.8	129.8	49.4	43.2	590.1	35.6
13	5.422	38.87	309.8	175.6	559.8	129.9	49.4	43.2	588.6	35.0
14	5.622	37.65	309.8	175.6	559.5	129.8	50.3	43.2	587.9	36.2
15	5.859	36.31	309.7	175.6	559.8	130.1	50.1	43.2	589.5	35.3
16	5.795	36.66	309.7	175.6	560.0	130.1	50.4	43.2	588.9	35.3
17	5.622	37.65	309.7	175.6	559.5	130.2	49.7	43.4	588.5	35.6
18	5.735	37.00	309.7	175.6	559.5	130.2	51.4	43.2	589.4	35.2
19	5.706	37.16	309.7	175.6	559.7	130.1	49.7	43.3	588.6	36.3
20	5.667	37.39	309.8	175.6	559.8	130.1	50.1	43.2	588.8	35.5
21	5.751	36.91	309.7	175.6	559.8	130.5	49.3	43.5	589.6	35.0
22	5.665	37.40	309.8	175.6	559.7	130.5	49.8	43.3	588.3	36.8
23	5.629	37.61	309.8	175.6	559.6	130.5	50.5	43.2	589.8	35.9
24	5.545	38.11	309.8	175.7	560.1	130.5	49.5	43.2	589.9	35.3
25	5.910	36.03	309.8	175.7	559.7	130.5	51.1	43.2	588.2	35.9
26	5.828	36.48	309.8	175.6	559.4	130.5	50.1	43.3	588.9	36.0
27	5.718	37.10	309.8	175.6	560.1	130.5	49.3	43.4	589.9	35.3
28	5.762	36.84	309.7	175.6	559.8	130.5	50.0	43.5	588.9	35.2
29	5.573	37.94	309.8	175.6	559.5	130.6	50.0	43.3	588.2	36.3
30	5.854	36.34	309.7	175.7	559.6	130.5	49.7	43.3	589.3	35.5
31	5.650	37.49	309.8	175.6	559.8	130.5	51.0	43.5	589.3	35.0
32	5.800	36.63	309.7	175.6	559.6	130.6	50.1	43.2	589.3	36.3
Avg.:	5.635	37.58	309.8	175.6	559.6	129.9	49.9	43.2	588.9	35.6
Min:	5.279	36.03	309.7	175.5	559.1	128.0	48.7	43.1	587.3	35.0
Max:	5.910	39.81	309.8	175.7	560.1	130.6	51.4	43.5	590.1	36.8
Range:	0.631	3.77	0.2	0.1	1.0	2.6	2.7	0.4	2.8	1.8
Std. Dev.:	0.146	0.86	0.1	0.0	0.2	0.7	0.6	0.1	0.7	0.5

All test results within limits of test method

# IQT™ Results - Run Details

Run ID: cn45

ISS version: 3.40a, rev. 13c<sup>1</sup> / 2014-04-28

Setpoint: 576.5

Test Method: ASTM D6890-13b

Inj. #	ID	DCN	Charge P.	Inj. P.	Test T.	Trans. T.	Nozzle T.	Coolant T.	Air B. T.	Pump T.
1	4.052	50.52	309.8	175.6	560.1	130.2	51.1	44.2	590.2	35.2
2	3.982	51.33	309.8	175.7	559.7	130.5	50.0	44.0	588.7	36.4
3	4.119	49.76	309.8	175.7	559.4	130.8	51.0	43.9	588.2	35.8
4	4.034	50.71	309.8	175.7	559.8	130.8	51.4	43.9	589.4	35.3
5	4.046	50.58	309.8	175.6	559.8	130.8	51.3	44.1	588.6	36.0
6	4.064	50.37	309.8	175.7	559.8	130.8	51.4	44.2	588.9	36.6
7	4.070	50.30	309.9	175.6	560.1	130.8	50.4	44.2	589.6	35.7
8	4.034	50.72	309.9	175.7	559.9	130.8	50.4	44.2	588.3	35.3
9	4.008	51.02	309.8	175.7	559.4	130.8	50.7	44.2	588.9	35.2
10	4.045	50.59	309.8	175.7	559.9	131.1	51.1	44.2	589.6	36.0
11	4.096	50.01	309.8	175.7	559.8	131.2	50.1	44.2	588.5	35.4
12	3.918	52.09	309.8	175.7	559.8	131.2	51.1	44.2	589.5	35.0
13	4.045	50.59	309.9	175.7	559.8	131.1	50.7	44.2	589.6	37.2
14	4.025	50.82	309.8	175.6	559.4	131.2	50.5	44.2	588.3	36.1
15	4.030	50.76	309.8	175.7	559.8	131.2	50.9	44.2	589.5	35.6
16	4.058	50.44	309.8	175.7	559.8	131.4	51.4	44.2	589.6	35.3
17	4.001	51.10	309.8	175.7	559.5	131.5	50.0	44.2	588.6	36.1
18	4.079	50.21	309.8	175.7	559.5	131.5	50.4	44.2	590.0	35.8
19	3.966	51.51	309.9	175.6	559.7	131.6	49.7	44.2	589.6	35.3
20	4.096	50.02	309.8	175.7	559.5	131.9	51.4	44.2	588.2	36.0
21	4.154	49.38	309.8	175.7	559.5	131.9	51.7	44.2	589.9	36.6
22	3.944	51.77	309.8	175.7	559.7	132.0	50.4	44.2	589.6	35.7
23	4.051	50.53	309.8	175.7	559.3	131.7	50.7	44.2	588.2	35.3
24	4.174	49.17	309.9	175.7	559.5	131.5	51.4	44.1	589.9	36.6
25	4.045	50.59	309.7	175.7	559.8	131.8	50.6	44.3	589.6	37.0
26	4.130	49.64	309.7	175.6	559.4	131.8	50.1	44.3	588.5	36.0
27	4.156	49.36	309.8	175.7	559.4	131.5	50.4	44.2	589.6	35.5
28	4.043	50.61	309.9	175.7	559.5	131.5	50.4	44.2	589.9	35.2
29	4.095	50.02	309.8	175.6	559.3	131.5	50.4	44.2	588.6	36.2
30	4.016	50.93	309.9	175.7	559.3	131.6	50.7	44.2	589.9	36.0
31	3.971	51.45	309.8	175.7	559.5	131.8	50.4	44.3	589.6	35.3
32	3.993	51.19	309.8	175.7	559.1	131.9	50.5	44.2	588.5	35.1
Avg.:	4.048	50.55	309.8	175.7	559.6	131.3	50.7	44.2	589.2	35.8
Min:	3.918	49.17	309.7	175.6	559.1	130.2	49.7	43.9	588.2	35.0
Max:	4.174	52.09	309.9	175.7	560.1	132.0	51.7	44.3	590.2	37.2
Range:	0.256	2.92	0.2	0.1	1.0	1.9	1.9	0.4	2.0	2.1
Std. Dev.:	0.060	0.69	0.0	0.0	0.2	0.5	0.5	0.1	0.6	0.6

All test results within limits of test method

# IQT™ Results - Run Details

Run ID: cn60

ISS version: 3.40a, rev. 13c<sup>1</sup> / 2014-04-28

Setpoint: 576.5

Test Method: ASTM D6890-13b

Inj. #	ID	DCN	Charge P.	Inj. P.	Test T.	Trans. T.	Nozzle T.	Coolant T.	Air B. T.	Pump T.
1	3.251	61.86	309.8	175.7	559.6	130.5	50.7	43.8	588.9	35.3
2	3.242	62.02	309.9	175.6	559.6	130.2	48.4	43.9	589.2	35.3
3	3.354	60.09	309.7	175.6	559.5	130.3	50.5	43.9	588.2	35.3
4	3.321	60.65	309.8	175.6	559.6	130.8	50.3	43.9	588.9	35.6
5	3.206	62.66	309.8	175.6	559.8	131.1	49.6	43.9	589.4	35.2
6	3.244	61.98	309.8	175.6	559.7	131.1	50.7	43.9	588.3	36.3
7	3.181	63.12	309.8	175.7	559.1	131.0	50.9	43.9	589.6	35.6
8	3.052	65.60	309.8	175.7	560.0	131.2	50.4	43.8	589.6	35.0
9	3.265	61.61	309.8	175.6	559.8	131.2	50.7	43.9	588.2	37.7
10	3.144	63.80	309.8	175.7	559.2	131.2	51.1	43.9	588.9	36.4
11	3.096	64.73	309.8	175.6	559.8	131.2	49.3	44.0	590.2	35.7
12	3.217	62.46	309.8	175.7	560.2	131.5	50.1	43.9	588.9	35.3
13	3.186	63.03	309.8	175.6	559.9	131.5	50.4	43.9	588.1	35.1
14	3.218	62.44	309.8	175.7	559.5	131.4	50.7	43.9	589.5	37.3
15	3.183	63.08	309.7	175.7	559.9	131.5	49.0	43.9	589.3	36.3
16	3.175	63.24	309.8	175.7	559.5	131.4	50.7	43.9	588.3	35.6
17	3.152	63.67	309.8	175.7	559.8	131.5	49.8	43.9	589.6	35.3
18	3.183	63.09	309.8	175.6	559.9	131.5	50.2	43.9	589.9	35.6
19	3.143	63.82	309.8	175.7	559.8	131.6	49.6	43.9	588.6	37.0
20	3.215	62.51	309.8	175.6	559.3	131.9	50.3	43.9	589.2	36.0
21	3.169	63.35	309.8	175.7	559.8	131.8	50.7	43.9	590.5	35.6
22	3.216	62.47	309.8	175.6	559.7	131.5	49.7	43.9	589.3	35.3
23	3.067	65.31	309.8	175.7	558.9	131.6	48.7	43.9	588.2	36.3
24	3.153	63.64	309.7	175.7	559.5	131.6	49.3	43.9	589.6	36.0
25	3.234	62.16	309.8	175.7	559.7	131.8	50.7	44.0	589.3	35.4
26	3.208	62.62	309.8	175.7	559.4	131.7	50.4	43.9	588.6	35.1
27	3.179	63.17	309.8	175.7	559.7	131.8	50.4	44.2	590.2	36.5
28	3.133	64.02	310.0	175.7	559.8	131.8	50.7	43.9	589.6	35.6
29	3.240	62.05	309.8	175.7	558.9	131.9	52.1	43.9	588.2	35.3
30	3.176	63.21	309.8	175.6	559.2	131.5	49.3	44.1	589.8	36.6
31	3.183	63.08	309.8	175.7	559.5	131.5	49.7	43.9	589.9	36.0
32	3.197	62.83	309.8	175.6	559.4	131.3	49.9	44.2	588.2	35.3
Avg.:	3.193	62.90	309.8	175.7	559.6	131.3	50.2	43.9	589.1	35.8
Min:	3.052	60.09	309.7	175.6	558.9	130.2	48.4	43.8	588.1	35.0
Max:	3.354	65.60	310.0	175.7	560.2	131.9	52.1	44.2	590.5	37.7
Range:	0.302	5.50	0.3	0.1	1.3	1.7	3.7	0.4	2.5	2.7
Std. Dev.:	0.063	1.14	0.0	0.0	0.3	0.4	0.8	0.1	0.7	0.7

All test results within limits of test method

# IQT™ Results - Run Details

Fuel ID: ch

ISS version: 3.40a, rev. 13c<sup>1</sup> / 2014-04-28

Setpoint: 576.5

Test Method: ASTM D6890-13b

Inj. #	ID	DCN	Charge P.	Inj. P.	Test T.	Trans. T.	Nozzle T.	Coolant T.	Air B. T.	Pump T.
1	9.948	24.19	309.7	175.7	559.5	129.8	50.9	44.3	587.7	35.2
2	9.743	24.53	309.8	175.7	560.0	129.9	51.4	44.2	589.5	36.7
3	9.567	24.83	309.8	175.7	560.0	129.9	50.8	44.2	588.9	35.9
4	9.839	24.37	309.8	175.6	559.4	129.9	51.0	44.2	587.5	35.3
5	8.597	26.70	309.8	175.7	559.6	129.8	49.7	44.2	589.0	35.1
6	9.994	24.12	309.8	175.7	559.9	130.1	51.6	44.2	589.3	35.6
7	9.886	24.29	309.8	175.7	559.8	130.2	51.7	44.3	587.7	35.2
8	9.959	24.18	309.9	175.7	559.5	130.5	50.7	44.2	588.6	35.6
9	9.776	24.47	309.8	175.7	559.9	130.8	51.0	44.2	589.3	35.3
10	10.297	23.65	309.8	175.6	559.5	130.8	51.4	44.2	588.2	37.0
11	10.128	23.91	309.8	175.7	559.5	131.0	51.4	44.2	588.9	36.3
12	10.443	23.43	309.8	175.6	559.8	130.8	50.1	44.2	589.8	35.6
13	10.008	24.10	309.8	175.7	559.8	130.7	50.4	44.2	588.2	35.3
14	9.052	25.78	309.8	175.7	559.5	130.5	50.1	44.2	588.2	36.3
15	10.341	23.58	309.7	175.7	560.0	130.9	49.5	44.2	589.5	35.8
16	10.191	23.81	309.9	175.7	559.8	130.8	50.7	44.2	588.6	35.3
17	9.907	24.26	309.8	175.7	559.8	130.8	50.4	44.2	588.6	36.3
18	7.533	29.32	309.8	175.7	560.2	130.8	50.3	44.2	589.9	36.0
19	10.201	23.79	309.8	175.7	560.4	130.8	50.7	44.3	588.9	35.3
20	9.429	25.07	309.8	175.6	560.1	130.8	50.4	44.2	587.3	35.0
21	10.031	24.06	309.8	175.7	559.8	130.9	50.7	44.2	588.9	37.4
22	10.141	23.89	309.8	175.7	560.1	130.9	50.2	44.2	589.6	36.2
23	9.829	24.39	309.7	175.7	560.0	131.1	50.4	44.2	587.9	35.7
24	9.550	24.86	309.8	175.7	559.8	130.8	50.7	44.2	588.6	35.3
25	9.706	24.59	309.8	175.6	560.2	130.5	50.4	44.2	589.6	35.7
26	9.844	24.36	309.8	175.7	560.4	130.5	50.0	44.3	588.5	36.9
27	10.125	23.91	309.9	175.7	559.8	130.5	50.2	44.4	588.2	36.0
28	9.618	24.74	309.8	175.7	559.9	130.5	50.8	44.2	589.4	35.4
29	10.085	23.97	309.9	175.7	560.1	130.6	50.4	44.3	588.5	35.2
30	10.214	23.78	309.8	175.7	559.8	130.7	51.4	44.2	588.2	35.8
31	9.067	25.75	309.9	175.7	560.1	130.5	51.2	44.3	589.6	35.3
32	9.971	24.16	309.9	175.7	560.1	130.6	51.7	44.2	588.6	35.3
Avg.:	9.782	24.46	309.8	175.7	559.9	130.6	50.7	44.2	588.7	35.8
Min:	7.533	23.43	309.7	175.6	559.4	129.8	49.5	44.2	587.3	35.0
Max:	10.443	29.32	309.9	175.7	560.4	131.1	51.7	44.4	589.9	37.4
Range:	2.910	5.89	0.2	0.1	1.0	1.3	2.2	0.2	2.6	2.4
Std. Dev.:	0.570	1.11	0.0	0.0	0.3	0.4	0.6	0.0	0.7	0.6

Average value of 'Ignition Delay' is above upper limit of 6.5

Value of 'DCN' calculated using:  $DCN = 83.99 * ((ID - 1.512)^{-0.658}) + 3.547$



# IQT™ Results - Run Details

el ID: 8576

ISS version: 3.40a, rev. 13c<sup>1</sup> / 2014-04-28

Setpoint: 567.5

Test Method: ASTM D6890-13b

Inj. #	ID	DCN	Charge P.	Inj. P.	Test T.	Trans. T.	Nozzle T.	Coolant T.	Air B. T.	Pump T.
1	4.534	45.62	310.6	176.5	560.4	129.8	50.1	45.3	590.9	35.2
2	4.687	44.28	310.5	176.4	560.8	129.8	50.7	45.3	589.9	36.7
3	4.520	45.74	310.6	176.4	560.0	130.1	50.4	45.3	589.3	36.0
4	4.592	45.10	310.5	176.4	560.2	130.1	50.4	45.4	590.8	35.3
5	4.577	45.23	310.6	176.5	560.4	130.4	50.4	45.5	590.1	35.0
6	4.610	44.94	310.6	176.5	560.1	130.5	49.9	45.5	589.8	36.6
7	4.646	44.62	310.6	176.4	560.7	130.8	50.0	45.5	591.0	35.8
8	4.512	45.82	310.5	176.4	560.7	130.9	49.7	45.5	590.2	35.3
9	4.592	45.09	310.6	176.4	560.1	131.0	50.4	45.5	589.6	35.1
10	4.603	45.00	310.4	176.5	560.4	131.2	49.5	45.3	590.9	36.3
11	4.553	45.45	310.6	176.4	560.3	131.2	50.1	45.3	590.2	35.6
12	4.585	45.15	310.5	176.4	560.1	131.2	50.0	45.4	590.1	35.2
13	4.732	43.89	310.6	176.5	560.1	131.2	50.4	45.5	590.6	35.7
14	4.627	44.79	310.5	176.5	560.3	131.5	50.1	45.4	589.6	35.3
15	4.619	44.85	310.6	176.5	560.5	131.5	50.4	45.6	590.8	36.2
16	4.496	45.96	310.5	176.5	560.5	131.5	50.7	45.5	590.2	36.2
17	4.625	44.80	310.6	176.4	560.1	131.5	50.8	45.6	589.6	35.5
18	4.584	45.16	310.6	176.4	560.8	131.8	49.7	45.4	591.2	35.2
19	4.646	44.62	310.5	176.4	560.8	131.9	49.7	45.5	590.5	37.6
20	4.677	44.36	310.4	176.4	560.4	131.9	49.7	45.5	589.9	36.6
21	4.510	45.83	310.6	176.5	560.8	131.9	50.4	45.5	591.2	35.9
22	4.586	45.15	310.6	176.4	560.8	131.9	49.6	45.6	590.6	35.4
23	4.517	45.77	310.5	176.4	560.3	131.8	50.3	45.6	589.4	35.2
24	4.669	44.43	310.6	176.4	560.4	131.9	49.7	45.6	591.2	36.7
25	4.654	44.56	310.6	176.5	560.5	131.9	50.0	45.5	590.9	36.0
26	4.553	45.45	310.4	176.4	560.2	131.9	50.1	45.6	589.6	35.4
27	4.608	44.96	310.7	176.4	560.5	131.9	50.2	45.6	591.2	35.2
28	4.629	44.77	310.6	176.4	560.8	131.9	49.7	45.6	590.9	37.3
29	4.613	44.91	310.5	176.5	560.4	131.9	50.1	45.5	589.9	36.7
30	4.616	44.89	310.6	176.4	560.8	131.9	50.4	45.6	591.5	36.0
31	4.602	45.01	310.5	176.5	560.8	131.9	50.0	45.6	591.2	35.5
32	4.533	45.63	310.6	176.4	560.1	132.2	50.1	45.6	589.9	35.2
Avg.:	4.597	45.05	310.6	176.4	560.4	131.3	50.1	45.5	590.4	35.8
Min:	4.496	43.89	310.4	176.4	560.0	129.8	49.5	45.3	589.3	35.0
Max:	4.732	45.96	310.7	176.5	560.8	132.2	50.8	45.6	591.5	37.6
Range:	0.236	2.07	0.4	0.1	0.8	2.4	1.3	0.3	2.3	2.6
Std. Dev.:	0.057	0.50	0.1	0.0	0.3	0.7	0.3	0.1	0.6	0.7

All test results within limits of test method

# IQT™ Results - Run Details

ID: heptane

ISS version: 3.40a, rev. 13c<sup>1</sup> / 2014-04-28

Setpoint: 567.5

Test Method: ASTM D6890-13b

Inj. #	ID	DCN	Charge P.	Inj. P.	Test T.	Trans. T.	Nozzle T.	Coolant T.	Air B. T.	Pump T.
1	3.893	52.39	310.2	176.9	558.8	128.1	48.7	45.3	589.1	35.8
2	3.673	55.27	310.2	176.9	559.4	128.4	48.9	45.3	589.8	35.3
3	3.881	52.54	310.3	176.7	559.2	128.4	48.9	45.2	588.2	36.5
4	3.882	52.53	310.3	176.6	559.0	128.7	48.7	45.4	588.5	36.0
5	3.877	52.60	310.1	176.6	559.2	128.9	49.3	45.4	589.9	35.3
6	3.842	53.03	310.2	176.7	559.7	129.0	49.0	45.3	588.6	37.0
7	3.840	53.05	310.2	176.5	559.1	129.1	48.9	45.3	588.0	36.7
8	3.742	54.32	310.1	176.6	559.1	129.1	48.7	45.3	589.6	35.8
9	3.863	52.76	310.1	176.5	559.2	129.3	49.0	45.3	588.6	35.3
10	3.920	52.07	310.2	176.5	559.1	129.4	49.0	45.3	588.8	36.2
11	3.856	52.86	310.1	176.6	559.4	129.4	49.0	45.4	590.0	37.0
12	3.882	52.53	310.1	176.5	559.2	129.4	48.8	45.3	588.9	36.0
13	3.856	52.85	310.3	176.5	558.8	129.5	49.0	45.4	588.3	35.4
14	3.835	53.12	310.1	176.6	559.1	129.5	48.7	45.4	589.7	35.1
15	3.920	52.07	310.3	176.7	559.1	129.5	49.3	45.4	589.1	36.7
16	3.808	53.46	310.2	176.6	558.9	129.6	49.1	45.3	589.1	35.7
17	3.796	53.62	310.4	176.5	559.5	129.8	49.1	45.4	589.9	35.3
18	3.811	53.42	310.2	176.5	559.5	129.8	49.3	45.3	588.6	36.7
19	3.828	53.21	310.1	176.5	559.0	129.8	49.2	45.4	588.8	36.7
20	3.729	54.51	310.2	176.6	559.1	129.8	49.7	45.3	589.6	35.7
21	3.847	52.97	310.2	176.5	559.1	129.8	49.0	45.3	588.8	35.3
22	3.836	53.11	310.1	176.5	559.0	129.8	49.6	45.3	589.2	36.0
23	3.903	52.27	310.1	176.6	559.5	129.9	50.8	45.4	590.2	36.7
24	3.858	52.82	310.2	176.5	559.4	129.9	49.8	45.3	588.9	35.9
25	3.825	53.24	310.0	176.5	559.1	129.9	50.1	45.3	588.6	35.3
26	3.703	54.86	310.0	176.6	559.5	129.9	50.4	45.5	589.9	35.3
27	3.769	53.98	310.0	176.5	559.5	130.0	49.9	45.4	589.9	37.0
28	3.854	52.88	309.9	176.5	559.4	130.0	50.0	45.4	588.2	35.9
29	3.786	53.75	310.1	176.5	559.3	130.1	49.8	45.3	589.5	35.3
30	3.750	54.21	310.1	176.5	559.5	130.1	50.0	45.4	589.8	35.1
31	3.958	51.60	310.2	176.4	559.1	130.1	50.3	45.4	588.6	36.3
32	3.716	54.67	310.3	176.5	559.1	130.1	50.0	45.6	589.9	35.6
Avg.:	3.829	53.19	310.2	176.6	559.2	129.5	49.4	45.4	589.1	35.9
Min:	3.673	51.60	309.9	176.4	558.8	128.1	48.7	45.2	588.0	35.1
Max:	3.958	55.27	310.4	176.9	559.7	130.1	50.8	45.6	590.2	37.0
Range:	0.286	3.67	0.5	0.6	0.9	2.0	2.1	0.3	2.2	1.9
Std. Dev.:	0.068	0.87	0.1	0.1	0.2	0.5	0.6	0.1	0.6	0.6

All test results within limits of test method

# Appendix D: Master fuel data sheet.

		IGNITION DELAYS														
		IQT			331			10% CHRR			5% CHRR			310		
Fuel	DCN	IGD	std(IQT)	2x std	IGD	std(331)	2x std	IGD	std(10%)	2x std	IGD	std(5%)	2x std	IGD	std(310)	2x std
CN30	37.58	5.635	0.146	0.292	5.6369	0.1425	0.285	5.9119	0.1955	0.391	5.7963	0.2198	0.4396	4.8913	0.1711	0.3422
JP5	44.97	4.607	0.075	0.15	4.6169	0.0755	0.151	4.7594	0.0746	0.1492	4.65	0.074	0.148	4.4112	0.0814	0.1628
F76	49.57	4.137	0.079	0.158	4.1575	0.073	0.146	4.2888	0.0568	0.1136	4.1862	0.0661	0.1322	3.9413	0.0981	0.1962
CN45	50.55	4.048	0.06	0.12	4.0294	0.062	0.124	4.1781	0.0519	0.1038	4.085	0.0552	0.1104	3.6694	0.0697	0.1394
nC7	53.76	3.785	0.067	0.134	3.8281	0.0916	0.1832	3.9619	0.1067	0.2134	3.8681	0.0883	0.1766	3.6219	0.1067	0.2134
CN60	62.9	3.193	0.063	0.126	3.1744	0.0688	0.1376	3.3169	0.0614	0.1228	3.2075	0.0673	0.1346	2.9475	0.0999	0.1998
nC10	65.88	3.085	0.042	0.084	3.0681	0.0437	0.0874	3.1963	0.0499	0.0998	3.1013	0.0465	0.093	2.8687	0.052	0.104
nC16	118.85	2.13	0.033	0.066	2.1344	0.0349	0.0698	2.235	0.0313	0.0626	2.1463	0.0342	0.0684	1.8563	0.0527	0.1054

Tol-Hex	DCN	IGD	std(IQT)	2x std	IGD	std(331)	2x std	IGD	std(10%)	2x std	IGD	std(5%)	2x std	IGD	std(310)	2x std
50/50	55.9	3.627	0.079	0.158	3.6144	0.0786	0.1572	3.7987	0.0626	0.1252	3.67	0.0818	0.1636	3.1844	0.0928	0.1856
60/40	49.58	4.136	0.175	0.35	4.1563	0.1791	0.3582	4.3919	0.1609	0.3218	4.2669	0.1909	0.3818	3.5044	0.1268	0.2536
65/35	44.84	4.621	0.256	0.512	4.6519	0.2475	0.495	4.9438	0.2438	0.4876	4.7806	0.2571	0.5142	3.9094	0.1317	0.2634
70/30	39.05	5.395	0.514	1.028	5.4244	0.5141	1.0282	5.9244	0.6094	1.2188	5.7012	0.6179	1.2358	4.4656	0.317	0.634
72/28	37.09	5.718	0.439	0.878	5.7713	0.4466	0.8932	6.3481	0.5225	1.045	6.1031	0.5417	1.0834	4.6794	0.2992	0.5984
74/26	32.58	6.536	0.186	0.372	6.6119	0.1661	0.3322	7.5281	0.4973	0.9946	7.2131	0.5797	1.1594	5.2444	0.1508	0.3016
75/25	27.5	8.243	0.209	0.418	8.5612	0.8208	1.6416	11.6269	0.8612	1.7224	11.46	1.0833	2.1666	6.6744	1.2144	2.4288

		Physical/Chemical Delay Separation Methods											
		mindP (WSU)			25% mindP			50% mindP			ddP		
Fuel	DCN	IGD	std(WSU)	2x std	IGD	std(25%)	2x std	IGD	std(50%)	2x std	IGD	std(ddP)	2x std
CN30	37.58	3.2794	0.0785	0.157	0.415	0.3259	0.6518	1.815	0.1277	0.2554	0.7056	0.1219	0.2438
JP5	44.97	3.4025	0.3419	0.6838	0.9031	0.4233	0.8466	1.5169	0.2773	0.5546	1.3519	0.4616	0.9232
F76	49.57	3.0538	0.4546	0.9092	0.9081	0.2875	0.575	1.39	0.2321	0.4642	1.2237	0.1506	0.3012
CN45	50.55	2.6206	0.3699	0.7398	0.7062	0.0864	0.1728	1.1231	0.0959	0.1918	1.0875	0.1474	0.2948
nC7	53.76	2.9275	0.3823	0.7646	0.9225	0.0978	0.1956	1.2775	0.1003	0.2006	1.2369	0.092	0.184
CN60	62.9	1.5456	0.1992	0.3984	0.5838	0.0472	0.0944	0.8238	0.045	0.09	0.8144	0.042	0.084
nC10	65.88	2.1362	0.431	0.862	0.6181	0.0429	0.0858	0.8956	0.0492	0.0984	0.8837	0.0246	0.0492
nC16	118.85	1.4163	0.0555	0.111	0.4031	0.0586	0.1172	0.6694	0.0547	0.1094	0.6563	0.0854	0.1708

Tol-Hex	DCN	IGD	std(WSU)	2x std	IGD	std(25%)	2x std	IGD	std(50%)	2x std	IGD	std(ddP)	2x std
50/50	55.9	1.7944	0.1424	0.2848	0.7087	0.0383	0.0766	0.9688	0.038	0.076	0.9113	0.0872	0.1744
60/40	49.58	2.2425	0.1444	0.2888	0.6013	0.0948	0.1896	1.1012	0.0465	0.093	1.2275	0.1551	0.3102
65/35	44.84	2.5731	0.1478	0.2956	0.4525	0.1868	0.3736	1.1919	0.0923	0.1846	1.1437	0.5016	1.0032
70/30	39.05	3.0219	0.132	0.264	0.3094	0.1935	0.387	1.3081	0.1016	0.2032	0.9675	0.5413	1.0826
72/28	37.09	3.2131	0.1374	0.2748	0.3275	0.1737	0.3474	1.4781	0.1312	0.2624	1.0275	0.5197	1.0394
74/26	32.58	3.5781	0.0843	0.1686	0.3706	0.1252	0.2504	1.4356	0.1266	0.2532	0.5375	0.5688	1.1376
75/25	27.5	4.1588	0.1773	0.3546	0.4938	0.1418	0.2836	1.2688	0.1644	0.3288	0.9681	0.1774	0.3548

nC7 CHRR Data			
CHRR %	IGD	std(IGD)	2x std
2	3.7688	0.0914	0.1828
3	3.8106	0.0941	0.1882
4	3.8431	0.0945	0.189
5	3.8681	0.0883	0.1766
6	3.8919	0.0907	0.1814
7	3.9131	0.0897	0.1794
8	3.9294	0.0884	0.1768
9	3.9463	0.0889	0.1778
10	3.9619	0.0905	0.181
IQT	3.785	0.067	0.134

Fuel Properties Analysis				
Fuel	DCN	Modified Drop Diameter (m)	Weber Number	Break Up Time (s)
CN30	37.58	0.001647	812663	0.001893
JP5	44.97	0.004715	759917	0.00177
F76	49.57	0.002491	805656	0.001877
CN45	50.55	0.001755	712002	0.001659
nC7	53.76	0.005453	814630	0.001898
CN60	62.9	0.001871	810663	0.001889
nC10	65.88	0.005445	833871	0.001943
nC16	118.85	0.002288	882910	0.002057

Laurence Livermore Kinetics Chemical Delay Comparison (331 Standard ddP Separation)							
Fuel	DCN	IGD <sub>c</sub> - LLK	IGD <sub>c</sub> - ddP	Fuel	DCN	IGD <sub>c</sub> - LLK	IGD <sub>c</sub> - ddP
nC7	53.76	1.73	2.5912	75/25	27.5	6.8	7.5931
nC10	65.88	1.47	2.1844	70/30	39.05	4.88	4.4569
nC16	118.85	1.35	1.4781	65/35	44.84	3.6	3.5082
				60/40	49.58	2.82	2.9288

## Appendix E: Plotter code and all generated plots of results.

This script plots various metrics of diesel ignition based on IQT analysis  
J.L. Mendelson 31JUL16

```
close all
clear all
clc
```

### Phys/Chem Separation

```
WSU = xlsread('Master Fuel Data Sheet', 'Sheet1', 'D25:D32');
WSU_tol = xlsread('Master Fuel Data Sheet', 'Sheet1', 'D35:D41');
mindP25 = xlsread('Master Fuel Data Sheet', 'Sheet1', 'G25:G32');
mindP25_tol = xlsread('Master Fuel Data Sheet', 'Sheet1', 'G35:G41');
mindP50 = xlsread('Master Fuel Data Sheet', 'Sheet1', 'J25:J32');
mindP50_tol = xlsread('Master Fuel Data Sheet', 'Sheet1', 'J35:J41');
ddP = xlsread('Master Fuel Data Sheet', 'Sheet1', 'M25:M32');
ddP_tol = xlsread('Master Fuel Data Sheet', 'Sheet1', 'M35:M41');

IGD331 = xlsread('Master Fuel Data Sheet', 'Sheet1', 'G4:G11');
IGD331_tol = xlsread('Master Fuel Data Sheet', 'Sheet1', 'G14:G20');

chem_WSU = IGD331 - WSU;
chem_WSU_tol = IGD331_tol - WSU_tol;
chem_mindP25 = IGD331 - mindP25;
chem_mindP25_tol = IGD331_tol - mindP25_tol;
chem_mindP50 = IGD331 - mindP50;
chem_mindP50_tol = IGD331_tol - mindP50_tol;
chem_ddP = IGD331 - ddP;
chem_ddP_tol = IGD331_tol - ddP_tol;

fuels = {'CN30', 'JP5', 'F76', 'CN45', 'nc7', 'CN60', 'nc10', 'nc16'};
split = {'Physical', 'Chemical'};
fig = 1;
for i = 1:8;
    figure(fig)
    plot = [WSU(i) chem_WSU(i); mindP25(i) chem_mindP25(i); mindP50(i) chem_mindP50(i); ddP(i) chem_ddP(i)];
    bar(plot, 'stacked');
    title(fuels{i})
    set(gca, 'XTick', 1:4, 'XTickLabel', {'WSU' '25% mindP' '50% mindP' 'ddP'})
    ylabel('Ignition Delay (ms)');
    legend(split)
    grid on;
    plotfixer;
    fig = fig + 1;
end

tols = {'50/50', '60/40', '65/35', '70/30', '72/28', '74/26', '75/25'};

for i = 1:7;
    figure(fig)
    plot = [WSU_tol(i) chem_WSU_tol(i); mindP25_tol(i) chem_mindP25_tol(i); mindP50_tol(i) chem_mindP50_tol(i);
    ddP_tol(i) chem_ddP_tol(i)];
    bar(plot, 'stacked');
    title(tols{i})
    set(gca, 'XTick', 1:4, 'XTickLabel', {'WSU' '25% mindP' '50% mindP' 'ddP'})
    ylabel('Ignition Delay (ms)');
    legend(split)
    grid on;
    plotfixer;
    fig = fig + 1;
end
```

### WSU variance for 8 analyzed fuels and Tol-Hex blends

```
WSU = xlsread('Master Fuel Data Sheet', 'Sheet1', 'D25:D32');
WSU_tol = xlsread('Master Fuel Data Sheet', 'Sheet1', 'D35:D41');
IGD331 = xlsread('Master Fuel Data Sheet', 'Sheet1', 'G4:G11');
IGD331_tol = xlsread('Master Fuel Data Sheet', 'Sheet1', 'G14:G20');
chem_WSU = IGD331 - WSU;
chem_WSU_tol = IGD331_tol - WSU_tol;

split = {'Physical', 'Chemical'};

figure(fig)
fig = fig + 1;
```

```

plot = [WSU chem_WSU];
bar(plot, 'stacked');
set(gca, 'XTick',1:8, 'XTickLabel',fuels)
title('WSU Method for Analyzed Fuels (Compared to IGD 331)')
xlabel('Fuel')
ylabel('Ignition Delay (ms)')
legend(split,'Location','NorthEast')
grid on;
plotfixer;

figure(fig)
fig = fig + 1;
plot = [flip(WSU_tol) flip(chem_WSU_tol)];
bar(plot, 'stacked');
set(gca, 'XTick',1:7, 'XTickLabel',flip(toIs))
title('WSU Method for Tol-Hex Blends (Compared to IGD 331)')
xlabel('Fuel (% Tol / % Hex)')
ylabel('Ignition Delay (ms)')
legend(split,'Location','NorthEast')
grid on;
plotfixer;

```

#### 25% mindP variance for 8 analyzed fuels and Tol-Hex blends

```

mindP25 = xlsread('Master Fuel Data Sheet', 'Sheet1', 'G25:G32');
mindP25_tol = xlsread('Master Fuel Data Sheet', 'Sheet1', 'G35:G41');
IGD331 = xlsread('Master Fuel Data Sheet', 'Sheet1', 'G4:G11');
IGD331_tol = xlsread('Master Fuel Data Sheet', 'Sheet1', 'G14:G20');
chem_mindP25 = IGD331 - mindP25;
chem_mindP25_tol = IGD331_tol - mindP25_tol;

split = {'Physical', 'Chemical'};

figure(fig)
fig = fig + 1;
plot = [mindP25 chem_mindP25];
bar(plot, 'stacked');
set(gca, 'XTick',1:8, 'XTickLabel',fuels)
title('25% mindP Method for Analyzed Fuels (Compared to IGD 331)')
xlabel('Fuel')
ylabel('Ignition Delay (ms)')
legend(split,'Location','NorthEast')
grid on;
plotfixer;

figure(fig)
fig = fig + 1;
plot = [flip(mindP25_tol) flip(chem_mindP25_tol)];
bar(plot, 'stacked');
set(gca, 'XTick',1:7, 'XTickLabel',flip(toIs))
title('25% mindP Method for Tol-Hex Blends (Compared to IGD 331)')
xlabel('Fuel (% Tol / % Hex)')
ylabel('Ignition Delay (ms)')
legend(split,'Location','NorthEast')
grid on;
plotfixer;

```

#### 50% mindP variance for 8 analyzed fuels and Tol-Hex blends

```

mindP50 = xlsread('Master Fuel Data Sheet', 'Sheet1', 'J25:J32');
mindP50_tol = xlsread('Master Fuel Data Sheet', 'Sheet1', 'J35:J41');
IGD331 = xlsread('Master Fuel Data Sheet', 'Sheet1', 'G4:G11');
IGD331_tol = xlsread('Master Fuel Data Sheet', 'Sheet1', 'G14:G20');
chem_mindP50 = IGD331 - mindP50;
chem_mindP50_tol = IGD331_tol - mindP50_tol;

split = {'Physical', 'Chemical'};

figure(fig)
fig = fig + 1;
plot = [mindP50 chem_mindP50];
bar(plot, 'stacked');
set(gca, 'XTick',1:8, 'XTickLabel',fuels)
title('50% mindP Method for Analyzed Fuels (Compared to IGD 331)')
xlabel('Fuel')
ylabel('Ignition Delay (ms)')
legend(split,'Location','NorthEast')
grid on;
plotfixer;

figure(fig)

```

```

fig = fig + 1;
plot = [flip(mindP50_tol) flip(chem_mindP50_tol)];
bar(plot, 'stacked');
set(gca, 'XTick',1:7, 'XTickLabel',flip(toIs))
title('50% mindP Method for Tol-Hex Blends (Compared to IGD 331)')
xlabel('Fuel (% Tol / % Hex)')
ylabel('Ignition Delay (ms)')
legend(split, 'Location', 'NorthEast')
grid on;
plotfixer;

```

#### ddP variance for 8 analyzed fuels and Tol-Hex blends

```

ddP = xlsread('Master Fuel Data Sheet', 'Sheet1', 'M25:M32');
ddP_tol = xlsread('Master Fuel Data Sheet', 'Sheet1', 'M35:M41');
IGD331 = xlsread('Master Fuel Data Sheet', 'Sheet1', 'G4:G11');
IGD331_tol = xlsread('Master Fuel Data Sheet', 'Sheet1', 'G14:G20');
chem_ddP = IGD331 - ddP;
chem_ddP_tol = IGD331_tol - ddP_tol;

```

```
split = {'Physical', 'Chemical'};
```

```

figure(fig)
fig = fig + 1;
plot = [ddP chem_ddP];
bar(plot, 'stacked');
set(gca, 'XTick',1:8, 'XTickLabel',fuels)
title('ddP Method for Analyzed Fuels (Compared to IGD 331)')
xlabel('Fuel')
ylabel('Ignition Delay (ms)')
legend(split, 'Location', 'NorthEast')
grid on;
plotfixer;

```

```

figure(fig)
fig = fig + 1;
plot = [flip(ddP_tol) flip(chem_ddP_tol)];
bar(plot, 'stacked');
set(gca, 'XTick',1:7, 'XTickLabel',flip(toIs))
title('ddP Method for Tol-Hex Blends (Compared to IGD 331)')
xlabel('Fuel (% Tol / % Hex)')
ylabel('Ignition Delay (ms)')
legend(split, 'Location', 'NorthEast')
grid on;
plotfixer;

```

#### Ignition Delay Methods for 8 Major Fuels

```

IGD_IQT = xlsread('Master Fuel Data Sheet', 'Sheet1', 'D4:D11');
error_IQT = xlsread('Master Fuel Data Sheet', 'Sheet1', 'F4:F11');
IGD_331 = xlsread('Master Fuel Data Sheet', 'Sheet1', 'G4:G11');
error_331 = xlsread('Master Fuel Data Sheet', 'Sheet1', 'I4:I11');
IGD_310 = xlsread('Master Fuel Data Sheet', 'Sheet1', 'P4:P11');
error_310 = xlsread('Master Fuel Data Sheet', 'Sheet1', 'R4:R11');
IGD_10 = xlsread('Master Fuel Data Sheet', 'Sheet1', 'J4:J11');
error_10 = xlsread('Master Fuel Data Sheet', 'Sheet1', 'L4:L11');
IGD_5 = xlsread('Master Fuel Data Sheet', 'Sheet1', 'M4:M11');
error_5 = xlsread('Master Fuel Data Sheet', 'Sheet1', 'P4:P11');
IGD_mindP = xlsread('Master Fuel Data Sheet', 'Sheet1', 'D25:D32');
error_mindP = xlsread('Master Fuel Data Sheet', 'Sheet1', 'F25:F32');
methods = {'IQT', '331', '310', '10% CHRR', '5% CHRR', 'mindP'};
plot = [];
errorplot = [];
for i=1:8
    plot = [plot; IGD_IQT(i), IGD_331(i), IGD_310(i), IGD_10(i), IGD_5(i), IGD_mindP(i)];
    errorplot = [errorplot; error_IQT(i), error_331(i), error_310(i), error_10(i), error_5(i), error_mindP(i)];
end
figure(fig)
fig = fig + 1;
bar(plot)
hold on;
numgroups = size(plot, 1);
numbars = size(plot, 2);
groupwidth = min(0.8, numbars/(numbars+1.5));
for i = 1:numbars
    % Based on barweb.m by Bolu Ajiboye from MATLAB File Exchange
    x = (1:numgroups) - groupwidth/2 + (2*i-1) * groupwidth / (2*numbars); % Aligning error bar with
individual bar
    errorbar(x, plot(:,i), errorplot(:,i), 'k', 'linestyle', 'none');
end
fuels = {'CN30', 'JP5', 'F76', 'CN45', 'nc7', 'CN60', 'nc10', 'nc16'};

```

```

set(gca, 'XTick',1:8, 'XTickLabel',fuels)
grid on;
legend(methods)
plotfixer;
title('Fuel Ignition Delays for Various Methods for Analyzed Fuels')
xlabel('Fuel')
ylabel('Igniton Delay (ms)')

```

#### Ignition Delay Methods for Tol-Hex blends w/ JP5, F76

```

IGD_IQT_tol = xlsread('Master Fuel Data Sheet', 'Sheet1', 'D14:D20');
error_IQT_tol = xlsread('Master Fuel Data Sheet', 'Sheet1', 'F14:F20');
IGD_331_tol = xlsread('Master Fuel Data Sheet', 'Sheet1', 'G14:G20');
error_331_tol = xlsread('Master Fuel Data Sheet', 'Sheet1', 'I14:I20');
IGD_310_tol = xlsread('Master Fuel Data Sheet', 'Sheet1', 'P14:P20');
error_310_tol = xlsread('Master Fuel Data Sheet', 'Sheet1', 'R14:R20');
IGD_10_tol = xlsread('Master Fuel Data Sheet', 'Sheet1', 'J14:J20');
error_10_tol = xlsread('Master Fuel Data Sheet', 'Sheet1', 'L14:L20');
IGD_5_tol = xlsread('Master Fuel Data Sheet', 'Sheet1', 'M14:M20');
error_5_tol = xlsread('Master Fuel Data Sheet', 'Sheet1', 'O14:O20');
IGD_mindP_tol = xlsread('Master Fuel Data Sheet', 'Sheet1', 'D35:D41');
error_mindP_tol = xlsread('Master Fuel Data Sheet', 'Sheet1', 'F35:F41');

IGD_IQT_conv = xlsread('Master Fuel Data Sheet', 'Sheet1', 'D5:D6');
error_IQT_conv = xlsread('Master Fuel Data Sheet', 'Sheet1', 'F5:F6');
IGD_331_conv = xlsread('Master Fuel Data Sheet', 'Sheet1', 'G5:G6');
error_331_conv = xlsread('Master Fuel Data Sheet', 'Sheet1', 'I5:I6');
IGD_310_conv = xlsread('Master Fuel Data Sheet', 'Sheet1', 'P5:P6');
error_310_conv = xlsread('Master Fuel Data Sheet', 'Sheet1', 'R5:R6');
IGD_10_conv = xlsread('Master Fuel Data Sheet', 'Sheet1', 'J5:J6');
error_10_conv = xlsread('Master Fuel Data Sheet', 'Sheet1', 'L5:L6');
IGD_5_conv = xlsread('Master Fuel Data Sheet', 'Sheet1', 'M5:M6');
error_5_conv = xlsread('Master Fuel Data Sheet', 'Sheet1', 'P5:P6');
IGD_mindP_conv = xlsread('Master Fuel Data Sheet', 'Sheet1', 'D26:D27');
error_mindP_conv = xlsread('Master Fuel Data Sheet', 'Sheet1', 'F26:F27');
methods = {'IQT', '331', '310', '10% CHRR', '5% CHRR', 'mindP'};
plot = [];
errorplot = [];

for i=1:7
    plot = [plot; IGD_IQT_tol(8-i), IGD_331_tol(8-i), IGD_310_tol(8-i), IGD_10_tol(8-i), IGD_5_tol(8-i),
    IGD_mindP_tol(8-i)];
    errorplot = [errorplot; error_IQT_tol(8-i), error_331_tol(8-i), error_310_tol(8-i), error_10_tol(8-i),
    error_5_tol(8-i), error_mindP_tol(8-i)];
end

for i=1:2
    plot = [plot; IGD_IQT_conv(i), IGD_331_conv(i), IGD_310_conv(i), IGD_10_conv(i), IGD_5_conv(i),
    IGD_mindP_conv(i)];
    errorplot = [errorplot; error_IQT_conv(i), error_331_conv(i), error_310_conv(i), error_10_conv(i),
    error_5_conv(i), error_mindP_conv(i)];
end

figure(fig)
fig = fig + 1;
bar(plot)
hold on;
numgroups = size(plot, 1);
numbars = size(plot, 2);
groupwidth = min(0.8, numbars/(numbars+1.5));
for i = 1:numbars
    % Based on barweb.m by Bolu Ajiboye from MATLAB File Exchange
    x = (1:numgroups) - groupwidth/2 + (2*i-1) * groupwidth / (2*numbars); % Aligning error bar with
individual bar
    errorbar(x, plot(:,i), errorplot(:,i), 'k', 'linestyle', 'none');
end
tols2 = {'75/25', '74/26', '72/28', '70/30', '65/35', '60/40', '50/50', 'JP5', 'F76'};
set(gca, 'XTick',1:9, 'XTickLabel',tols2)
grid on;
legend(methods, 'Location', 'NorthEast')
title('Fuel Ignition Delays for Various Methods for Tol-Hex Blends')
xlabel('Fuel (% Tol / % Hex)')
ylabel('Igniton Delay (ms)')
plotfixer;

```

#### Ignition delays relative to IQT for each fuel

```

IGD_IQT = xlsread('Master Fuel Data Sheet', 'Sheet1', 'D4:D11');
error_IQT = xlsread('Master Fuel Data Sheet', 'Sheet1', 'F4:F11');
IGD_331 = xlsread('Master Fuel Data Sheet', 'Sheet1', 'G4:G11');
error_331 = xlsread('Master Fuel Data Sheet', 'Sheet1', 'I4:I11');

```

```

IGD_310 = xlsread('Master Fuel Data Sheet', 'Sheet1', 'P4:P11');
error_310 = xlsread('Master Fuel Data Sheet', 'Sheet1', 'R4:R11');
IGD_10 = xlsread('Master Fuel Data Sheet', 'Sheet1', 'J4:J11');
error_10 = xlsread('Master Fuel Data Sheet', 'Sheet1', 'L4:L11');
IGD_5 = xlsread('Master Fuel Data Sheet', 'Sheet1', 'M4:M11');
error_5 = xlsread('Master Fuel Data Sheet', 'Sheet1', 'P4:P11');
IGD_mindP = xlsread('Master Fuel Data Sheet', 'Sheet1', 'D25:D32');
error_mindP = xlsread('Master Fuel Data Sheet', 'Sheet1', 'F25:F32');

rel_331 = IGD_331 - IGD_IQT;
rel_310 = IGD_310 - IGD_IQT;
rel_10 = IGD_10 - IGD_IQT;
rel_5 = IGD_5 - IGD_IQT;
rel_mindP = IGD_mindP - IGD_IQT;
methods = {'331', '310', '10% CHRR', '5% CHRR', 'mindP'};
plot = [];
for i=1:8
    plot = [plot; rel_331(i), rel_310(i), rel_10(i), rel_5(i), rel_mindP(i)];
end
figure(fig)
fig = fig + 1;
bar(plot)
fuels = {'CN30', 'JP5', 'F76', 'CN45', 'nc7', 'CN60', 'nc10', 'nc16'};
set(gca, 'XTick', 1:8, 'XTickLabel', fuels)
grid on;
legend(methods, 'Location', 'SouthEast')
title('Fuel Ignition Delays Relative to IQT Ignition Delays for Analyzed Fuels')
xlabel('Fuel')
ylabel('Relative Igniton Delay (ms)')
plotfixer;

```

#### Ignition delays relative to IQT for each fuel w/o mindP

```

IGD_IQT = xlsread('Master Fuel Data Sheet', 'Sheet1', 'D4:D11');
error_IQT = xlsread('Master Fuel Data Sheet', 'Sheet1', 'F4:F11');
IGD_331 = xlsread('Master Fuel Data Sheet', 'Sheet1', 'G4:G11');
error_331 = xlsread('Master Fuel Data Sheet', 'Sheet1', 'I4:I11');
IGD_310 = xlsread('Master Fuel Data Sheet', 'Sheet1', 'P4:P11');
error_310 = xlsread('Master Fuel Data Sheet', 'Sheet1', 'R4:R11');
IGD_10 = xlsread('Master Fuel Data Sheet', 'Sheet1', 'J4:J11');
error_10 = xlsread('Master Fuel Data Sheet', 'Sheet1', 'L4:L11');
IGD_5 = xlsread('Master Fuel Data Sheet', 'Sheet1', 'M4:M11');
error_5 = xlsread('Master Fuel Data Sheet', 'Sheet1', 'P4:P11');

rel_331 = IGD_331 - IGD_IQT;
rel_310 = IGD_310 - IGD_IQT;
rel_10 = IGD_10 - IGD_IQT;
rel_5 = IGD_5 - IGD_IQT;
methods = {'331', '310', '10% CHRR', '5% CHRR'};
plot = [];
for i=1:8
    plot = [plot; rel_331(i), rel_310(i), rel_10(i), rel_5(i)];
end
figure(fig)
fig = fig + 1;
bar(plot)
fuels = {'CN30', 'JP5', 'F76', 'CN45', 'nc7', 'CN60', 'nc10', 'nc16'};
set(gca, 'XTick', 1:8, 'XTickLabel', fuels)
grid on;
legend(methods, 'Location', 'SouthEast')
title('Fuel Ignition Delays Relative to IQT Ignition Delays for Analyzed Fuels')
xlabel('Fuel')
ylabel('Relative Igniton Delay (ms)')
plotfixer;

```

#### Ignition delays relative to nc7 331

```

IGD_IQT = xlsread('Master Fuel Data Sheet', 'Sheet1', 'D4:D11');
error_IQT = xlsread('Master Fuel Data Sheet', 'Sheet1', 'F4:F11');
IGD_331 = xlsread('Master Fuel Data Sheet', 'Sheet1', 'G4:G11');
error_331 = xlsread('Master Fuel Data Sheet', 'Sheet1', 'I4:I11');
IGD_310 = xlsread('Master Fuel Data Sheet', 'Sheet1', 'P4:P11');
error_310 = xlsread('Master Fuel Data Sheet', 'Sheet1', 'R4:R11');
IGD_10 = xlsread('Master Fuel Data Sheet', 'Sheet1', 'J4:J11');
error_10 = xlsread('Master Fuel Data Sheet', 'Sheet1', 'L4:L11');
IGD_5 = xlsread('Master Fuel Data Sheet', 'Sheet1', 'M4:M11');
error_5 = xlsread('Master Fuel Data Sheet', 'Sheet1', 'P4:P11');
IGD_mindP = xlsread('Master Fuel Data Sheet', 'Sheet1', 'D25:D32');
error_mindP = xlsread('Master Fuel Data Sheet', 'Sheet1', 'F25:F32');
methods = {'IQT', '331', '310', '10% CHRR', '5% CHRR', 'mindP'};
plot = [];

```



```

for i=1:4
    plot = [plot; IGD_IQT(i)/IGD_IQT(5), IGD_331(i)/IGD_331(5), IGD_310(i)/IGD_310(5), IGD_10(i)/IGD_10(5),
    IGD_5(i)/IGD_5(5), IGD_mindP(i)/IGD_mindP(5)];
end
for i=6:8
    plot = [plot; IGD_IQT(i)/IGD_IQT(5), IGD_331(i)/IGD_331(5), IGD_310(i)/IGD_310(5), IGD_10(i)/IGD_10(5),
    IGD_5(i)/IGD_5(5), IGD_mindP(i)/IGD_mindP(5)];
end
figure(fig)
fig = fig + 1;
bar(plot)
fuels = {'CN30', 'JP5', 'F76', 'CN45', 'CN60', 'nc10', 'nc16'};
set(gca, 'XTick',1:7, 'XTickLabel',fuels)
grid on;
legend(methods)
title('Fuel Ignition Delays for Various Methods Relative to nc7')
xlabel('Fuel')
ylabel('Fuel Delay / nc7 Delay')
plotfixer;

```

#### nc7 Cumulative Heat Release Rate IGD values 2%-10%

```

CHRR = xlsread('Master Fuel Data Sheet', 'Sheet1', 'C45:C53');
figure(fig)
fig = fig+1;
bar(CHRR)
percentages = {'2', '3', '4', '5', '6', '7', '8', '9', '10'};
set(gca, 'XTick',1:9, 'XTickLabel',percentages);
grid on;
xlabel('CHRR Percentage (%)');
ylabel('Ignition Delay (ms)');
title('nc7 CHRR Ignition Delays');
axis([0 10 3.7 4]);
plotfixer;

```

#### nc7 Cumulative Heat Release Rate Analysis w/ IQT

```

CHRR = xlsread('Master Fuel Data Sheet', 'Sheet1', 'C45:C53');
IQTref = xlsread('Master Fuel Data Sheet', 'Sheet1', 'C54');
relval = CHRR-IQTref;

figure(fig)
fig = fig+1;
bar(relval)
percentages = {'2', '3', '4', '5', '6', '7', '8', '9', '10'};
set(gca, 'XTick',1:9, 'XTickLabel',percentages);
grid on;
xlabel('CHRR Percentage (%)');
ylabel('Relative Ignition Delay (ms)');
title('nc7 CHRR Ignition Delays Relative to IQT Delay');
plotfixer;

```

#### Modified Droplet Diameter/weber #/Break-up Time vs. DCN

```

dropdiam = xlsread('Master Fuel Data Sheet', 'Sheet1', 'I45:I52');
weber = xlsread('Master Fuel Data Sheet', 'Sheet1', 'J45:J52');
breakup = xlsread('Master Fuel Data Sheet', 'Sheet1', 'K45:K52');

figure(fig)
fig = fig + 1;
bar(dropdiam);
fuels = {'CN30', 'JP5', 'F76', 'nc7', 'CN45', 'CN60', 'nc10', 'nc16'};
set(gca, 'XTick',1:8, 'XTickLabel',fuels);
grid on;
title('Modified Droplet Diameter vs. Fuel')
xlabel('Fuel')
ylabel('Modified Droplet Diameter')
plotfixer;

figure(fig)
fig = fig + 1;
bar(dropdiam);
DCN = num2cell(xlsread('Master Fuel Data Sheet', 'Sheet1', 'H45:H52'))';
set(gca, 'XTick',1:8, 'XTickLabel',DCN);
grid on;
title('Modified Droplet Diameter vs. DCN')
xlabel('DCN')
ylabel('Modified Droplet Diameter')
plotfixer;

```

```

figure(fig)
fig = fig + 1;
bar(weber);
fuels = {'CN30', 'JP5', 'F76', 'nC7', 'CN45', 'CN60', 'nC10', 'nC16'};
set(gca, 'XTick',1:8, 'XTickLabel',fuels);
grid on;
title('Weber Number vs. Fuel')
xlabel('Fuel')
ylabel('Weber Number')
plotfixer;

figure(fig)
fig = fig + 1;
bar(weber);
set(gca, 'XTick',1:8, 'XTickLabel',DCN);
grid on;
title('Modified Droplet Diameter vs. DCN')
xlabel('DCN')
ylabel('Modified Droplet Diameter')
plotfixer;

figure(fig)
fig = fig + 1;
bar(breakup);
fuels = {'CN30', 'JP5', 'F76', 'nC7', 'CN45', 'CN60', 'nC10', 'nC16'};
set(gca, 'XTick',1:8, 'XTickLabel',fuels);
grid on;
title('Break-up Time vs. Fuel')
xlabel('Fuel')
ylabel('Break-up Time (s)')
plotfixer;

figure(fig)
fig = fig + 1;
bar(breakup);
set(gca, 'XTick',1:8, 'XTickLabel',DCN);
grid on;
title('Break-up Time vs. DCN')
xlabel('DCN')
ylabel('Break-up Time (s)')
plotfixer;

```

#### Laurence Livermore Kinetics Comparison - Conventional

```

llchem_conv = xlsread('Master Fuel Data Sheet', 'Sheet1', 'D58:D60');
ddPchem_conv = xlsread('Master Fuel Data Sheet', 'Sheet1', 'E58:E60');
llchem_tol = xlsread('Master Fuel Data Sheet', 'Sheet1', 'H58:H61');
ddPchem_tol = xlsread('Master Fuel Data Sheet', 'Sheet1', 'I58:I61');

plot = [];
for i = 1:3
    plot=[plot; ddPchem_conv(i), llchem_conv(i)]
end
LLlegend = {'ddP Chem Delay (compared to 331 standard)', 'Laurence Livermore Kinetics Chem Delay'};
figure(fig)
fig = fig + 1;
bar(plot)
llfuels_conv = {'Heptane (nC7)', 'Decane (nC10)', 'Hexadecane (nC16)'};
set(gca, 'XTick',1:3, 'XTickLabel',llfuels_conv);
grid on;
title('LLK Delay Comparison for Pure Component Fuels');
xlabel('Fuel')
ylabel('Chemical Ignition Delay (ms)')
legend(LLlegend, 'Location', 'NorthEast');

```

#### Laurence Livermore Kinetics Comparison - Tol-Hex

```

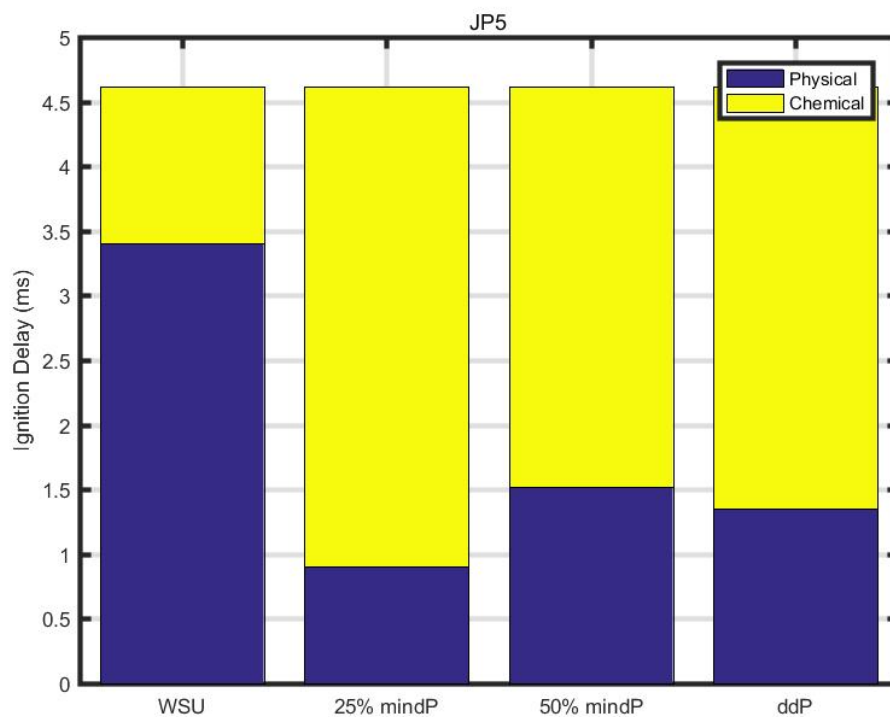
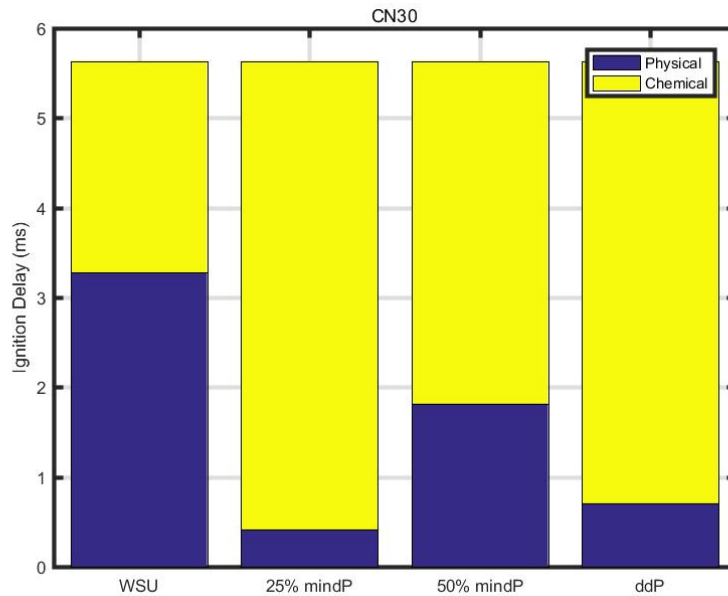
plot = [];
for i = 1:4
    plot=[plot; ddPchem_tol(i), llchem_tol(i)]
end
figure(fig)
fig = fig + 1;
bar(plot)
llfuels_tol = {'75/25', '70/30', '65/35', '60/40'};
set(gca, 'XTick',1:4, 'XTickLabel',llfuels_tol);
title('LLK Chem Delay Comparison for Tol-Hex Blends');
xlabel('Fuel (% Tol / % Hex)')
ylabel('Chemical Ignition Delay (ms)')

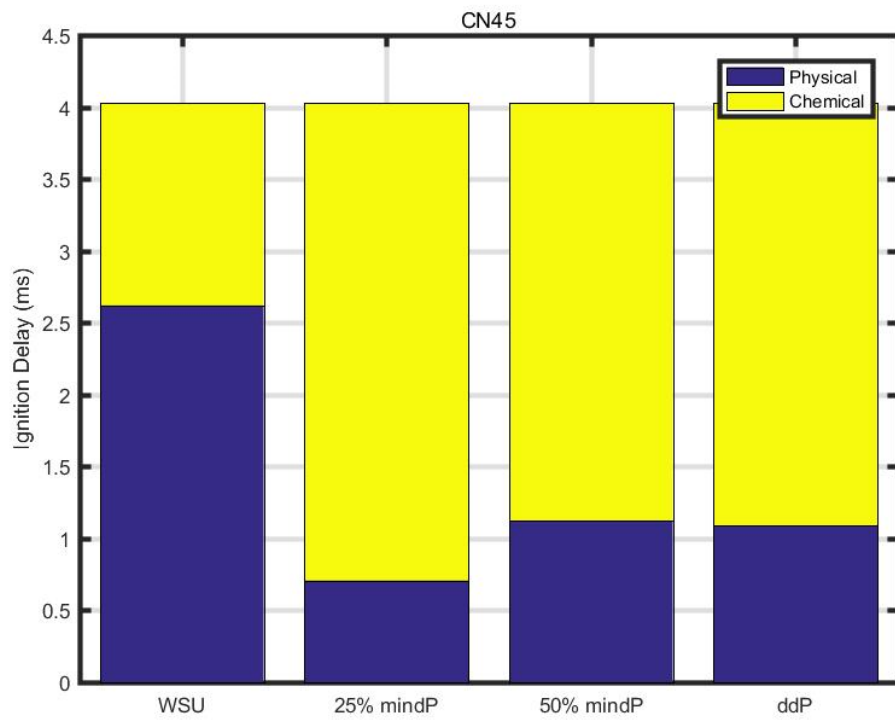
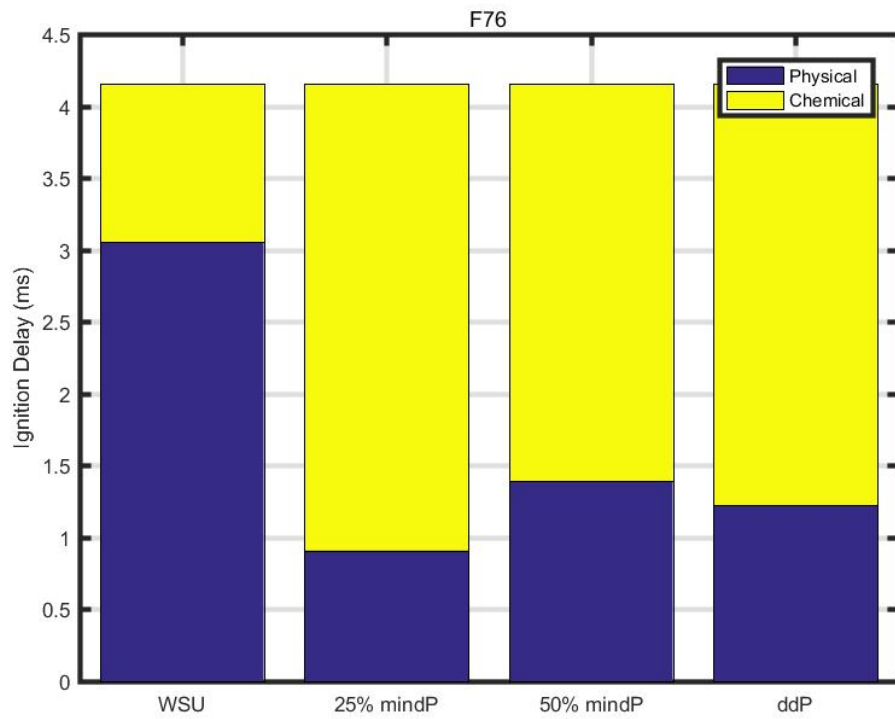
```

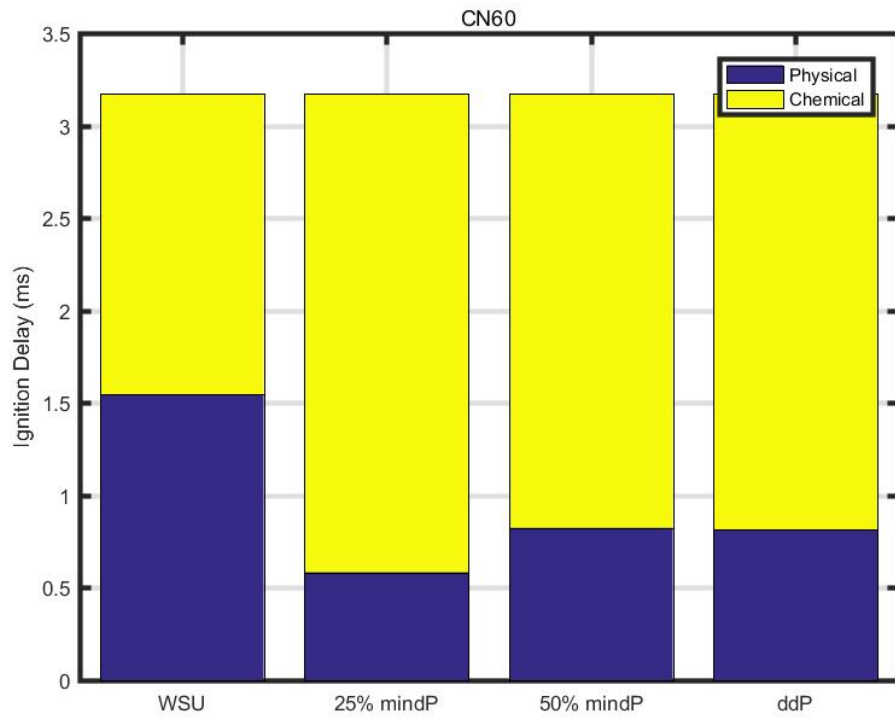
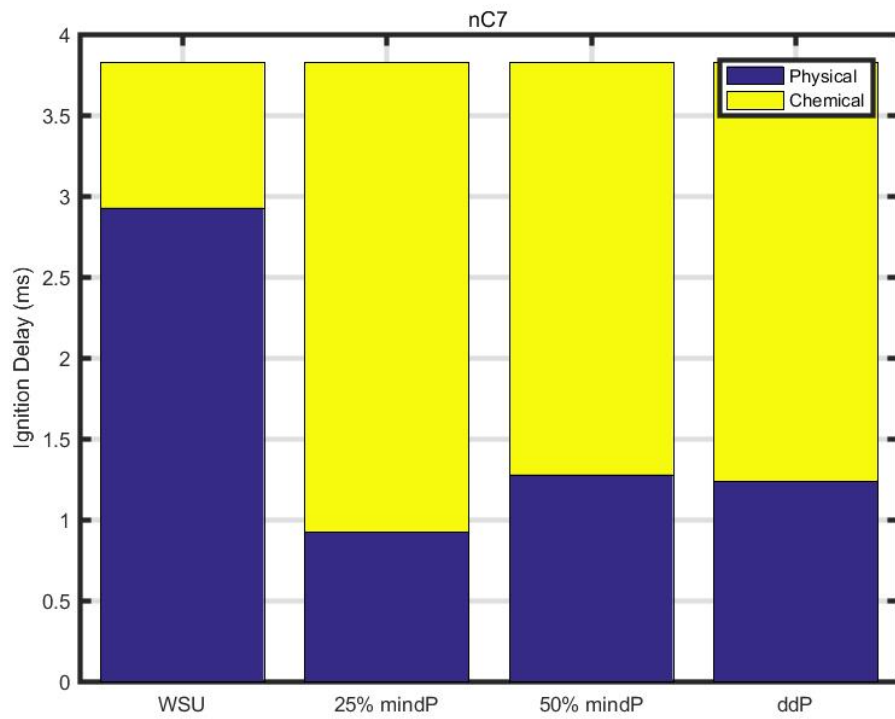
```
grid on;  
Legend(LLlegend, 'Location', 'NorthEast');
```

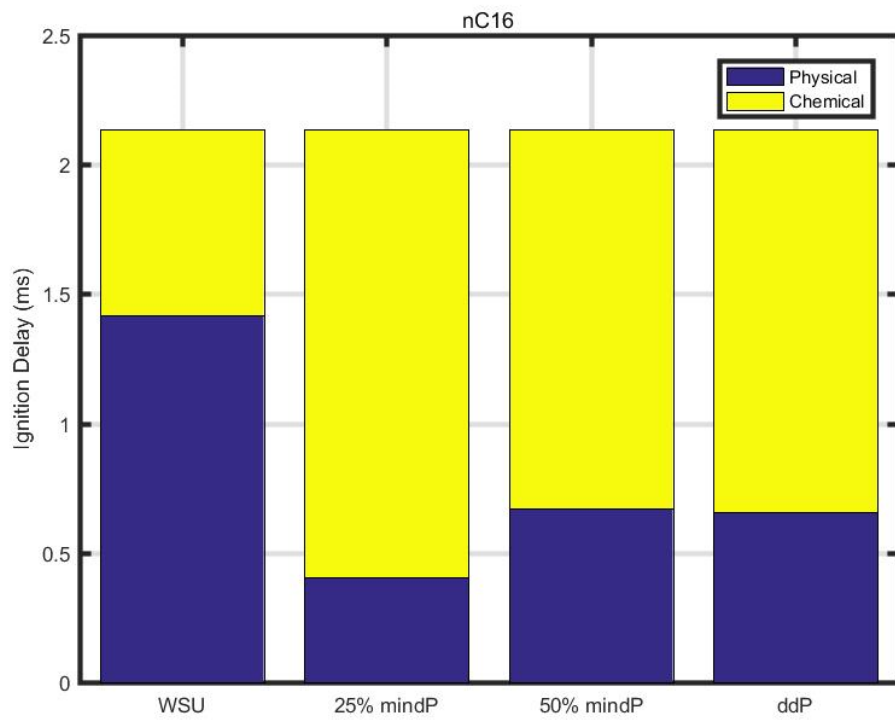
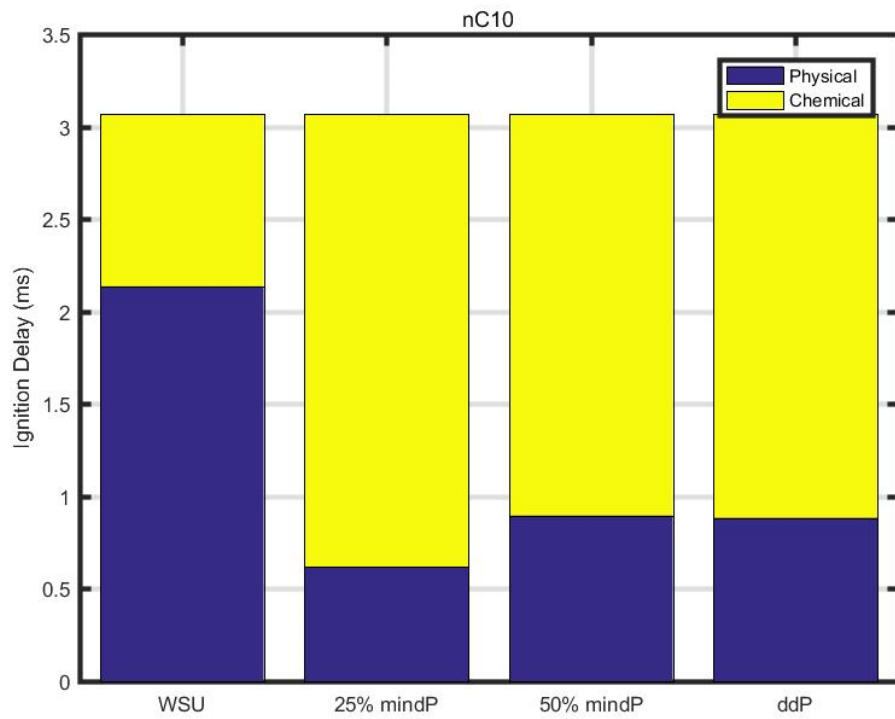
#### Saving figures to a presentation directory

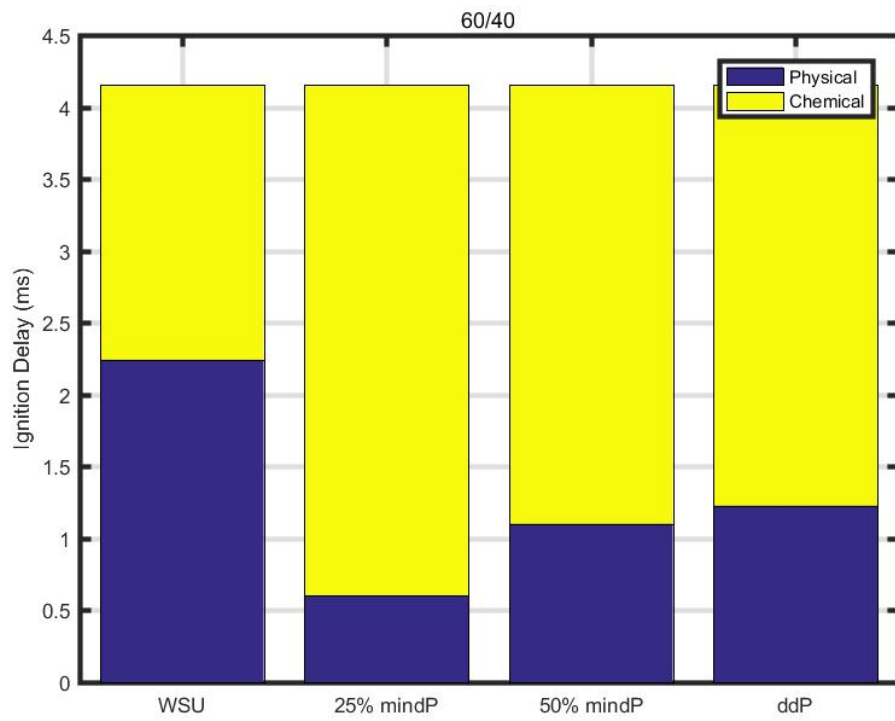
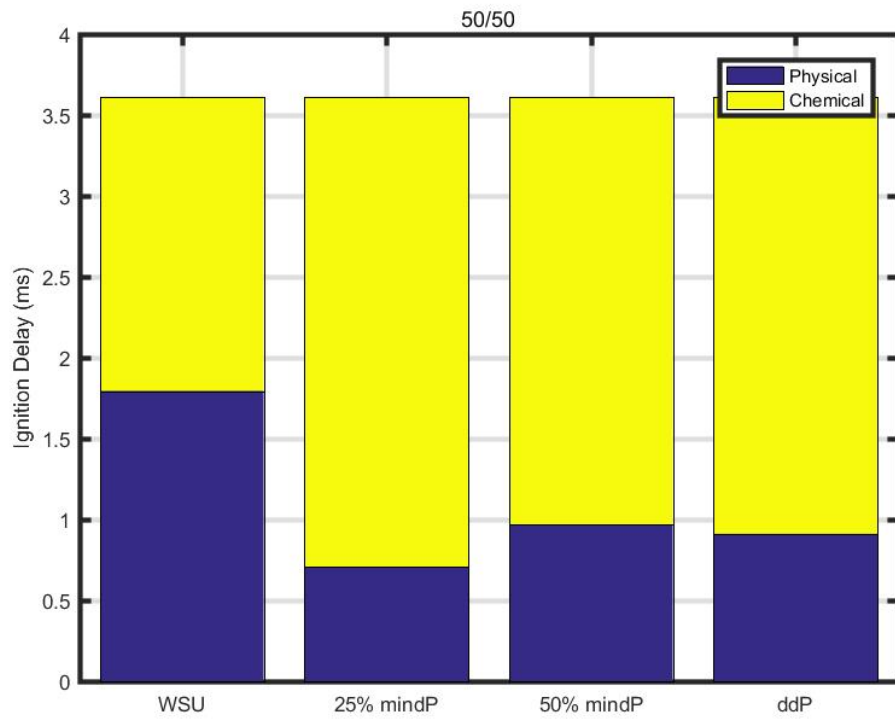
```
for loopIndex = 1:(fig-1)  
    baseFileName = sprintf('figure_%d.jpg', loopIndex);  
    fullFileName = fullfile('C:\DIRECTORYNAME', baseFileName);  
    saveas(figure(loopIndex), fullFileName);  
end
```

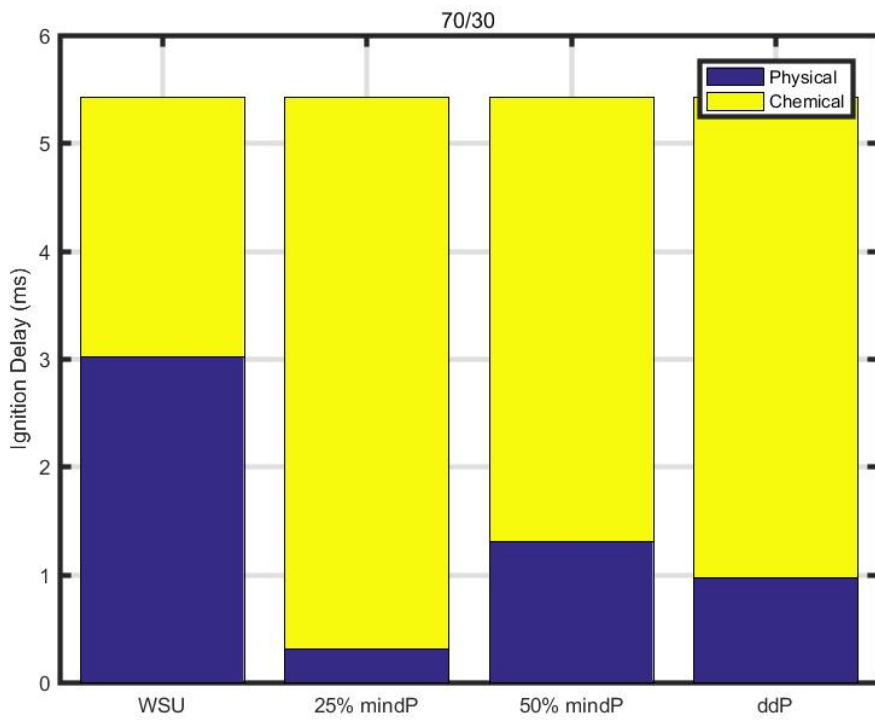
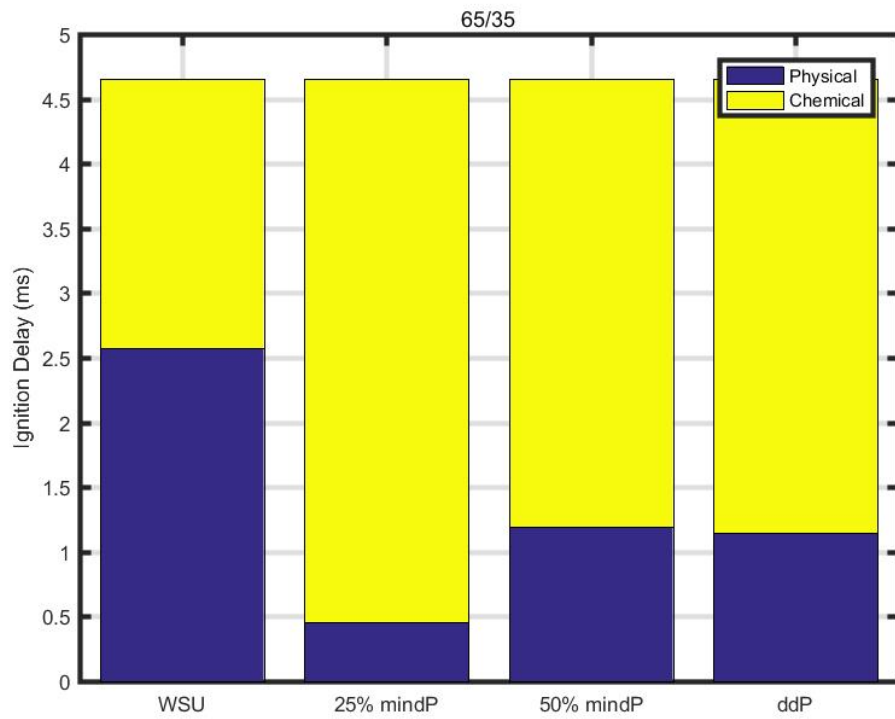




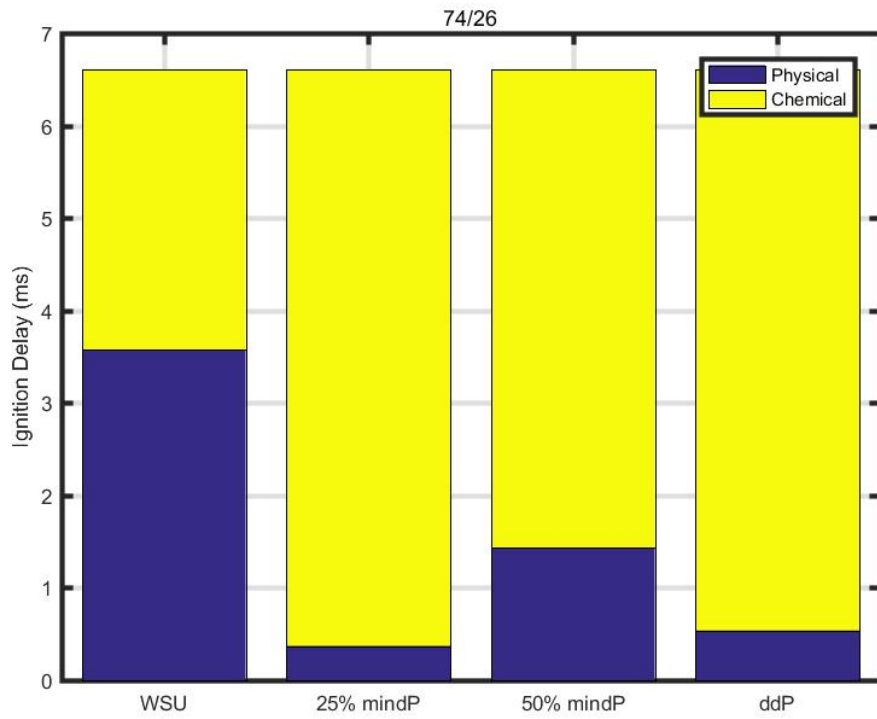
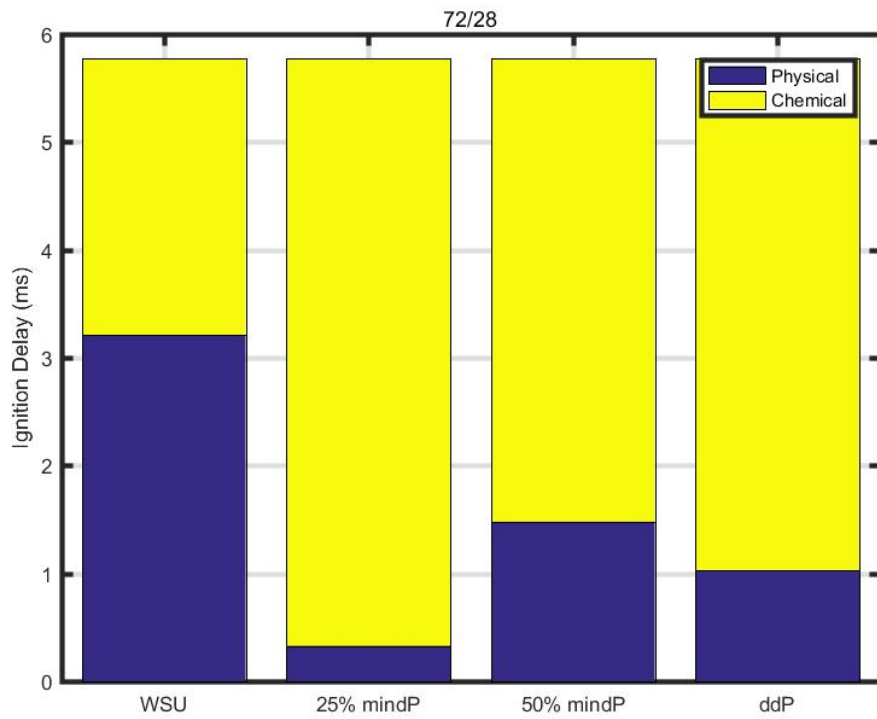


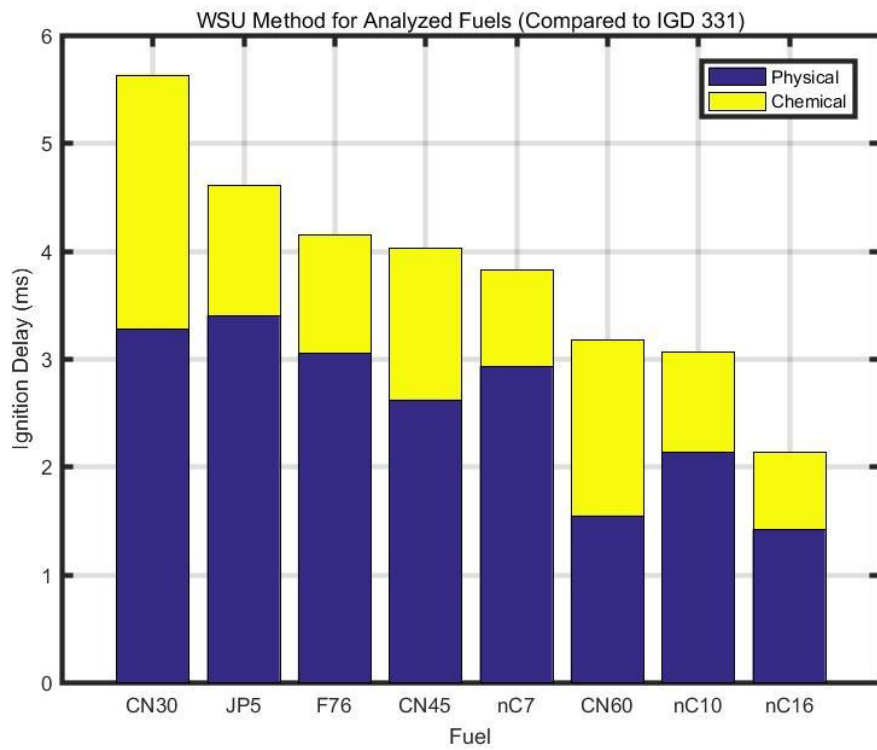
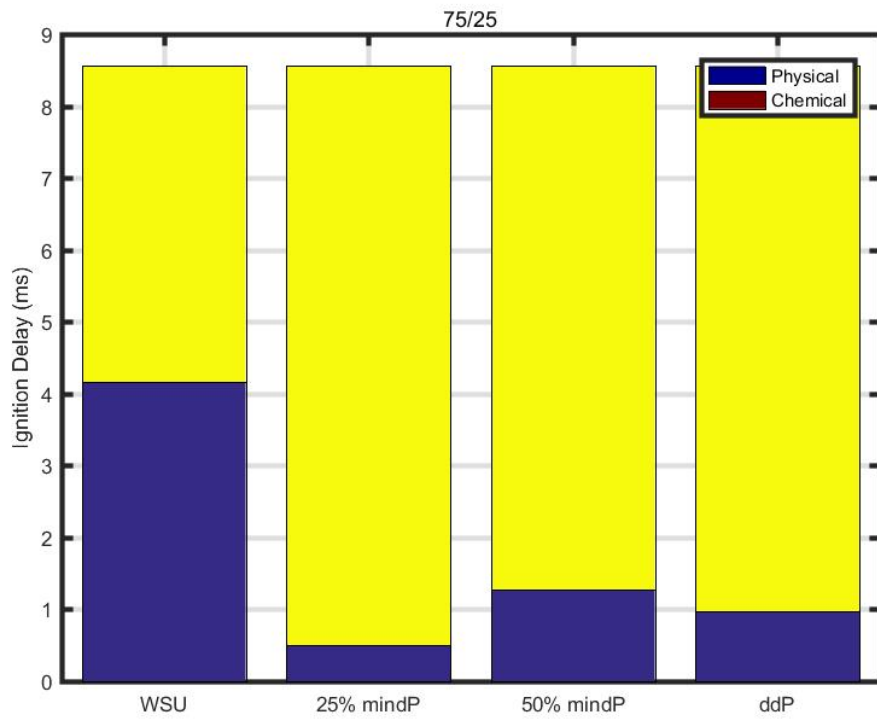


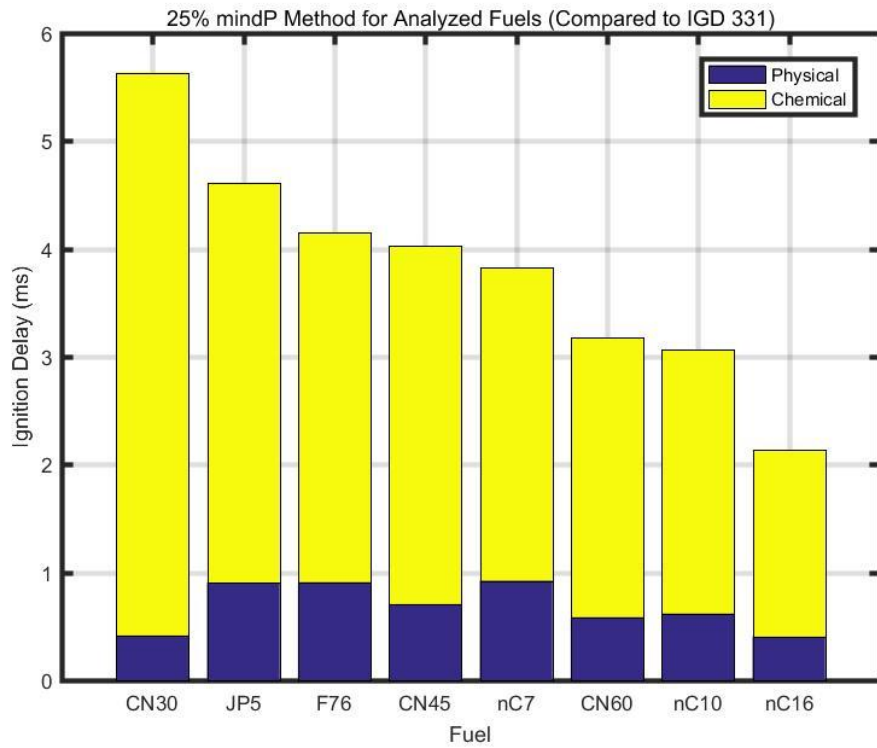
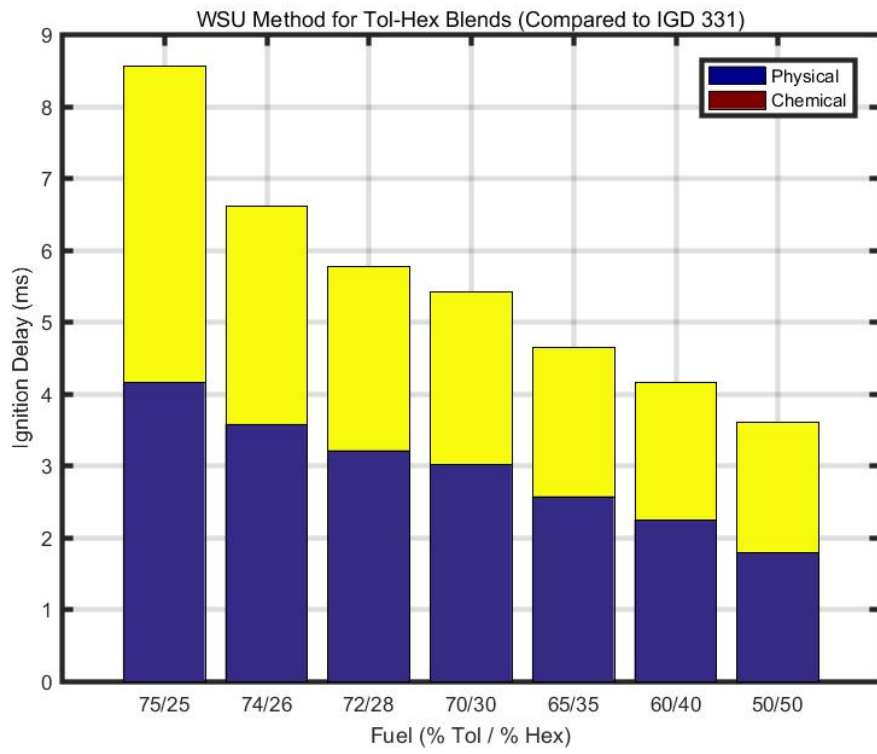


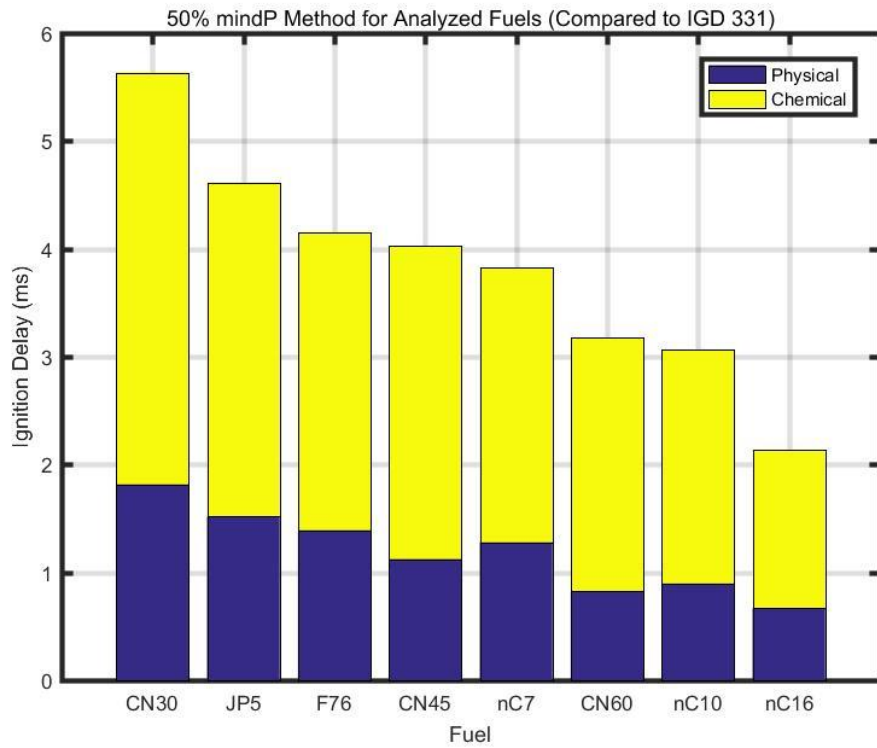
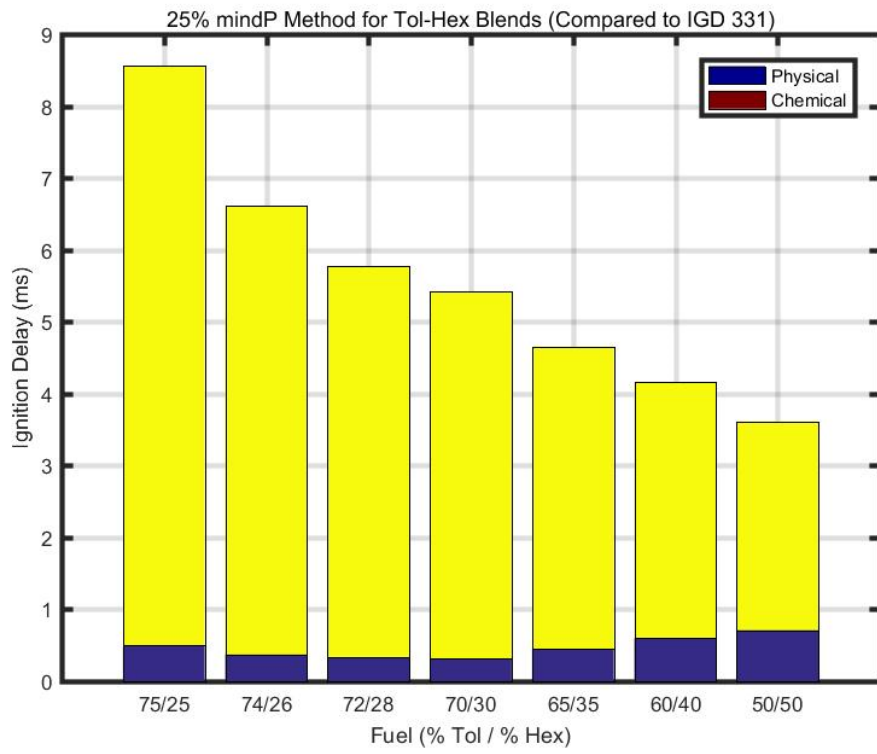


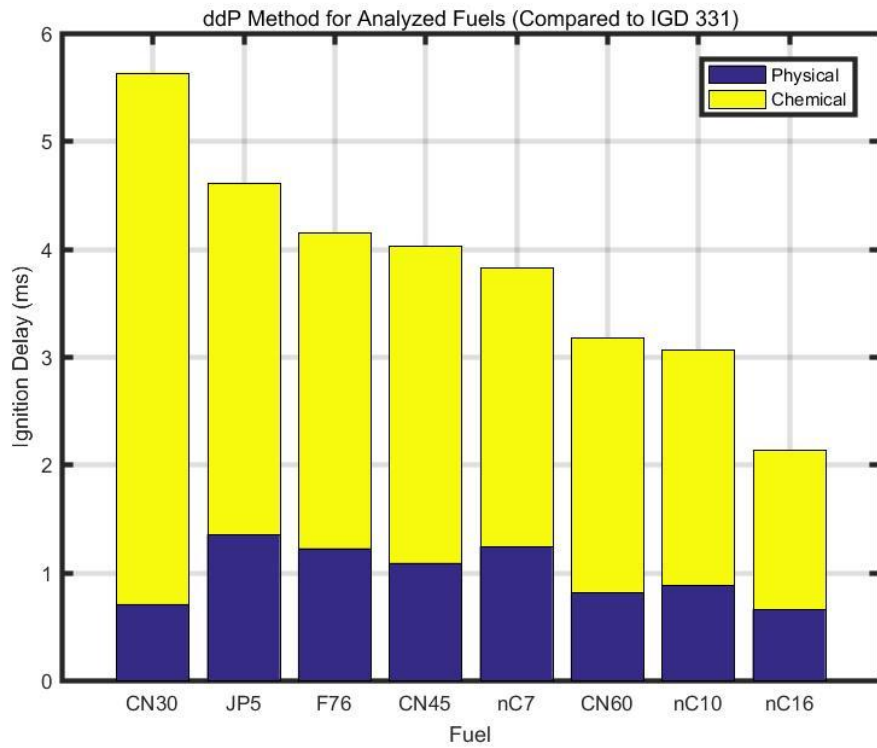
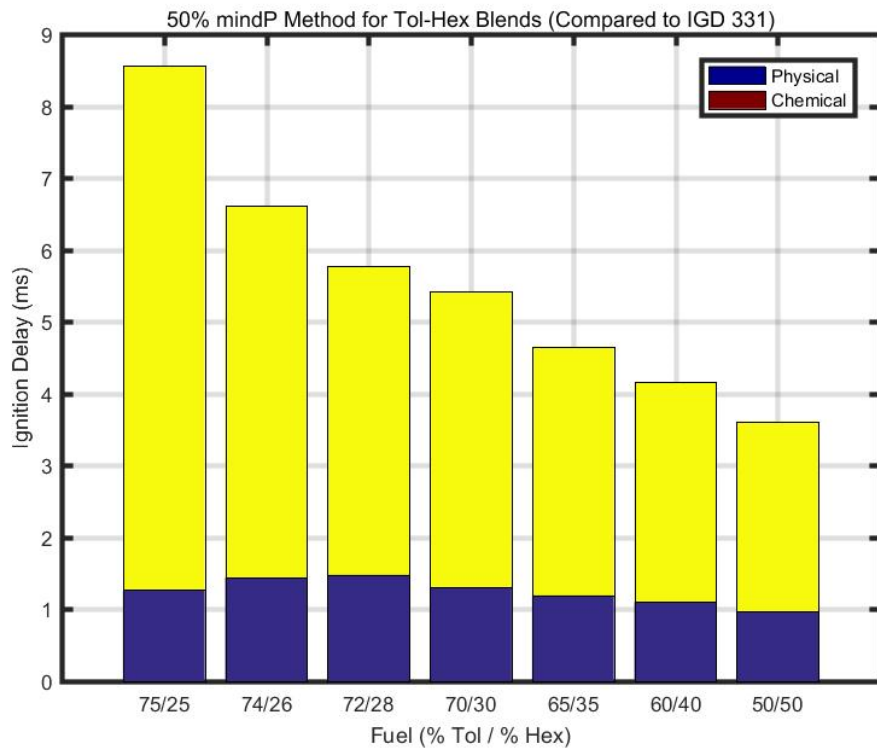


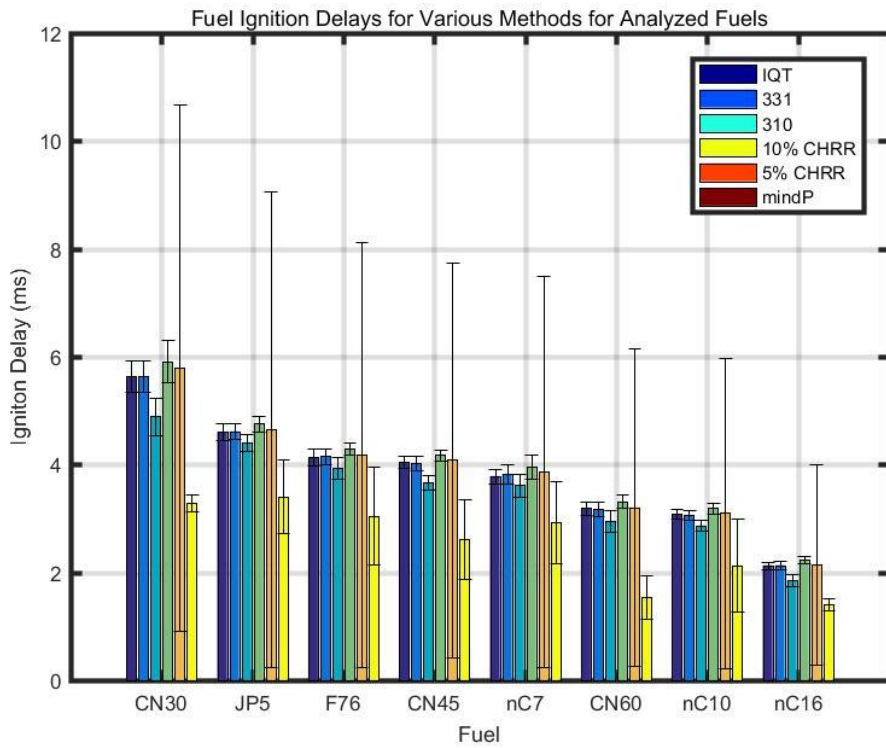
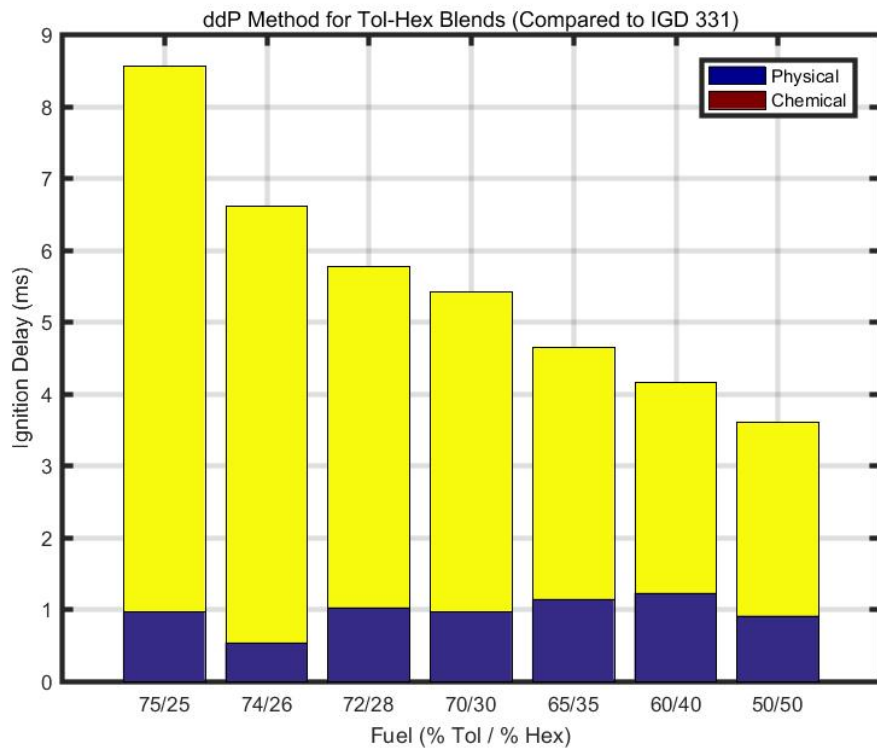


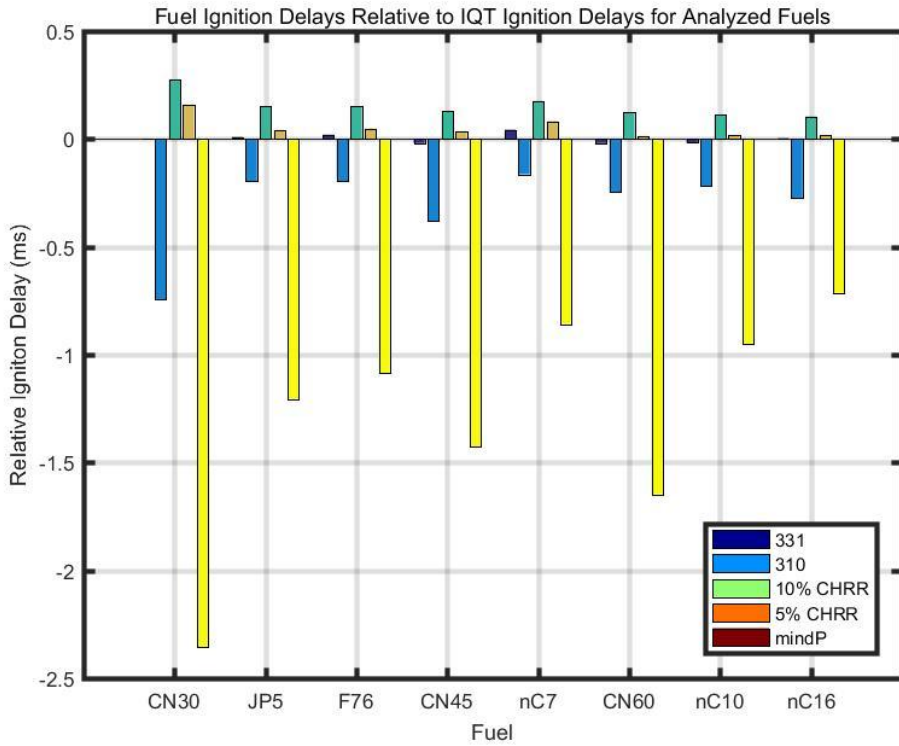
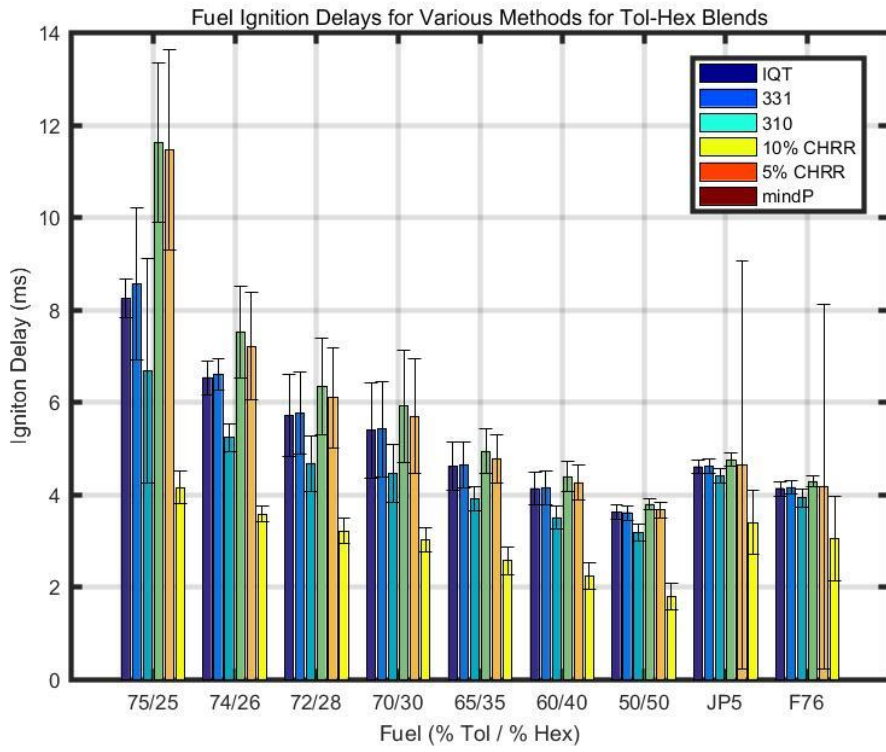


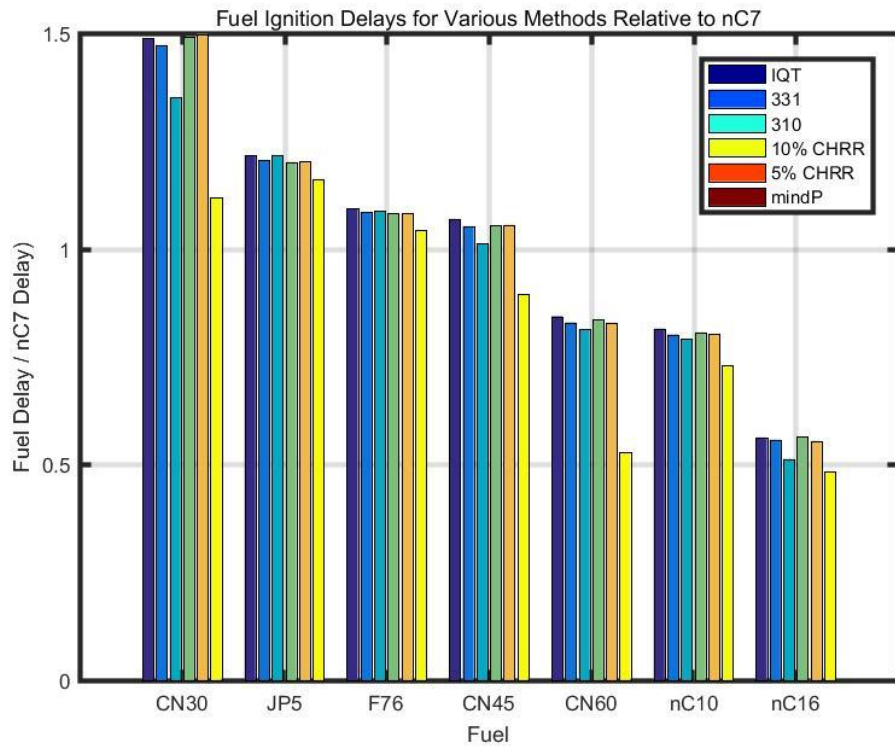
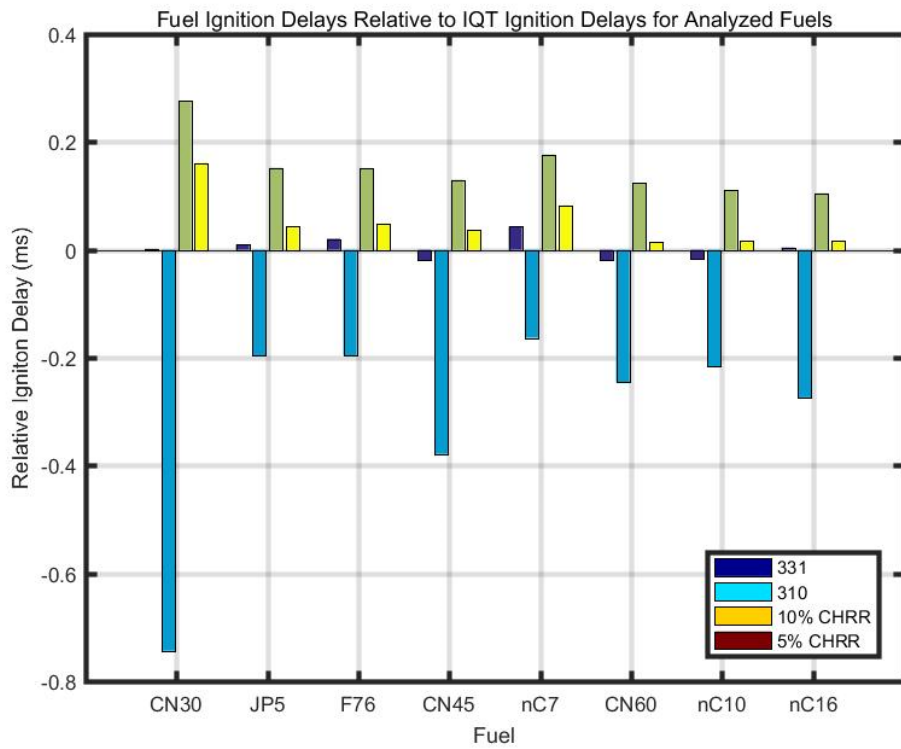




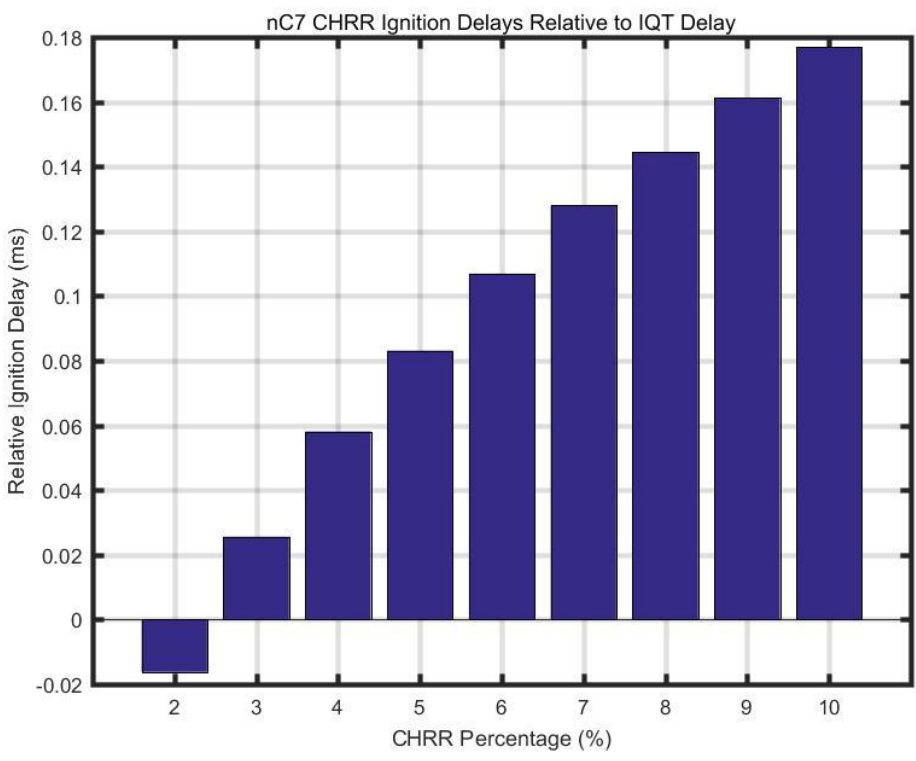
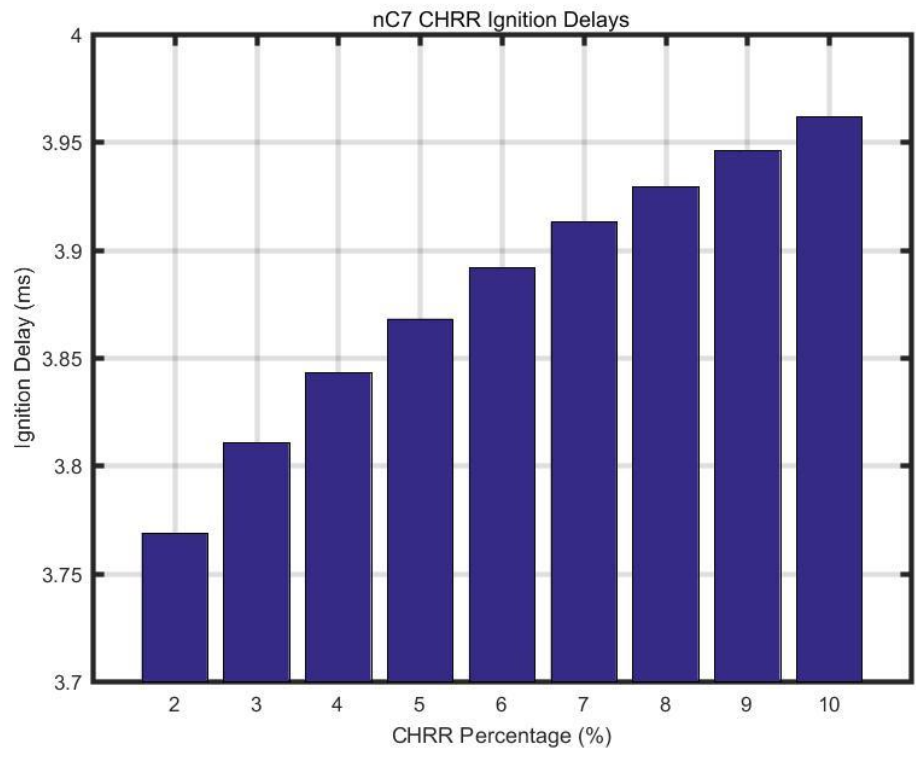


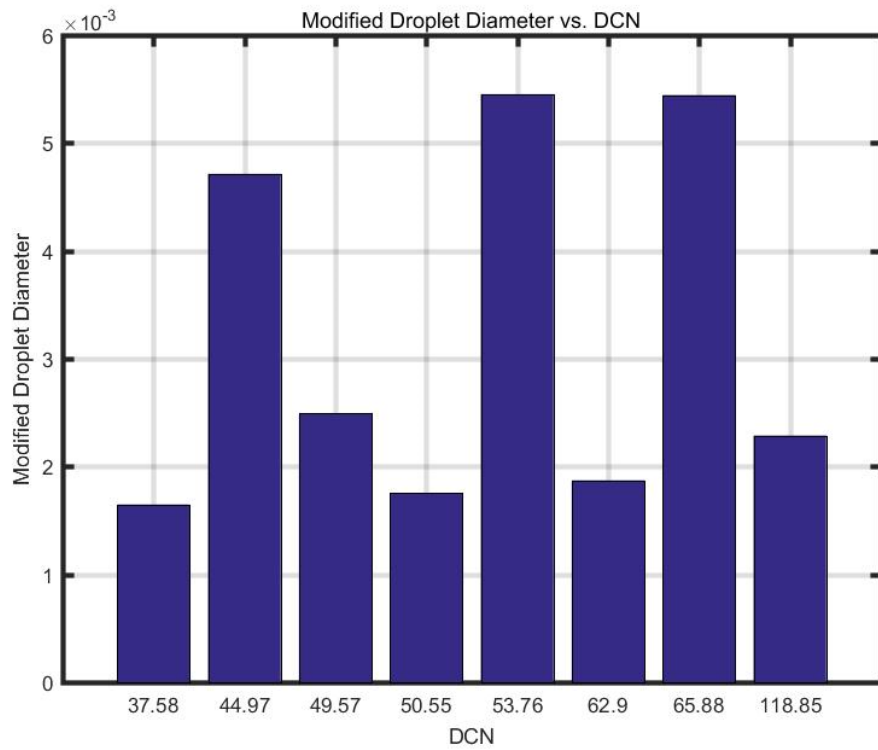
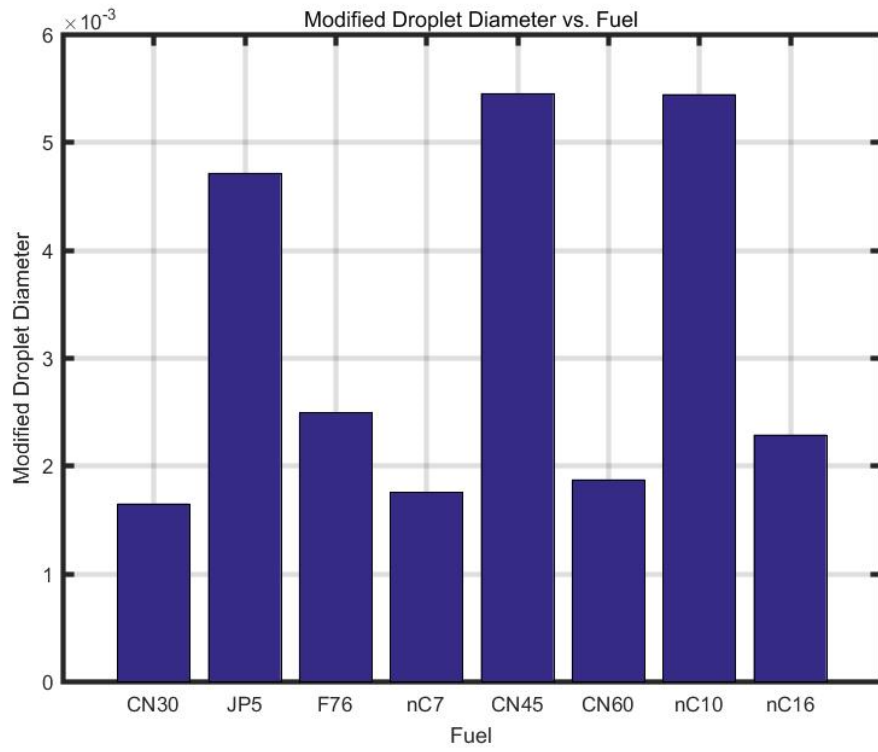


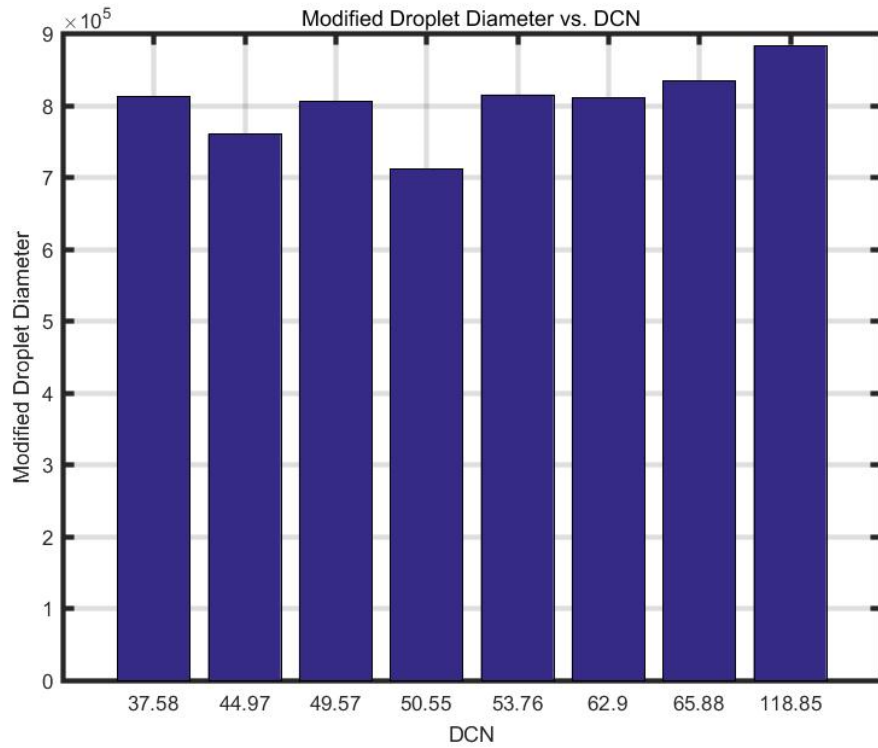
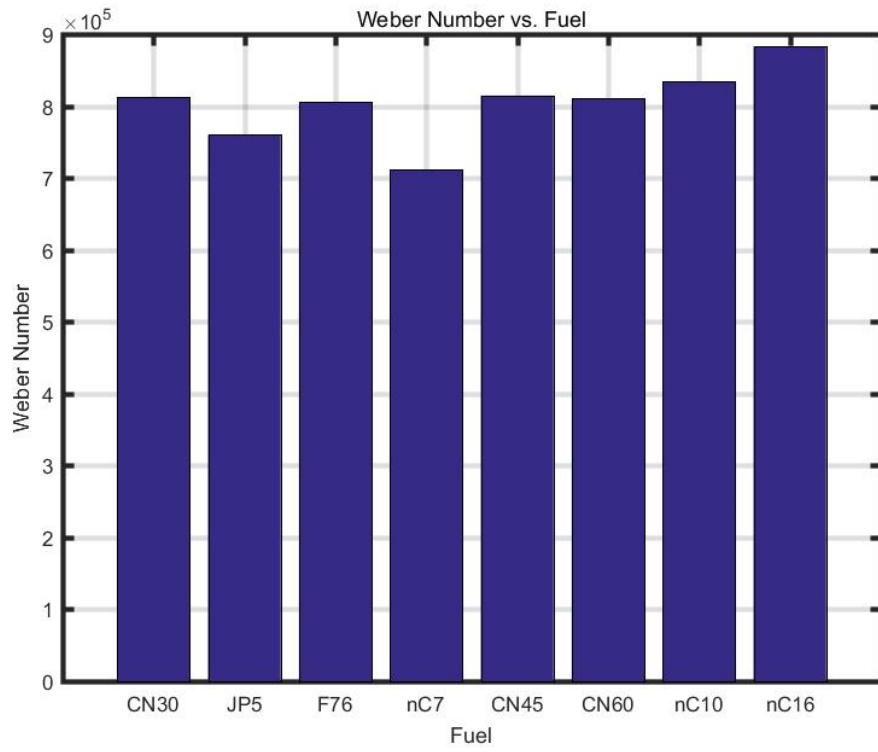


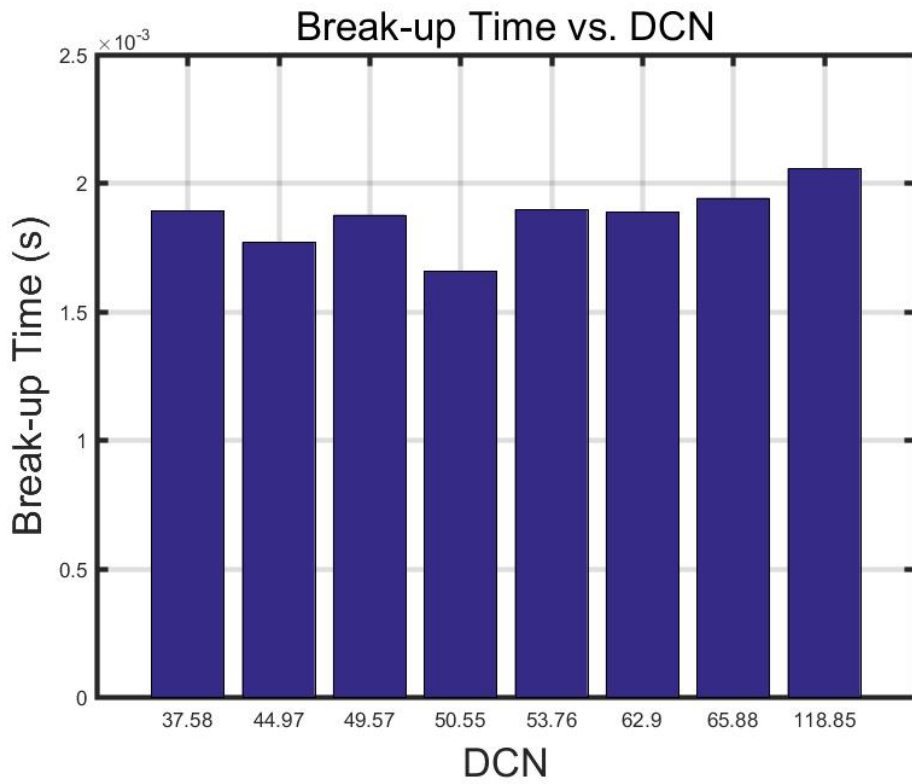
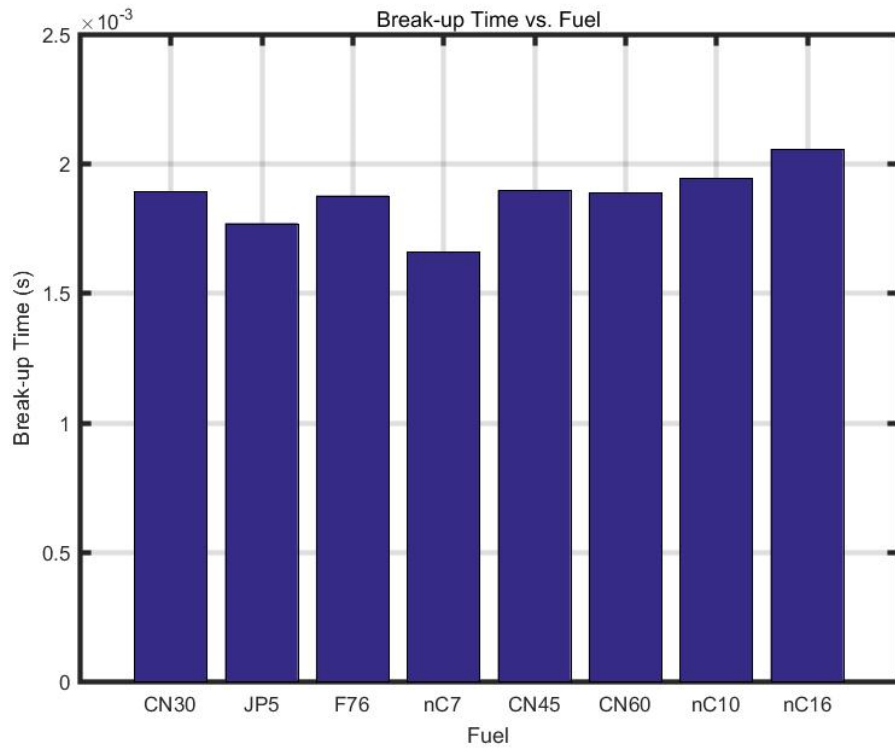


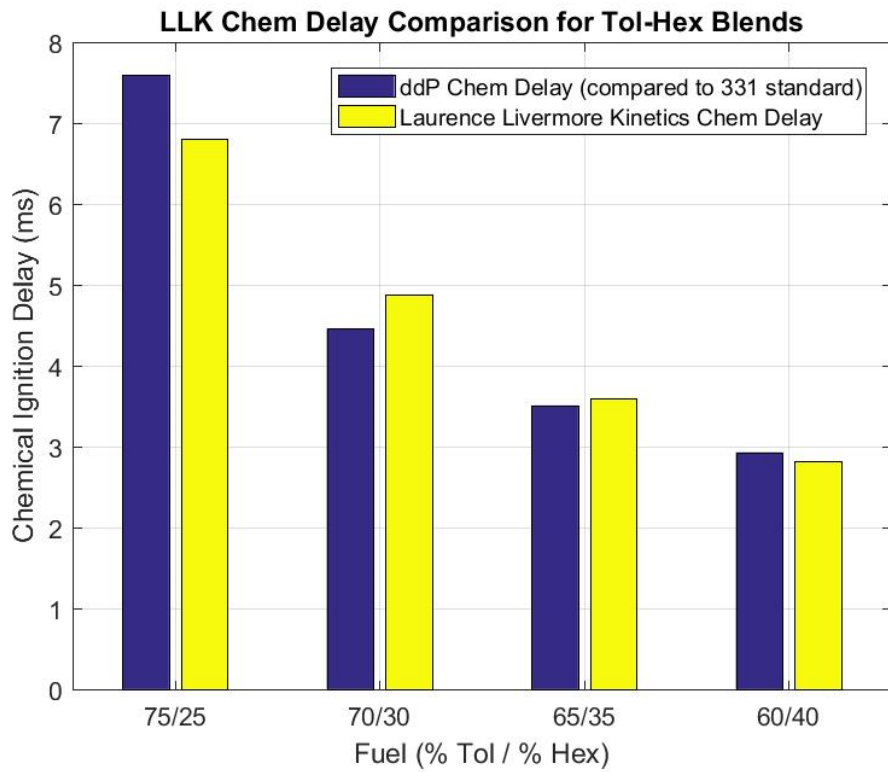
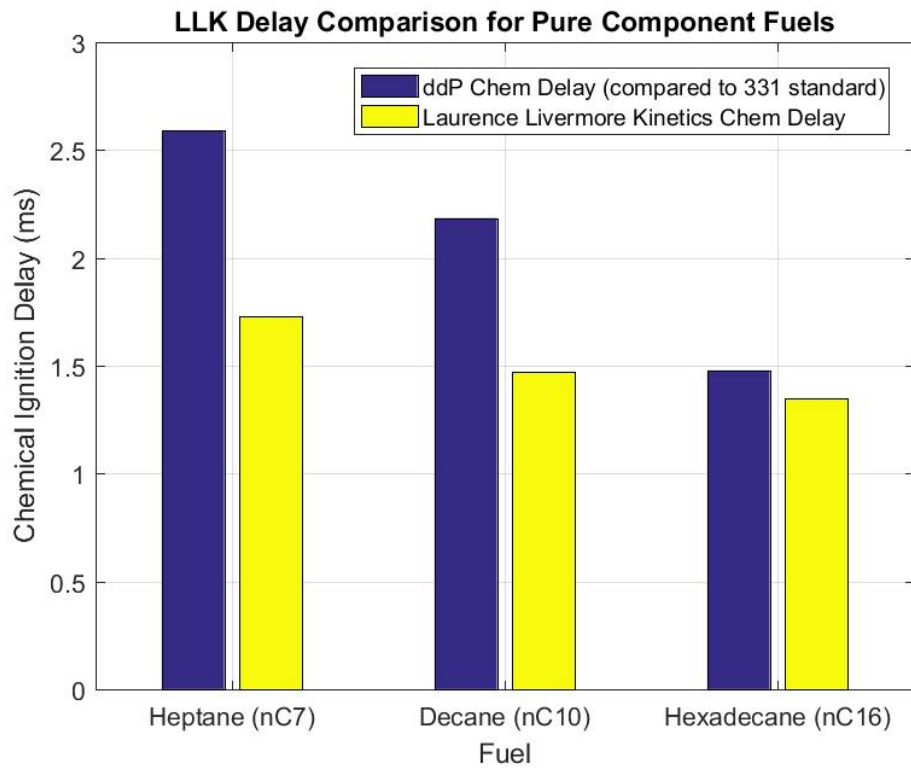












## Appendix F: POI Location Code - CAPT Len Hamilton, USN (Ret.)

```
%this program find IGD and POI based on 8th order polyfit of pressure trace
%L.J. Hamilton 7-14-2016

clear all
format compact
close all
clc

for k=1:32
    % have all 32 for CN30, 45 and 60
    num=1599; %1597 CN60 (DCN 62.9), 1595 CN30 (DCN 37.6), 1598 CN45 (DCN 50.6)
    filename = strcat('Run',num2str(num),'_Inj',num2str(k),'.pre'); %change below also
    data=importdata(filename);
    data=csvread(filename,2,0);

    time=data(:,1);
    Pvesse1=data(:,2)*101.325/14.7;

    lift=data(:,3);
    SOI(k) = time(min(find(lift > 0.05*max(lift))));

    P1 = mean(Pvesse1(100:150)); %kPa - initial air pressure of spray vessel
    cutloc = min(find(Pvesse1 > 1.10*P1)); %determining the position of the cutoff value
    Pvesse1drop = Pvesse1(1:cutloc); %creating a new matrix of only the pressure drop signal

    %curvefit pressure drop signal
    time2 = time(1:size(Pvesse1drop));
    COEF = polyfit(time2,Pvesse1drop,8);
    Pvesse1dropfit = polyval(COEF,time2);

    dPvesse1 = diff(Pvesse1dropfit); %1st derivative of pressure
    ddPvesse1 = diff(Pvesse1dropfit,2); %2nd derivative of pressure
    cumsumdP = cumsum(dPvesse1);
    time3 = time(1:size(dPvesse1));
    time4 = time(1:size(ddPvesse1));

    [mincumsumdP,POIloc]=min(cumsumdP); %returns inflection point location
    POI(k) = time(POIloc);
    IGD(k) = POI(k)-SOI(k);

    figure(1)
    subplot(311)
    plot(time, Pvesse1, time2,Pvesse1dropfit,'r')
    title('Pressure Fitting visual')
    xlabel('Time');ylabel('Pressure')
    legend('Measured P', 'Fitted P', 'Location', 'SouthEast')
    axis([0 15 1900 2500])
    grid on

    subplot(312)
    plot(time3,dPvesse1,time4,100*ddPvesse1,'r')
    hold on
    xlabel('Time')
    legend('dP', 'ddP', 'Location', 'SouthEast')
    axis([0 15 -2 6])
    grid on

    subplot(313)
    plot(time3, cumsumdP)
    hold on
    xlabel('Time');ylabel('cumsumdP');
    axis([0 15 -200 200])
    grid on

end

figure(2)
subplot(211)
plot(POI)
```

```
xlabel('run#');ylabel('POI time');  
axis([0 32 6 11])  
text(1,10,['\fontsize{10}mean POI = ',num2str(mean(POI)),' msec'])  
text(1,9,['\fontsize{10}STD POI = ',num2str(std(POI)),' msec'])  
  
subplot(212)  
plot(IGD)  
xlabel('run#');ylabel('IGD time');  
axis([0 32 5 10])  
text(1,9,['\fontsize{10}mean IGD = ',num2str(mean(IGD)),' msec'])  
text(1,8,['\fontsize{10}STD IGD = ',num2str(std(IGD)),' msec'])
```

[Published with MATLAB® R2016a](#)

Appendix G: Cetane values for primary standard fuels (CN30, CN45, CN60) based on composition isocetane-cetane.

Cetane Vol (m <sup>3</sup> )	Isocetane Vol (m <sup>3</sup> )	CN	mass Cetane (kg)	mass Isocetane (kg)	mass fraction Cetane	mass fraction Isocetane
1	99	15.85	770	78507	0.009712779	0.990287221
2	98	16.7	1540	77714	0.019431196	0.980568804
3	97	17.55	2310	76921	0.029155255	0.970844745
4	96	18.4	3080	76128	0.038884961	0.961115039
5	95	19.25	3850	75335	0.04862032	0.95137968
6	94	20.1	4620	74542	0.058361335	0.941638665
7	93	20.95	5390	73749	0.068108012	0.931891988
8	92	21.8	6160	72956	0.077860357	0.922139643
9	91	22.65	6930	72163	0.087618373	0.912381627
10	90	23.5	7700	71370	0.097382067	0.902617933
11	89	24.35	8470	70577	0.107151442	0.892848558
12	88	25.2	9240	69784	0.116926503	0.883073497
13	87	26.05	10010	68991	0.126707257	0.873292743
14	86	26.9	10780	68198	0.136493707	0.863506293
15	85	27.75	11550	67405	0.146285859	0.853714141
16	84	28.6	12320	66612	0.156083718	0.843916282
17	83	29.45	13090	65819	0.165887288	0.834112712
17.647	82.353	30	13588.19	65305.929	0.172233243	0.827766757
18	82	30.3	13860	65026	0.175696575	0.824303425
19	81	31.15	14630	64233	0.185511583	0.814488417
20	80	32	15400	63440	0.195332319	0.804667681
21	79	32.85	16170	62647	0.205158786	0.794841214
22	78	33.7	16940	61854	0.214990989	0.785009011
23	77	34.55	17710	61061	0.224828935	0.775171065
24	76	35.4	18480	60268	0.234672627	0.765327373
25	75	36.25	19250	59475	0.24452207	0.75547793
26	74	37.1	20020	58682	0.254377271	0.745622729
27	73	37.95	20790	57889	0.264238234	0.735761766
28	72	38.8	21560	57096	0.274104963	0.725895037
29	71	39.65	22330	56303	0.283977465	0.716022535
30	70	40.5	23100	55510	0.293855744	0.706144256
31	69	41.35	23870	54717	0.303739804	0.696260196
32	68	42.2	24640	53924	0.313629652	0.686370348
33	67	43.05	25410	53131	0.323525293	0.676474707
34	66	43.9	26180	52338	0.33342673	0.66657327
35	65	44.75	26950	51545	0.34333397	0.65666603
35.294	64.706	44.9999	27176.38	51311.858	0.346247803	0.653752197
36	64	45.6	27720	50752	0.353247018	0.646752982
37	63	46.45	28490	49959	0.363165878	0.636834122
38	62	47.3	29260	49166	0.373090557	0.626909443
39	61	48.15	30030	48373	0.383021058	0.616978942



40	60	49	30800	47580	0.392957387	0.607042613
41	59	49.85	31570	46787	0.402899549	0.597100451
42	58	50.7	32340	45994	0.41284755	0.58715245
43	57	51.55	33110	45201	0.422801394	0.577198606
44	56	52.4	33880	44408	0.432761087	0.567238913
45	55	53.25	34650	43615	0.442726634	0.557273366
46	54	54.1	35420	42822	0.452698039	0.547301961
47	53	54.95	36190	42029	0.462675309	0.537324691
48	52	55.8	36960	41236	0.472658448	0.527341552
49	51	56.65	37730	40443	0.482647461	0.517352539
50	50	57.5	38500	39650	0.492642354	0.507357646
51	49	58.35	39270	38857	0.502643132	0.497356868
52	48	59.2	40040	38064	0.5126498	0.4873502
52.941	47.059	59.9999	40764.57	37317.787	0.522071458	0.477928542
53	47	60.05	40810	37271	0.522662363	0.477337637
54	46	60.9	41580	36478	0.532680827	0.467319173
55	45	61.75	42350	35685	0.542705196	0.457294804
56	44	62.6	43120	34892	0.552735477	0.447264523
57	43	63.45	43890	34099	0.562771673	0.437228327
58	42	64.3	44660	33306	0.572813791	0.427186209
59	41	65.15	45430	32513	0.582861835	0.417138165
60	40	66	46200	31720	0.592915811	0.407084189
61	39	66.85	46970	30927	0.602975724	0.397024276
62	38	67.7	47740	30134	0.61304158	0.38695842
63	37	68.55	48510	29341	0.623113383	0.376886617
64	36	69.4	49280	28548	0.633191139	0.366808861
65	35	70.25	50050	27755	0.643274854	0.356725146
66	34	71.1	50820	26962	0.653364532	0.346635468
67	33	71.95	51590	26169	0.663460178	0.336539822
68	32	72.8	52360	25376	0.673561799	0.326438201
69	31	73.65	53130	24583	0.683669399	0.316330601
70	30	74.5	53900	23790	0.693782984	0.306217016
71	29	75.35	54670	22997	0.703902558	0.296097442
72	28	76.2	55440	22204	0.714028128	0.285971872
73	27	77.05	56210	21411	0.724159699	0.275840301
74	26	77.9	56980	20618	0.734297276	0.265702724
75	25	78.75	57750	19825	0.744440864	0.255559136
76	24	79.6	58520	19032	0.754590468	0.245409532
77	23	80.45	59290	18239	0.764746095	0.235253905
78	22	81.3	60060	17446	0.774907749	0.225092251
79	21	82.15	60830	16653	0.785075436	0.214924564
80	20	83	61600	15860	0.795249161	0.204750839
81	19	83.85	62370	15067	0.805428929	0.194571071
82	18	84.7	63140	14274	0.815614747	0.184385253
83	17	85.55	63910	13481	0.825806618	0.174193382
84	16	86.4	64680	12688	0.83600455	0.16399545
85	15	87.25	65450	11895	0.846208546	0.153791454

86	14	88.1	66220	11102	0.856418613	0.143581387
87	13	88.95	66990	10309	0.866634756	0.133365244
88	12	89.8	67760	9516	0.87685698	0.12314302
89	11	90.65	68530	8723	0.887085291	0.112914709
90	10	91.5	69300	7930	0.897319694	0.102680306
91	9	92.35	70070	7137	0.907560195	0.092439805
92	8	93.2	70840	6344	0.917806799	0.082193201
93	7	94.05	71610	5551	0.928059512	0.071940488
94	6	94.9	72380	4758	0.938318339	0.061681661
95	5	95.75	73150	3965	0.948583285	0.051416715
96	4	96.6	73920	3172	0.958854356	0.041145644
97	3	97.45	74690	2379	0.969131557	0.030868443
98	2	98.3	75460	1586	0.979414895	0.020585105
99	1	99.15	76230	793	0.989704374	0.010295626
100	0	100	77000	0	1	0

Cetane Vol (m <sup>3</sup> )	Isocetane Vol (m <sup>3</sup> )	CN	moles Cetane	moles Isocetane	mole fraction Cetane	mole fraction Isocetane	density of mixture (kg/m <sup>3</sup> )
1	99	15.85	3400.441863	346685.8026	0.009713155	0.990286845	784.1941266
2	98	16.7	6800.883726	343183.9258	0.01943194	0.98056806	784.0881919
3	97	17.55	10201.32559	339682.049	0.02915636	0.97084364	783.9821957
4	96	18.4	13601.76745	336180.1722	0.03888642	0.96111358	783.876138
5	95	19.25	17002.20932	332678.2954	0.048622125	0.951377875	783.7700188
6	94	20.1	20402.65118	329176.4186	0.05836348	0.94163652	783.6638381
7	93	20.95	23803.09304	325674.5418	0.06811049	0.93188951	783.5575957
8	92	21.8	27203.53491	322172.665	0.07786316	0.92213684	783.4512916
9	91	22.65	30603.97677	318670.7883	0.087621494	0.912378506	783.3449257
10	90	23.5	34004.41863	315168.9115	0.097385498	0.902614502	783.2384981
11	89	24.35	37404.86049	311667.0347	0.107155176	0.892844824	783.1320086
12	88	25.2	40805.30236	308165.1579	0.116930534	0.883069466	783.0254572
13	87	26.05	44205.74422	304663.2811	0.126711577	0.873288423	782.9188438
14	86	26.9	47606.18608	301161.4043	0.136498308	0.863501692	782.8121684
15	85	27.75	51006.62795	297659.5275	0.146290734	0.853709266	782.705431
16	84	28.6	54407.06981	294157.6507	0.15608886	0.84391114	782.5986314
17	83	29.45	57807.51167	290655.7739	0.16589269	0.83410731	782.4917697
17.647	82.353	30	60007.59756	288390.0596	0.172238809	0.827761191	782.422597
18	82	30.3	61207.95354	287153.8971	0.175702229	0.824297771	782.3848457
19	81	31.15	64608.3954	283652.0203	0.185517482	0.814482518	782.2778594
20	80	32	68008.83726	280150.1435	0.195338455	0.804661545	782.1708108
21	79	32.85	71409.27913	276648.2667	0.205165152	0.794834848	782.0636998
22	78	33.7	74809.72099	273146.3899	0.214997578	0.785002422	781.9565264
23	77	34.55	78210.16285	269644.5131	0.224835738	0.775164262	781.8492905
24	76	35.4	81610.60472	266142.6363	0.234679638	0.765320362	781.7419919
25	75	36.25	85011.04658	262640.7595	0.244529282	0.755470718	781.6346308
26	74	37.1	88411.48844	259138.8828	0.254384676	0.745615324	781.527207
27	73	37.95	91811.9303	255637.006	0.264245824	0.735754176	781.4197205
28	72	38.8	95212.37217	252135.1292	0.274112731	0.725887269	781.3121712

29	71	39.65	98612.81403	248633.2524	0.283985403	0.716014597	781.2045591
30	70	40.5	102013.2559	245131.3756	0.293863844	0.706136156	781.0968841
31	69	41.35	105413.6978	241629.4988	0.30374806	0.69625194	780.9891461
32	68	42.2	108814.1396	238127.622	0.313638056	0.686361944	780.8813452
33	67	43.05	112214.5815	234625.7452	0.323533836	0.676466164	780.7734812
34	66	43.9	115615.0233	231123.8684	0.333435407	0.666564593	780.6655541
35	65	44.75	119015.4652	227621.9916	0.343342772	0.656657228	780.5575638
<b>35.294</b>	<b>64.706</b>	<b>44.9999</b>	<b>120015.1951</b>	<b>226592.4398</b>	<b>0.34625664</b>	<b>0.65374336</b>	<b>780.5258026</b>
36	64	45.6	122415.9071	224120.1148	0.353255937	0.646744063	780.4495103
37	63	46.45	125816.3489	220618.238	0.363174907	0.636825093	780.3413935
38	62	47.3	129216.7908	217116.3612	0.373099688	0.626900312	780.2332134
39	61	48.15	132617.2327	213614.4844	0.383030283	0.616969717	780.1249699
40	60	49	136017.6745	210112.6076	0.392966699	0.607033301	780.016663
41	59	49.85	139418.1164	206610.7308	0.402908941	0.597091059	779.9082925
42	58	50.7	142818.5583	203108.8541	0.412857013	0.587142987	779.7998586
43	57	51.55	146219.0001	199606.9773	0.422810921	0.577189079	779.691361
44	56	52.4	149619.442	196105.1005	0.43277067	0.56722933	779.5827997
45	55	53.25	153019.8838	192603.2237	0.442736265	0.557263735	779.4741747
46	54	54.1	156420.3257	189101.3469	0.452707712	0.547292288	779.3654859
47	53	54.95	159820.7676	185599.4701	0.462685014	0.537314986	779.2567333
48	52	55.8	163221.2094	182097.5933	0.472668178	0.527331822	779.1479169
49	51	56.65	166621.6513	178595.7165	0.482657209	0.517342791	779.0390364
50	50	57.5	170022.0932	175093.8397	0.492652112	0.507347888	778.930092
51	49	58.35	173422.535	171591.9629	0.502652892	0.497347108	778.8210835
52	48	59.2	176822.9769	168090.0861	0.512659554	0.487340446	778.7120109
<b>52.941</b>	<b>47.059</b>	<b>59.9999</b>	<b>180022.7927</b>	<b>164794.82</b>	<b>0.522081199</b>	<b>0.477918801</b>	<b>778.6093149</b>
53	47	60.05	180223.4187	164588.2093	0.522672103	0.477327897	778.6028741
54	46	60.9	183623.8606	161086.3325	0.532690545	0.467309455	778.4936731
55	45	61.75	187024.3025	157584.4557	0.542714885	0.457285115	778.3844078
56	44	62.6	190424.7443	154082.5789	0.552745128	0.447254872	778.2750781
57	43	63.45	193825.1862	150580.7021	0.562781279	0.437218721	778.1656841
58	42	64.3	197225.6281	147078.8253	0.572823343	0.427176657	778.0562256
59	41	65.15	200626.0699	143576.9486	0.582871326	0.417128674	777.9467025
60	40	66	204026.5118	140075.0718	0.592925234	0.407074766	777.837115
61	39	66.85	207426.9537	136573.195	0.60298507	0.39701493	777.7274627
62	38	67.7	210827.3955	133071.3182	0.613050841	0.386949159	777.6177458
63	37	68.55	214227.8374	129569.4414	0.623122551	0.376877449	777.5079642
64	36	69.4	217628.2792	126067.5646	0.633200206	0.366799794	777.3981178
65	35	70.25	221028.7211	122565.6878	0.643283812	0.356716188	777.2882065
66	34	71.1	224429.163	119063.811	0.653373373	0.346626627	777.1782302
67	33	71.95	227829.6048	115561.9342	0.663468895	0.336531105	777.068189
68	32	72.8	231230.0467	112060.0574	0.673570382	0.326429618	776.9580828
69	31	73.65	234630.4886	108558.1806	0.683677841	0.316322159	776.8479115
70	30	74.5	238030.9304	105056.3038	0.693791277	0.306208723	776.7376751
71	29	75.35	241431.3723	101554.427	0.703910695	0.296089305	776.6273734
72	28	76.2	244831.8141	98052.55023	0.7140361	0.2859639	776.5170065
73	27	77.05	248232.256	94550.67344	0.724167497	0.275832503	776.4065743

74	26	77.9	251632.6979	91048.79664	0.734304892	0.265695108	776.2960767
75	25	78.75	255033.1397	87546.91985	0.744448291	0.255551709	776.1855136
76	24	79.6	258433.5816	84045.04306	0.754597697	0.245402303	776.0748851
77	23	80.45	261834.0235	80543.16626	0.764753118	0.235246882	775.964191
78	22	81.3	265234.4653	77041.28947	0.774914558	0.225085442	775.8534313
79	21	82.15	268634.9072	73539.41267	0.785082023	0.214917977	775.742606
80	20	83	272035.3491	70037.53588	0.795255517	0.204744483	775.6317149
81	19	83.85	275435.7909	66535.65909	0.805435047	0.194564953	775.520758
82	18	84.7	278836.2328	63033.78229	0.815620617	0.184379383	775.4097353
83	17	85.55	282236.6746	59531.9055	0.825812234	0.174187766	775.2986467
84	16	86.4	285637.1165	56030.0287	0.836009902	0.163990098	775.1874921
85	15	87.25	289037.5584	52528.15191	0.846213626	0.153786374	775.0762715
86	14	88.1	292438.0002	49026.27512	0.856423413	0.143576587	774.9649848
87	13	88.95	295838.4421	45524.39832	0.866639268	0.133360732	774.853632
88	12	89.8	299238.884	42022.52153	0.876861195	0.123138805	774.742213
89	11	90.65	302639.3258	38520.64473	0.887089201	0.112910799	774.6307277
90	10	91.5	306039.7677	35018.76794	0.897323291	0.102676709	774.5191761
91	9	92.35	309440.2095	31516.89115	0.90756347	0.09243653	774.4075582
92	8	93.2	312840.6514	28015.01435	0.917809744	0.082190256	774.2958738
93	7	94.05	316241.0933	24513.13756	0.928062118	0.071937882	774.1841229
94	6	94.9	319641.5351	21011.26076	0.938320598	0.061679402	774.0723055
95	5	95.75	323041.977	17509.38397	0.948585189	0.051414811	773.9604214
96	4	96.6	326442.4189	14007.50718	0.958855896	0.041144104	773.8484707
97	3	97.45	329842.8607	10505.63038	0.969132725	0.030867275	773.7364533
98	2	98.3	333243.3026	7003.753588	0.979415682	0.020584318	773.6243691
99	1	99.15	336643.7444	3501.876794	0.989704772	0.010295228	773.512218
100	0	100	340044.1863	0	1	0	773.4

	Density (kg/m <sup>3</sup> )	Molar Mass (kg/mol)
n-hexadecane	770	0.22644
HMN	793	0.22645

## Appendix H: Calculation of individual fuel property values.

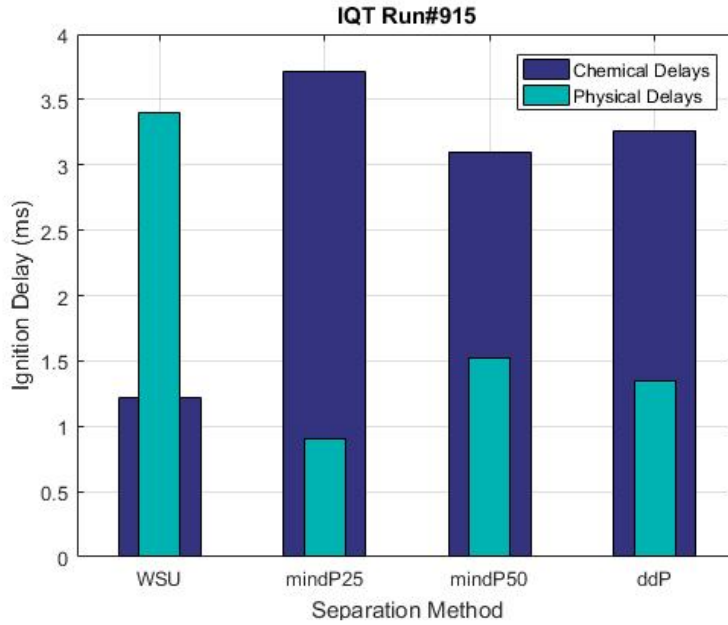
Fuel	DCN	density at 20 C (kg/m <sup>3</sup> )	viscosity at 20 C (mu/mPa s)	surface tension (N/M)	v_inj (m/s)	diameter (m) less C and Lam	Rej	Lam*	Dd(m)	Dd(mm)	Dd(um)
nC7	53.76	683.85	0.41	0.0187	214.8878645	4.2164E-07	358417.2345	19.14366681	5.38112E-06	0.005381116	5.381116046
nC10	65.88	729.87	0.922	0.0238	208.002981	5.7274E-07	164658.4986	3.785567533	1.44543E-06	0.001445434	1.445433918
nC16	118.85	773.8	3.44	0.0273	202.012365	6.9651E-07	45441.03722	0.271941792	1.26273E-07	0.000126273	0.126273466
CN30	37.58	782.42	3.579	0.0247	200.8964877	6.372E-07	43918.8125	0.251228811	1.06721E-07	0.000106721	0.106721302
CN45	50.55	780.53	3.516	0.0251	201.1395692	6.4595E-07	44651.72582	0.260312551	1.12099E-07	0.000112099	0.112099378
CN60	62.9	778.61	3.45	0.0255	201.3874149	6.5463E-07	45449.92901	0.270367603	1.17994E-07	0.000117994	0.117993907
JP5	44.97	800.9	1.51	0.0261	198.5652143	6.8922E-07	105318.4637	1.411363708	6.48489E-07	0.000648489	0.64848886
F76	49.57	848	3.24	0.0267	192.9720407	7.4652E-07	50506.2625	0.306551058	1.52565E-07	0.000152565	0.152564927

Fuel	DCN	Modified Drop Diameter (m)	Fuel	Weber Number	Fuel	Break Up Time (s)
nC7	53.76	0.005453456	nC7	712002.494	nC7	0.001658847
nC10	65.88	0.005335996	nC10	759917.029	nC10	0.00177048
nC16	118.85	0.00228838	nC16	805655.5237	nC16	0.001877043
CN30	37.58	0.001647173	CN30	814630.3888	CN30	0.001897953
CN45	50.55	0.001755221	CN45	812662.5819	CN45	0.001893368
CN60	62.9	0.001871076	CN60	810663.5401	CN60	0.001888711
JP5	44.97	0.004715121	JP5	833871.1669	JP5	0.001942781
F76	49.57	0.00249089	F76	882910.1629	F76	0.002057033

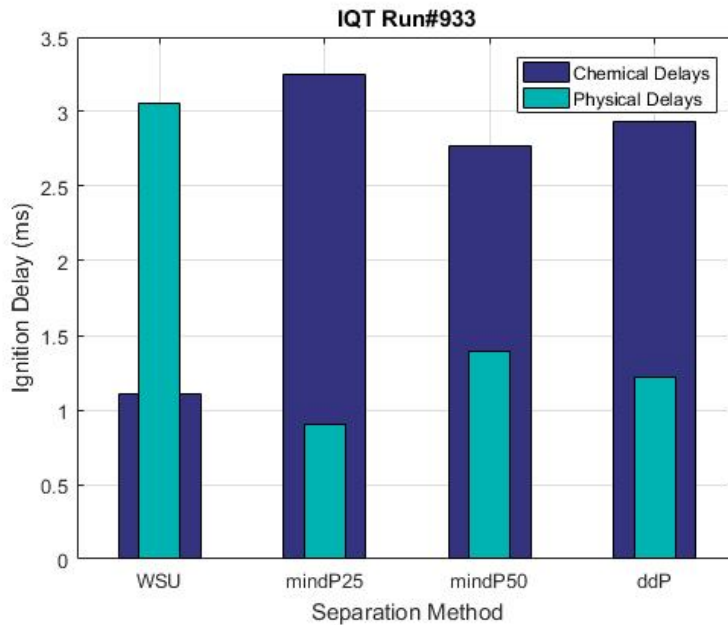
Fuel	DCN	Modified Droplet Diameter	Weber #	Break-up Time
CN30	37.58	0.001647173	814630.389	0.001897953
JP5	44.97	0.004715121	833871.167	0.001942781
F76	49.57	0.00249089	882910.163	0.002057033
CN45	50.55	0.001755221	812662.582	0.001893368
nC7	53.76	0.005453456	712002.494	0.001658847
CN60	62.9	0.001871076	810663.54	0.001888711
nC10	65.88	0.005335996	759917.029	0.00177048
nC16	118.85	0.00228838	805655.524	0.001877043

Appendix I: Physical and chemical ignition delay summaries for each fuel.

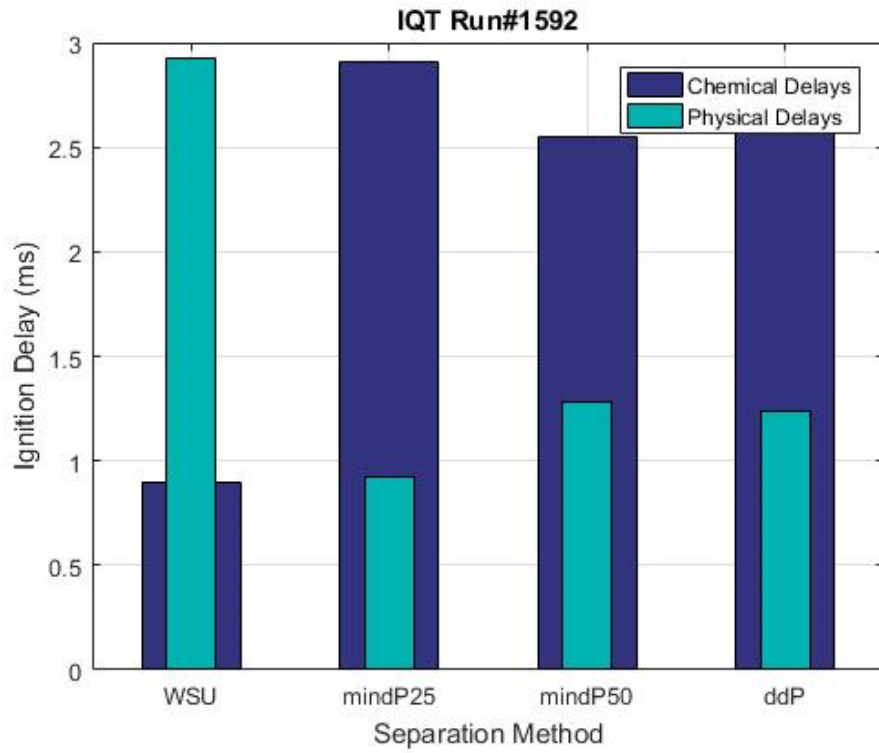
**JP5**



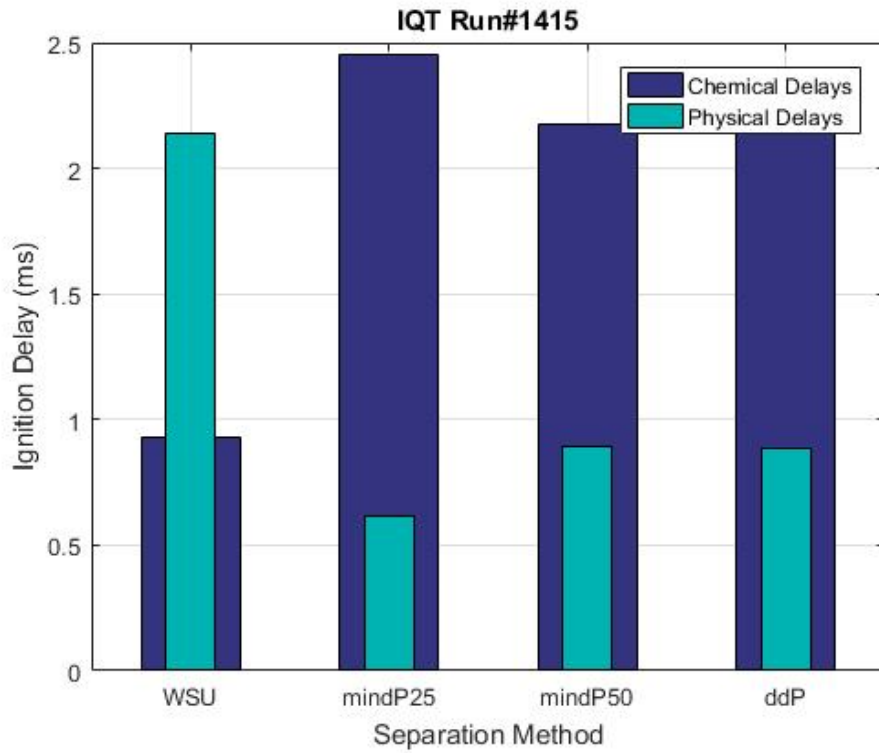
**F76**



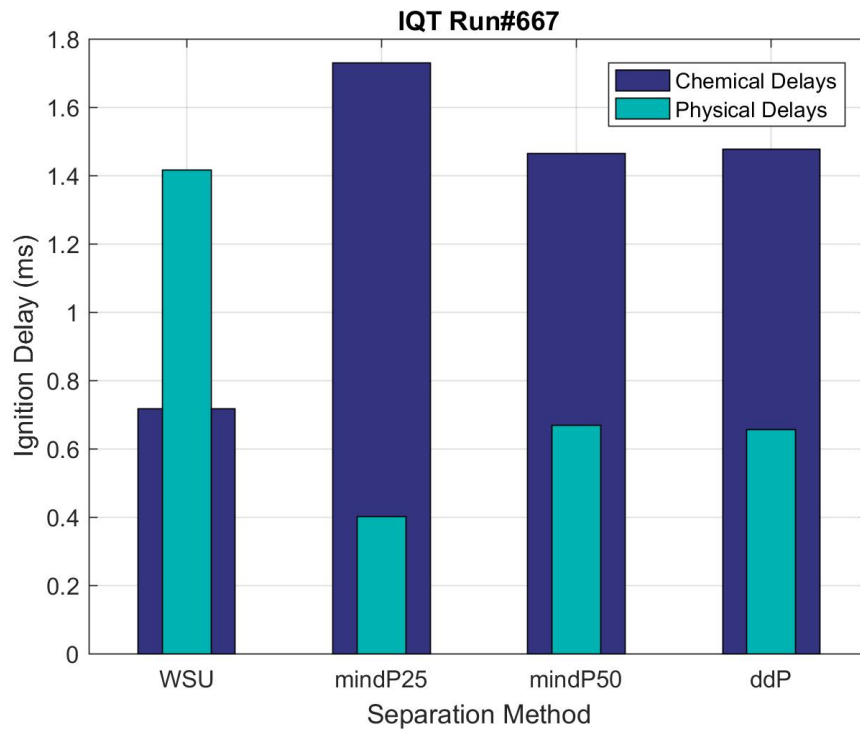
**nC7**



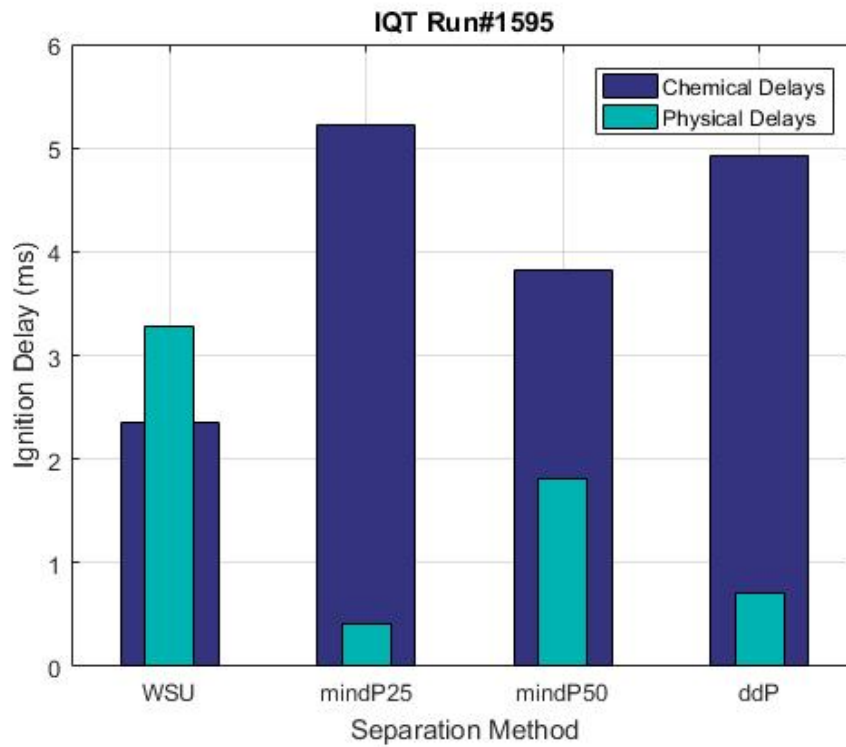
**nC10**



**nC16**

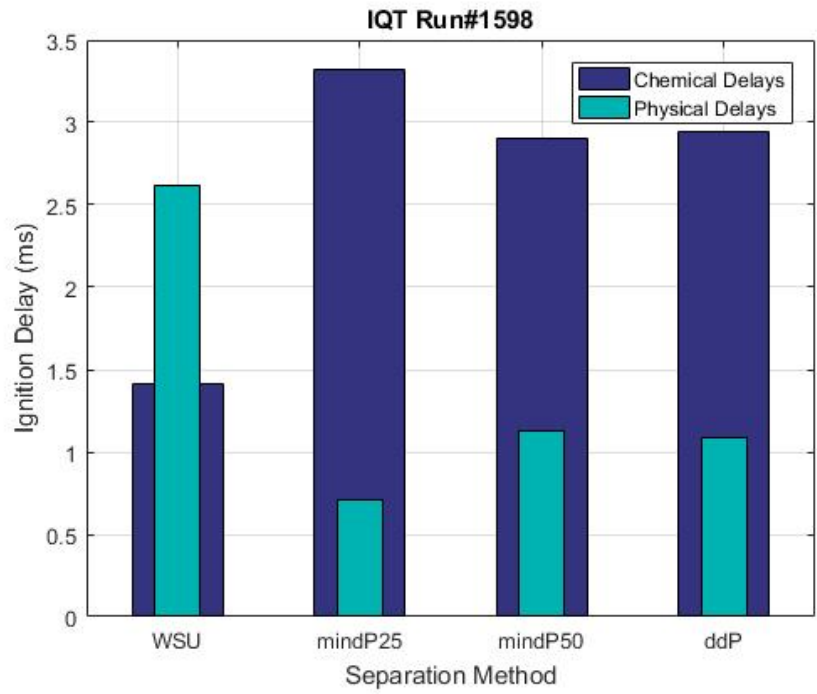


**CN30**

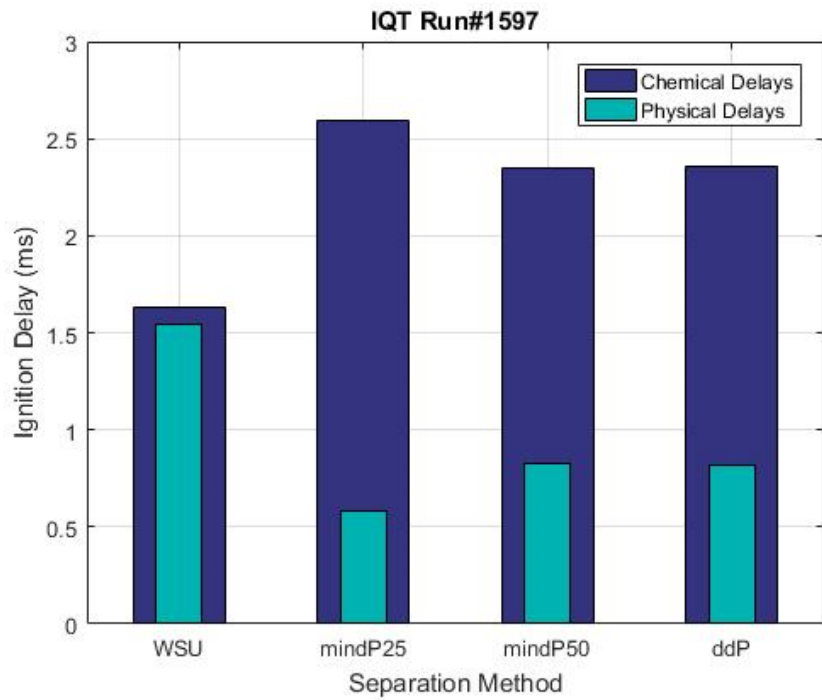




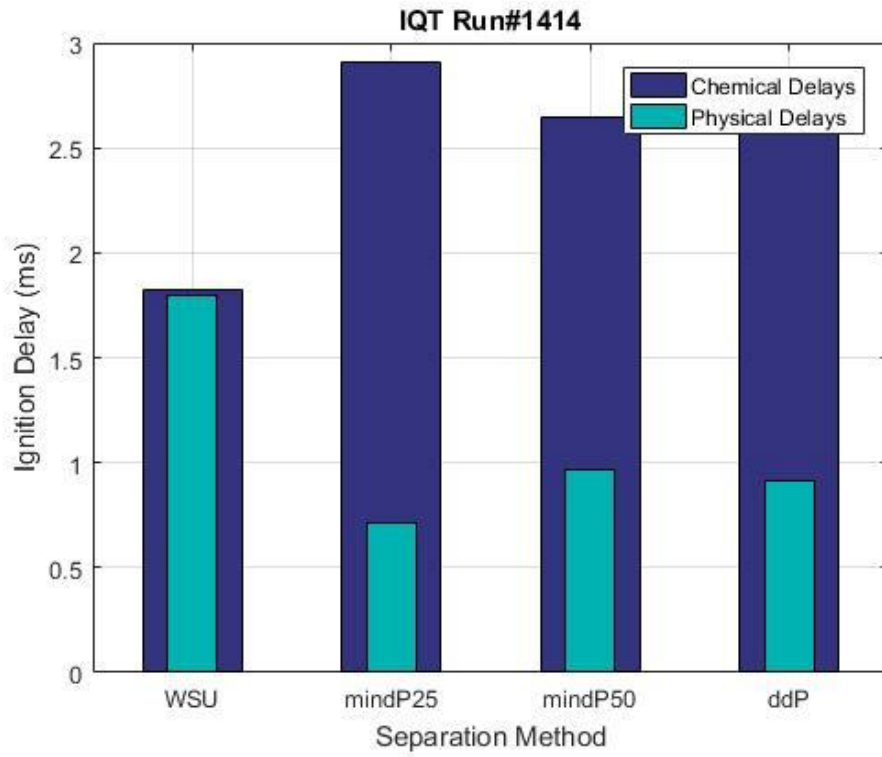
**CN45**



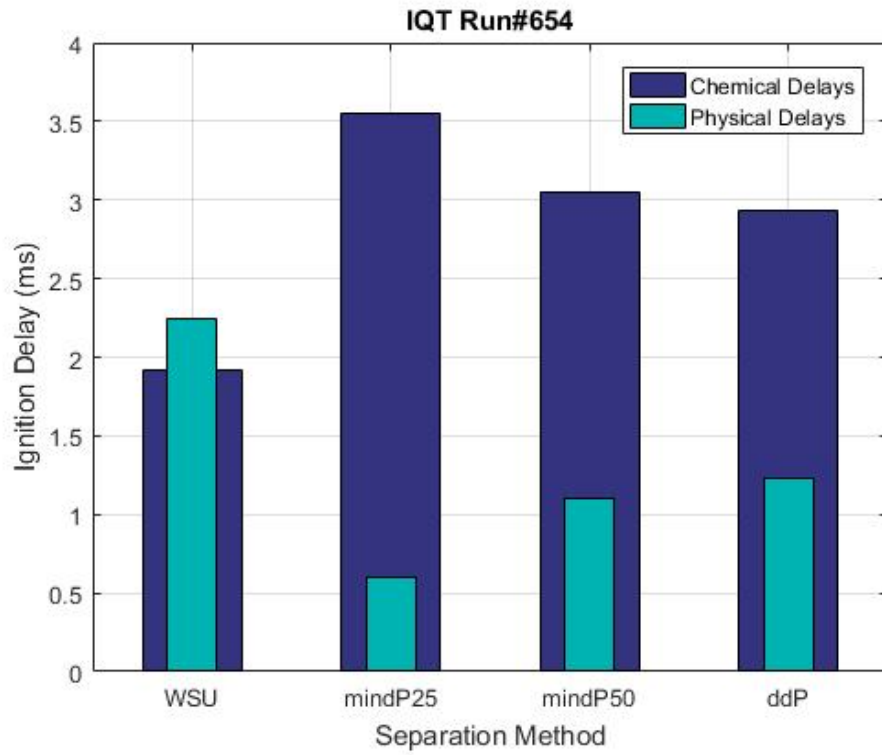
**CN60**



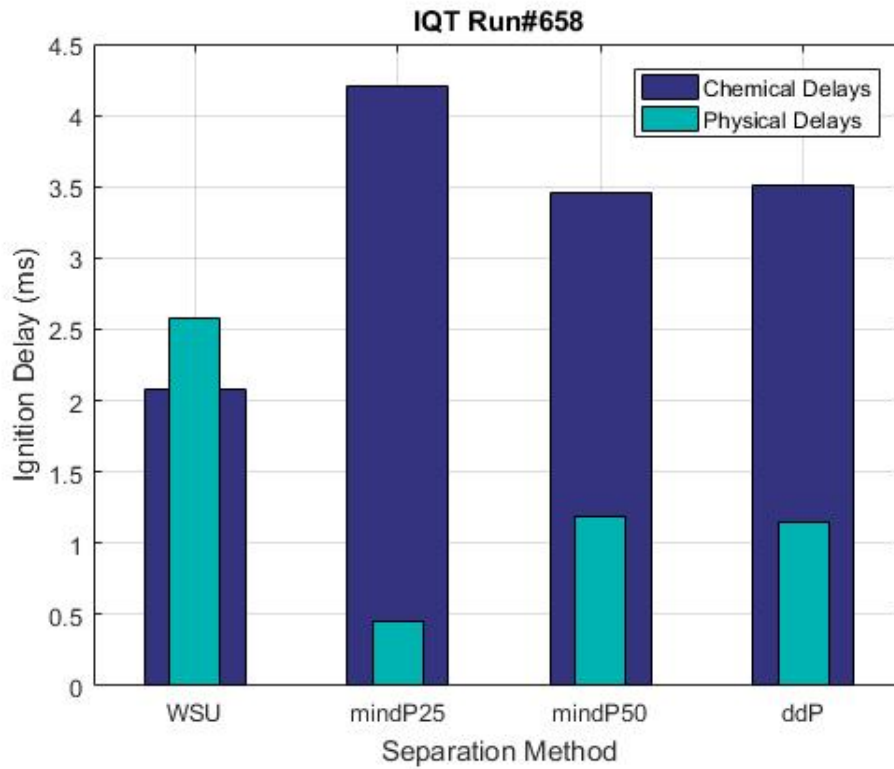
**50-50 Tol-Hex**



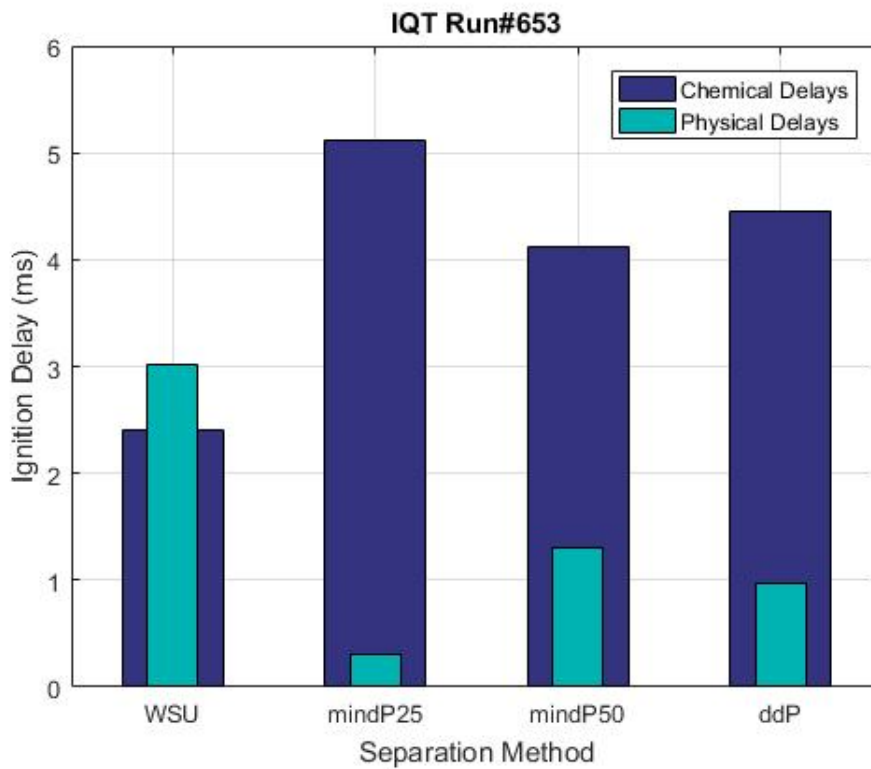
**60-40 Tol-Hex**



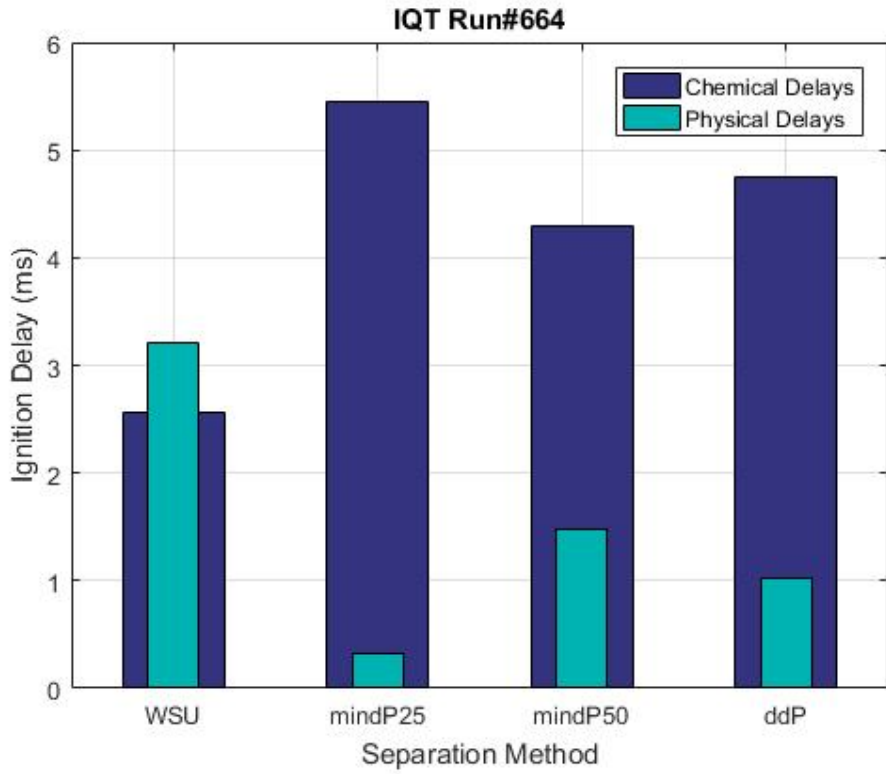
**65-35 Tol-Hex**



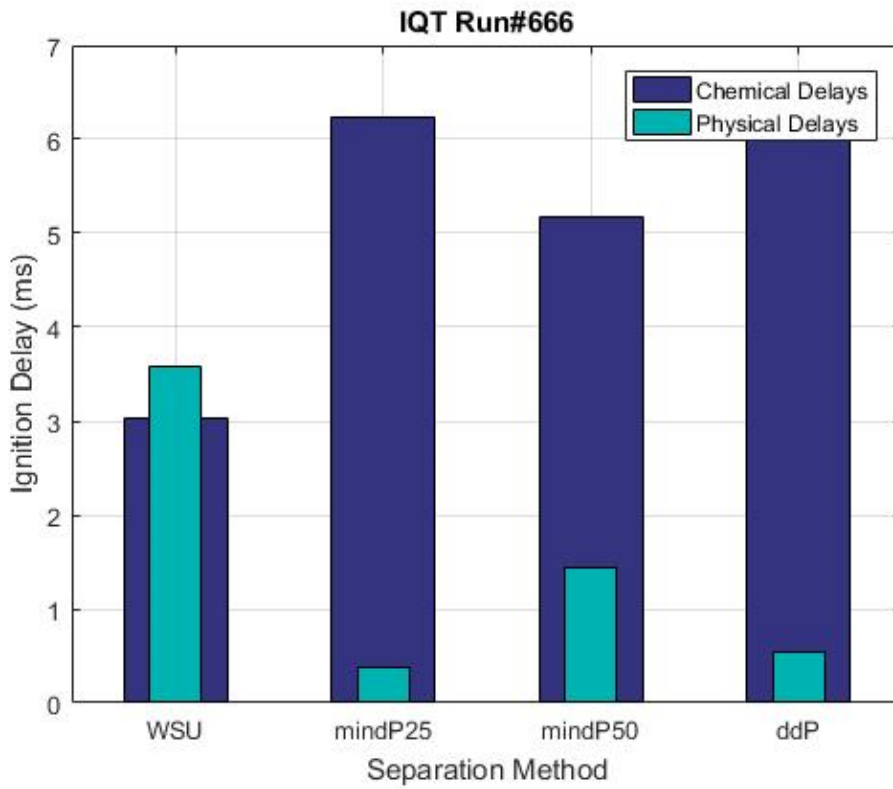
**70-30 Tol-Hex**



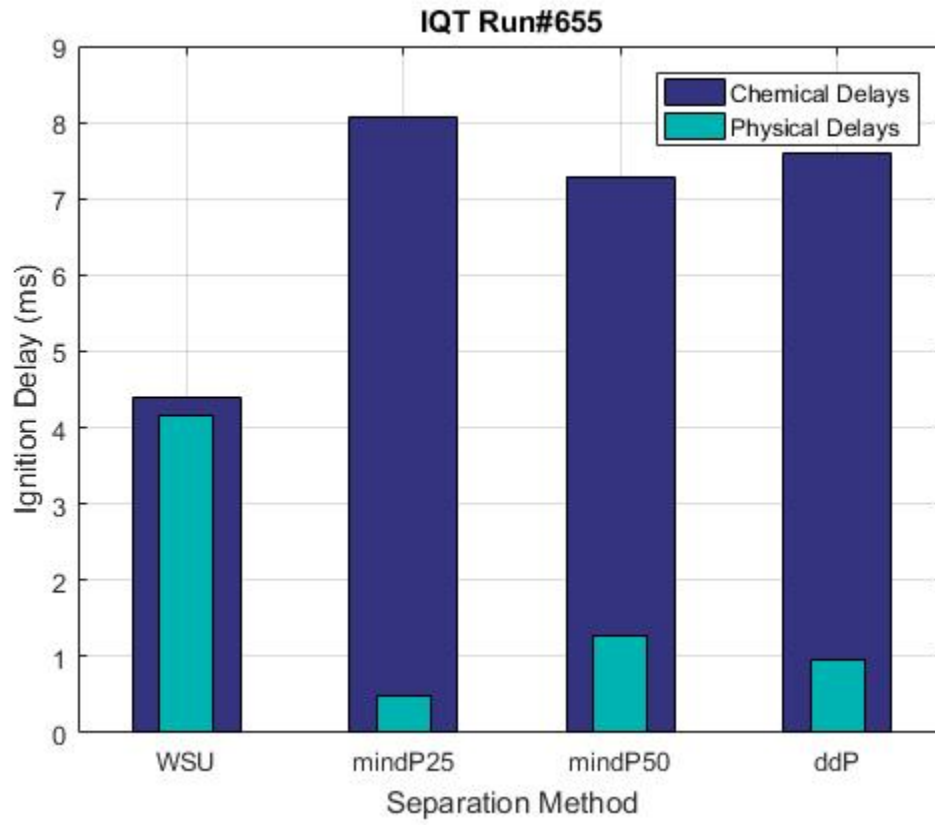
**72-28 Tol-Hex**



**74-26 Tol-Hex**



**75-25 Tol-Hex**



## Bibliography

- [1] Great Green Fleet. (n.d.). Retrieved October 20, 2016, from <http://greenfleet.dodlive.mil/energy/great-green-fleet/>
- [2] Mabus, R. (2011, May 4). US Navy Chief: I'm on a mission to stop using oil [Interview by P. McKenna]. In *New Scientist*. Retrieved October 24, 2016, from <https://www.newscientist.com/article/mg21028110.200-us-navy-chief-im-on-a-mission-to-stop-using-oil/#.Uk6vmT9y3gY>
- [3] Statement on Algae Biofuels in the Navy's Great Green Fleet. (n.d.). Retrieved October 24, 2016, from <http://algaebiomass.org/statement-on-algae-biofuels-in-the-navys-great-green-fleet/>
- [4] Matsunaga, M. (2014, July 3). Navy Looks to Biofuels to Sail the Great Green Fleet in 2016. Retrieved October 24, 2016, from [http://www.navy.mil/submit/display.asp?story\\_id=82044](http://www.navy.mil/submit/display.asp?story_id=82044)
- [5] Myers, M. (2016, January 20). Navy deploys first biofuel-powered Great Green Fleet to Asia-Pacific. *Navy Times*. Retrieved October 24, 2016, from <https://www.navytimes.com/story/military/2016/01/20/stennis-strike-group-sets-sail-10-percent-beef-fat-fuel-blend/79054624/>
- [6] Burnett, K. J. (2015). Diesel Engine Startup Characterization with Pure Component and Conventional Navy Fuels (Unpublished master's thesis). University of Maryland.
- [7] Allard, L. N., Webster, G. D., Hole, N. J., Ryan, T. W., III, Ott, D., & Fairbridge, C. W. (n.d.). Diesel Fuel Ignition Quality as Determined in the Ignition Quality Tester (IQT). Society of Automotive Engineers, 955-959. Retrieved October 28, 2016.
- [8] Allard, L. N., Hole, N. J., Webster, G. D., Ryan, T. W., III, Ott, D., Beregszaszy, A., . . . Rickeard, D. J. (1997). Diesel Fuel Ignition Quality as Determined in the Ignition Quality Tester (IQT) - Part II. Society of Automotive Engineers, 554-563. Retrieved October 28, 2016.
- [9] Allard, L. N., Webster, G. D., Ryan, T. W., III, Matheaus, A. C., Baker, G., Beregszaszy, A., . . . Jones, G. (2001). Diesel Fuel Ignition Quality as Determined in the Ignition Quality Tester (IQT) - Part IV. Society of Automotive Engineers, 119-128. Retrieved October 28, 2016.
- [10] Shrestha, Amit, Ziliang Zheng, Tamer Badawy, and Naeim Henein. "Development of JP-8 Surrogates and Their Validation Using Ignition Quality Tester." *SAE International* 7 (April 15, 2014): 337-51. Accessed July 13, 2016. doi:10.4271/2014-01-9077.
- [11] Bogin, G. E., Jr., Osecky, E., Chen, J. Y., Ratcliff, M. A., Luecke, J., Zigler, B. T., & Dean, A. M. (2014, June 16). Experiments and Computational Fluid Dynamics Modeling Analysis of Large n-Alkane Ignition Kinetics in the Ignition Quality Tester. *Energy and Fuels*, 28, 4781-4794. doi:10.1021/ef500769j

- [12] Guillen, D. P. (2012, July 25). The Autoignition of Cyclopentane in an Ignition Quality Tester. *Journal of the Minerals, Metals, and Materials Society*, 64(8), 985-989. doi:10.1007/s11837-012-0369-2
- [13] Bogin, G. E., Jr., Luecke, J., Ratcliff, M. A., Osecky, E., & Zigler, B. T. (2016). Effects of iso-octane/ethanol blend ratios on the observance of negative temperature coefficient behavior within the Ignition Quality Tester. Elsevier: *The Science and Technology of Fuel and Energy*, 186, 82-90. doi:10.1016/j.fuel.2016.08.021
- [14] Knothe, G., Matheaus, A. C., & Ryan, T. W., III. (2002, December 24). Cetane numbers of branched and straight-chain fatty esters determined in an ignition quality tester. *The Science and Technology of Fuel and Energy*, 82, 971-975. Retrieved October 28, 2016, from Science Direct.
- [15] Alfazazi, A., Kuti, O. A., Naser, N., Chung, S. H., & Sarathy, S. M. (2016, August 10). Two-stage Lagrangian modeling of ignition processes in ignition quality tester and constant volume combustion chambers. *The Science and Technology of Fuel and Energy*, 185, 589-598. doi:10.1016/j.fuel.2016.08.017
- [16] Naser, N., Yang, S. Y., Kalghatgi, G., & Chung, S. H. (2016, September 21). Relating the octane numbers of fuels to ignition delay times measured in an ignition quality tester (IQT). Elsevier: *The Science and Technology of Fuel and Energy*, 187, 117-127. doi:10.1016/j.fuel.2016.09.013
- [17] Diesel Fuel Ignition Quality Tester. (n.d.). Retrieved September 22, 2016, from <http://www.aet.ca/index.php?section=20>
- [18] Heywood, J. B. (1988). *Internal combustion engine fundamentals*. New Delhi: Tata McGraw Hill.
- [19] Luning Prak, D. J., Trulove, P. C., & Cowart, J. S. (2013, March 21). Density, Viscosity, Speed of Sound, Surface Tension, and Flash Point of Binary Mixtures of n-Hexadecane and 2,2,4,4,6,8,8- Heptamethylnonane and of Algal-Based Hydrotreated Renewable Diesel. *Journal of Chemical and Engineering Data*, (58), 920-926. Retrieved October 24, 2016, from <http://pubs.acs.org/doi/abs/10.1021/jc301337d>
- [20] Charles K. Westbrook, William J. Pitz, Olivier Herbinet, Henry J. Curran, Emma J. Silke. A comprehensive detailed chemical kinetic reaction mechanism for combustion of n-alkane hydrocarbons from n-octane to n-hexadecane. *Combustion and Flame*, Elsevier, 2008, 156, pp.181-199. <10.1016/j.combustame.2008.07.014>. <hal-00848875>